Investigating the Role of IFITM Proteins in the Viral Entry Mechanism of Early and Omicron Variants.

Tiffany Teoh

Supervisor: Efstathios (Stathis) Giotis and Nelson Fernandez

A thesis submitted for the degree of MSD Master of Science by Dissertation in Biological Sciences: Immunology (MSD)

School of Life Sciences.

University of Essex

February 2026

ABSTRACT

Severe acute respiratory syndrome coronavirus 2 (SARS-CoV-2) continues to pose a global health challenge due to the emergence of viral variants with altered entry mechanisms, making host restriction factors such as interferon-induced transmembrane proteins (IFITMs) critical determinants of infectivity. This study investigated the role of IFITM1, IFITM2, and IFITM3 in mediating the entry of early SARS-CoV-2 variants and Omicron subvariants using pseudotyped virus systems in human lung epithelial cells, with viral entry quantified by luciferase-based assays following IFITM overexpression. The results demonstrate that IFITM1 significantly restricts viral entry for several early variants, while IFITM2 exhibits consistent inhibitory effects across all variants examined. In contrast, IFITM3 overexpression does not significantly alter viral entry efficiency for any variant tested, indicating that IFITM3 does not play a major restrictive role in this experimental system. Collectively, these findings highlight distinct functional differences among IFITM family members and emphasise the importance of variant-specific entry pathways in shaping susceptibility to host restriction factors.

ACKNOWLEDGEMENT

I extend my heartfelt gratitude to all those who played a pivotal role in completing this research. Foremost, I owe immense thanks to my supervisors, Dr. Efstathios Giotis and Professor Nelson Fernandez, whose invaluable support and guidance were fundamental to the fruition of this work. Additionally, I am grateful to Dr. Greg Brooke and Professor Selwa Alsam for their additional guidance and insights.

My appreciation also goes out to the entire School of Life Science staff for their training and support, which was instrumental in my development and progress.

I am especially grateful to my family for their unwavering love and support. To my parents, thank you for everything you have done for me, particularly through significant health challenges. I also wish to pay heartfelt tribute to my late Uncle Peter. Without his support, I would not have come this far. He was my English and life mentor, and he remained a constant source of guidance and motivation. This thesis is for you.

To my friends and colleagues, thank you for your encouragement and kindness, which strengthened me throughout this journey.

Lastly, a special thanks to my lab mates Tukur, Deima, and Riaz for their collaboration, insights, and camaraderie. This journey would not have been the same without you all.

Table of Contents

LIST OF FIGURES

LIST OF TABLES

ABBREVIATIONS

***A549 ^{ACE2}*Cells**	A549 cells express ACE2 receptor
aa	Amino acid
ACE2	Angiotensin-converting enzyme-2
BLASTp	Basic Local Alignment Search Tool for proteins
CDC	Centres for Disease Control and Prevention
CO_2	Carbon dioxide
CoVs	Coronaviruses
CPM	Counts per million
DMEM	Dulbecco's Modified Eagle's medium
DMSO	Dimethyl sulfoxide
DNA	Deoxyribonucleic acid
EMBL-EBI	European Molecular Biology Laboratory's European Bioinformatics Institute
FP	Fusion peptide
GAPDH	Glyceraldehyde-3-phosphate dehydrogenase
GFP	Green fluorescent protein
GISAID	The Global Initiative on Sharing All Influenza Data
HA	Hemagglutinin
HAE	Human airway epithelial cells
HCoVs	Human coronaviruses
HEK293T	Human embryonic kidney 293 cell line expresses the large T antigen of simian virus 40 (SV40)
HIV	Human immunodeficiency virus
IAV	Influenza A Virus
IFITM	Interferon-induced transmembrane proteins
IFN	Interferon
IFNAR	interferon-α/β receptor
ISG	Interferon-stimulated genes
LVs	Lentivirus
NCBI	National Centre for Biotechnology Information
NK	Natural killer
NTD	N-terminal domain
PBS	Phosphate Buffered Saline (buffer solution)
PVs	Pseudotyped viruses
qRT-PCR	Quantitative real-time PCR
RBD	Receptor-binding domain
RFP	Red fluorescent protein
RLU	Relative Light Units
RNA	Ribonucleic acid
RNase-free	Free of ribonuclease (RNase) enzymes

S	Spike protein
SARS-CoV	Severe-acute-respiratory-syndrome-related coronavirus
SD	standard deviation
SGTF	Spike gene target failure
SGTL	Spike gene late detection
SHCoVs	Seasonal human coronaviruses
SNP	Single-nucleotide polymorphisms
sgmRNA	Subgenomic mRNAs
TMPRSS2	Transmembrane serine protease 2
TRS	Transcription-regulatory sequences
UDG	Uracil-DNA glycosylases
VOC	Variants of concern
VOI	Variant of interest
VSV	Vesicular stomatitis virus
VSVG	Vesicular Stomatitis Virus Glycoprotein
WHO	World Health Organisation
Δ-env	Without a functional envelope gene

CHAPTER ONE: INTRODUCTION

1.1 Overview of Coronaviruses and SARS-CoV-2

Coronaviruses are enveloped, positive-sense single-stranded ribonucleic acid (RNA) viruses belonging to the family Coronaviridae within the order Nidovirales (International Committee on Taxonomy of Viruses (ICTV)). They have large genomes (approximately ~30 kb; often described within a ~26–32 kb range) and are characterised by spike (S) glycoproteins that project from the viral envelope, giving them a distinctive crown-like appearance under electron microscopy (Fehr & Perlman, 2015; V'kovski et al., 2020). Coronaviruses infect a wide range of avian and mammalian hosts and can cause diseases of varying severity, ranging from mild respiratory infections to severe and potentially fatal illness (V'kovski et al., 2020). SARS-CoV-2, the causative agent of coronavirus disease 2019 (COVID-19), was first identified in late 2019 and rapidly spread globally, resulting in an unprecedented public health crisis (World Health Organisation, 2020; Wu et al., 2020). In contrast to previously circulating human coronaviruses, which typically cause mild upper respiratory tract infections, SARS-CoV-2 is associated with severe lower respiratory tract infection, systemic inflammation, and high transmissibility (V'kovski et al., 2020). These clinical and epidemiological characteristics are attributed in part to efficient mechanisms of cell entry and the virus's capacity to adapt through genetic variation (V'kovski et al., 2020).

The SARS-CoV-2 genome encodes multiple structural proteins, including spike (S), envelope (E), membrane (M), and nucleocapsid (N), as well as non-structural and accessory proteins that modulate viral replication and host responses (Bai et al., 2021; Islam et al., 2022). Among these, the spike protein plays a central role in viral infectivity by mediating attachment to host cells and triggering membrane fusion following receptor engagement and proteolytic activation (V'kovski et al., 2021; Yang & Rao, 2021). Consequently, spike-mediated entry is a key determinant of viral tropism, pathogenicity, and susceptibility to host restriction factors, making it a central focus of SARS-CoV-2 research and of this study (V'kovski et al., 2021).

1.2 The coronavirus family

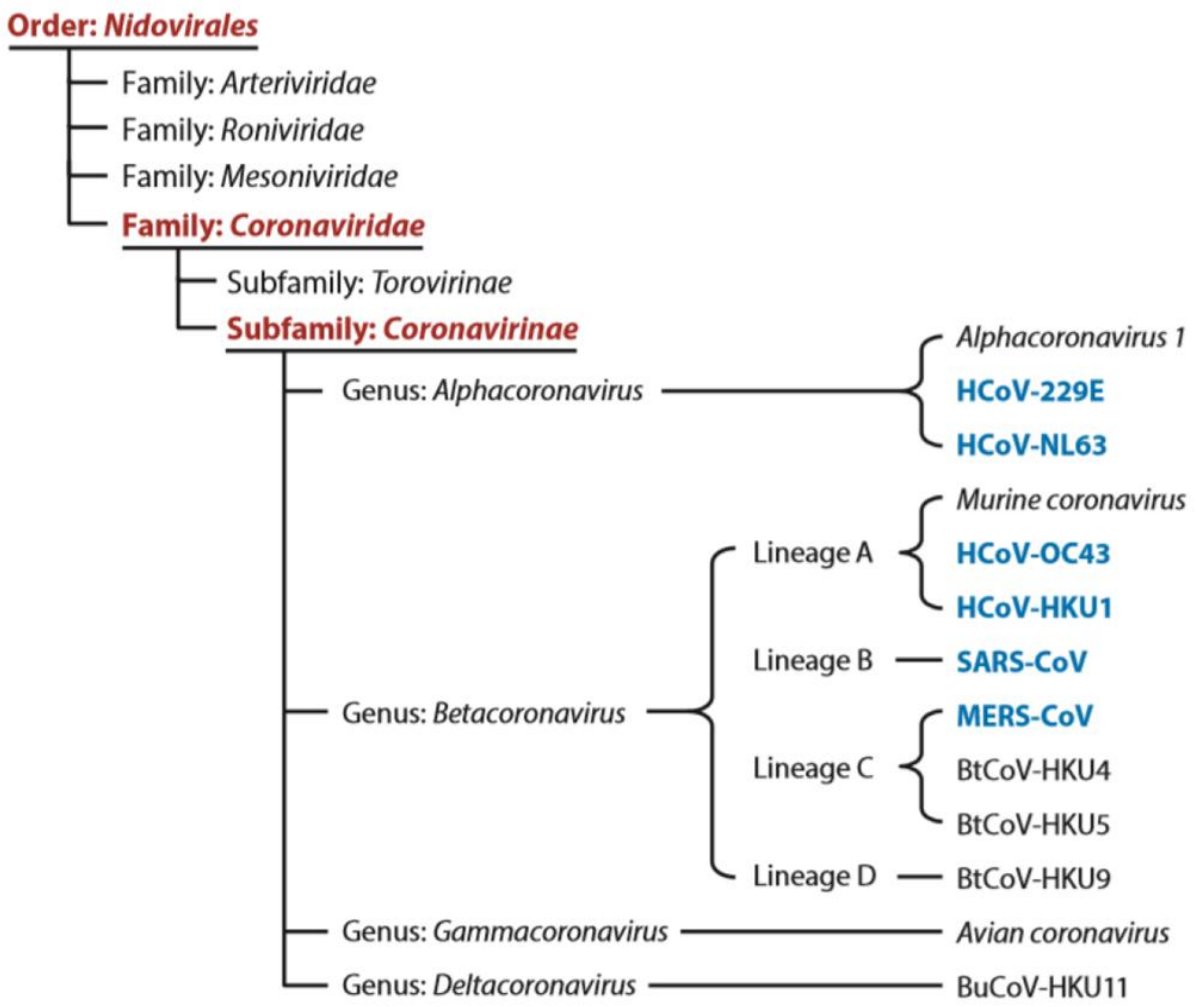

Figure 1: Classification scheme of HCoV and other coronaviruses.

Within the order Nidovirales, showing the four genera (Alpha-, Beta-, Gamma- and Deltacoronavirus) and representative human and animal coronavirus species, including major human pathogens (HCoV-229E, HCoV-NL63, HCoV-OC43, HCoV-HKU1, SARS-CoV, and MERS-CoV). Reproduced from Yan et al. (2020).

The family Coronaviridae is divided into four genera—Alphacoronavirus, Betacoronavirus, Gammacoronavirus, and Deltacoronavirus—distinguished primarily by genetic relatedness and typical host range (ICTV). Human coronaviruses are predominantly found within the alpha- and betacoronavirus genera (Fehr & Perlman, 2015; Su et al., 2016). While several endemic human coronaviruses, such as HCoV-229E and HCoV-OC43, typically cause mild respiratory illness, other

betacoronaviruses have been responsible for severe outbreaks, including SARS-CoV, MERS-CoV, and SARS-CoV-2 (Fehr & Perlman, 2015; Su et al., 2016; V'kovski et al., 2021).

Coronaviruses share a conserved genomic organisation, with replicase genes at the 5′ end of the genome and structural protein genes at the 3′ end (Fehr & Perlman, 2015; V'kovski et al., 2021). Despite this conserved framework, substantial diversity exists in spike (S) protein sequence and structure, contributing to differences in receptor usage, host specificity, and entry pathways (Li, 2016; V'kovski et al., 2021). This diversity enables coronaviruses to cross species barriers and adapt to new hosts (Su et al., 2016).

Within the Betacoronavirus genus, SARS-CoV-2 belongs to the subgenus Sarbecovirus, alongside SARS-CoV (ICTV). Viruses within this group can be genetically similar yet differ in transmissibility and pathogenicity (V'kovski et al., 2021). Comparative analyses show that variations in spike receptor-binding domains, protease activation requirements, and cleavage sites can strongly influence entry efficiency and disease outcome (Hoffmann et al., 2020; V'kovski et al., 2021; Walls et al., 2020). Understanding these shared and divergent features within the coronavirus family provides essential context for investigating how SARS-CoV-2 entry mechanisms are regulated and how host factors may differentially affect infection by distinct viral variants (V'kovski et al., 2021).

1.3 Proteolytic Activation of SARS-CoV-2 Spike: TMPRSS2 and cathepsins

Entry of SARS-CoV-2 into host cells depends on proteolytic activation of the spike (S) protein by host proteases (Figure 2). Following spike binding to the ACE2 receptor, cleavage at the S1/S2 and S2′ sites is required to expose the fusion machinery and trigger membrane fusion (Walls et al., 2020; Shang et al., 2020). This activation can occur at the plasma membrane or within endosomal compartments, depending on which proteases are available in the target cell (Hoffmann et al., 2020; Shang et al., 2020).

Transmembrane serine protease 2 (TMPRSS2) promotes spike activation at the cell surface, enabling rapid fusion of the viral envelope with the host plasma membrane (Hoffmann et al., 2020). This pathway is particularly efficient in cells with high TMPRSS2 expression, including populations within the lower respiratory tract, and has been linked to enhanced viral entry/replication in relevant models and more severe disease-associated phenotypes (Hoffmann et al., 2020; Meng et al., 2022). In contrast, in cells with low or absent TMPRSS2, SARS-CoV-2 can enter via endocytosis, where spike activation occurs within endosomes(Shang et al., 2020).

In the endosomal route, spike activation is mediated primarily by endosomal cysteine proteases, particularly cathepsin L, which are optimally active in acidic compartments (Shang et al., 2020). Following endocytosis, acidification of endosomes promotes cathepsin activity and supports proteolytic processing of the spike, exposing the fusion peptide and enabling fusion from within the endosome and release of the viral genome into the cytoplasm (Shang et al., 2020). Although this pathway is generally slower than TMPRSS2-mediated entry because it requires uptake and endosomal trafficking, it can broaden cellular tropism by enabling infection of cell types with limited TMPRSS2 expression (Shang et al., 2020; Peacock et al., 2022). This is especially relevant in the

upper airway, where TMPRSS2 expression is typically lower, and increased reliance on cathepsin-dependent entry has been associated with altered tissue tropism and reduced lower-airway pathogenicity in experimental systems (Meng et al., 2022; Peacock et al., 2022).

Notably, several SARS-CoV-2 variants, particularly within the Omicron lineage, show reduced dependence on TMPRSS2 and increased utilisation of cathepsin-mediated endosomal entry (Meng et al., 2022; Peacock et al., 2022). This shift in protease usage has important implications for transmissibility and tissue tropism, and may also alter sensitivity to host restriction factors that act within endosomal compartments (Meng et al., 2022; Peacock et al., 2022).

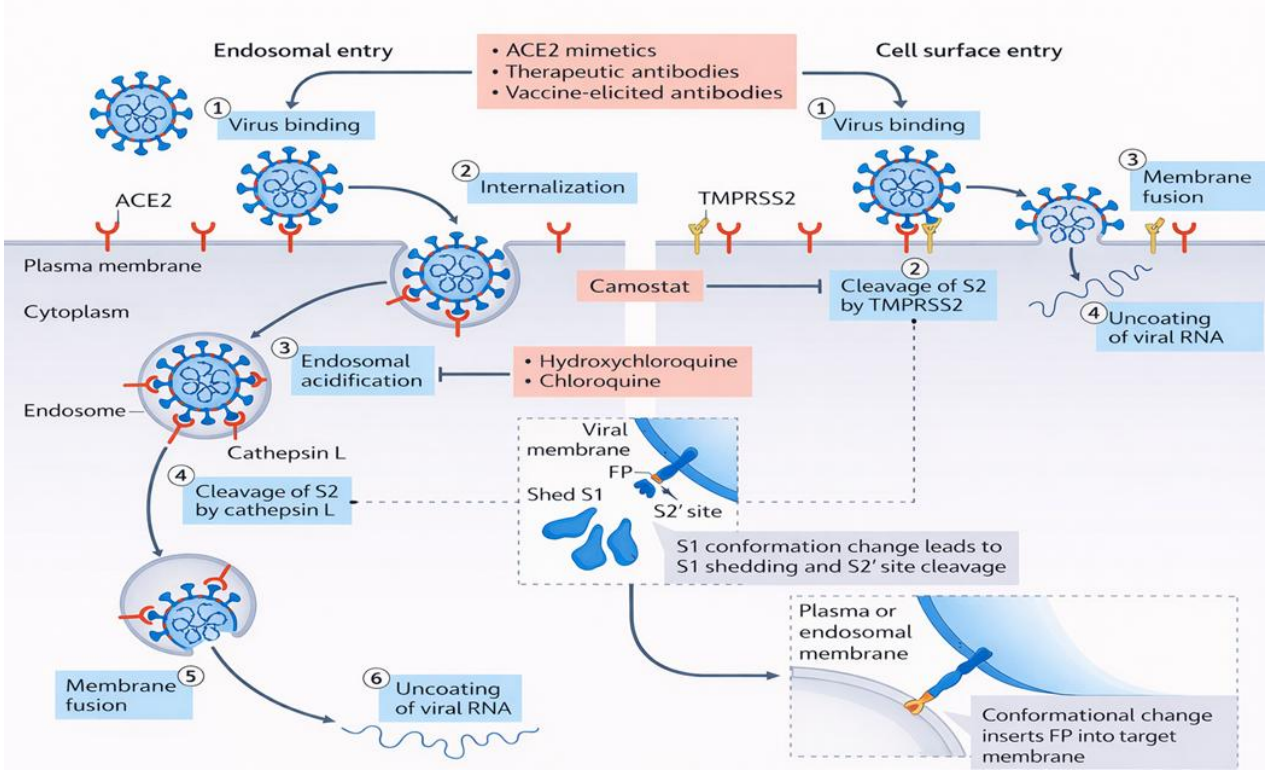

Figure 2: The viral entry of SARS-CoV-2

The entry of SARS-CoV-2 into host cells is a complex, multistep process that plays a crucial role in determining viral infectivity and pathogenicity. Central to this process are two distinct cleavage events of the spike (S) protein: one at the S1/S2 junction and the other at the S2′ site within the S2 subunit. These cleavage events are essential for activating the S protein and enabling membrane fusion between the virus and host cell. In SARS-CoV-2, the S1/S2 site contains a unique polybasic sequence cleaved by host cell proteases during viral maturation. However, the S2′ cleavage occurs only upon the virus binding to the angiotensin-converting enzyme 2 (ACE2) receptor on the surface of target cells. This binding event (Step 1) induces conformational changes in the S1 subunit, exposing the S2′ site for further processing. Cleavage of the S2′ site varies depending on the cellular entry pathway. In cells lacking sufficient expression of TMPRSS2, or where the virus-ACE2 complex does not encounter TMPRSS2, SARS-CoV-2 is internalised via clathrin-mediated endocytosis (Step 2) into endolysosomal compartments. The acidic environment activates cathepsins, which cleave the S2′ site (Steps 3 and 4). Alternatively, in the presence of TMPRSS2, S2′ cleavage occurs directly at the cell surface (Step 2), bypassing endocytosis. In both entry routes, cleavage at the S2′ site leads to exposure of the fusion peptide (FP) and dissociation of the S1 subunit. This triggers extensive conformational rearrangements within the S2 subunit, particularly in the heptad repeat one region, driving insertion of the fusion peptide into the host membrane (Step 5 for the endocytic route; Step 3 for the TMPRSS2-mediated pathway). Fusion of viral and cellular membranes forms a fusion pore through which viral RNA is released into the host cytoplasm, initiating uncoating and replication (Step 6 or Step 4, respectively) (Reproduced with modifications from Jackson et al., 2021).

1.4 The role of TMPRSS2 and cathepsins in SARS-CoV-2 viral entry

Building on the molecular overview described above, the following section explores how these proteases influence variant-specific entry dynamics. Entry of SARS-CoV-2 requires proteolytic activation of the spike protein, which can occur at the cell surface or within endosomal compartments, depending on the host proteases available. TMPRSS2 is a type II transmembrane serine protease that plays a critical role in viral pathogenesis, particularly for influenza viruses and SARS-CoV-2 (Iwata-Yoshikawa et al., 2019). In human airway epithelial cells, TMPRSS2 cleaves influenza haemagglutinin (HA), facilitating viral entry (Iwata-Yoshikawa et al., 2019). Similarly, TMPRSS2 cleaves the SARS-CoV-2 spike protein, a key step that promotes fusion of the viral and host membranes and enables efficient infection (Hoffmann et al., 2020; Mahoney et al., 2021). The importance of TMPRSS2-mediated spike processing is further supported by in vivo evidence: TMPRSS2-knockout mouse models show reduced disease severity and lower mortality after infection with influenza viruses and SARS-CoV-2 (Baby et al., 2025; Irham et al., 2020).

Because TMPRSS2 activity supports cell-surface entry, it has been explored as a therapeutic target. Several studies report that TMPRSS2 active-site inhibitors can reduce infection or disease severity, suggesting a potential strategy for treating both influenza and SARS-CoV-2 infections (Hoffmann et al., 2020; Mahoney et al., 2021; Baby et al., 2025).

In contrast, cathepsins are lysosomal proteases with diverse roles in cellular homeostasis and immune regulation, including protein degradation, antigen presentation, and chemokine processing (Allan & Yates, 2015). They are predominantly active within acidic endosomal and lysosomal compartments, where they contribute to antigen processing, innate immune signalling, and broader immune regulation (Yadati et al., 2020; Zhao et al., 2024). Several cathepsins, particularly cathepsin L, also play a recognised role in SARS-CoV-2 entry. When the virus is internalised by endocytosis, cathepsin L can cleave and activate spike within acidified endosomes, enabling endosomal fusion and release of the viral genome into the cytoplasm (Hoffmann et al., 2020; Shang et al., 2020). This

provides an alternative route of infection when TMPRSS2 expression or activity is limited (Shang et al., 2020).

Clinically, dysregulation of specific cathepsins is associated with diverse phenotypes, including impaired antigen presentation, lysosomal storage pathology, skeletal/connective tissue abnormalities, neurodegeneration, and altered inflammatory regulation (Ketterer et al., 2017). These outcomes reflect the broad physiological roles of cathepsins across tissues and immune pathways (Yadati et al., 2020; Zhao et al., 2024). In the context of SARS-CoV-2 infection, greater reliance on cathepsin-dependent endosomal entry may influence tissue tropism and innate immune activation, particularly in tissues with low TMPRSS2 expression (Shang et al., 2020).

1.5 Brief overview: SARS-CoV-2 replication cycle

Following ACE2 binding and entry, the viral envelope fuses with a host membrane and releases the positive-sense RNA genome into the cytoplasm. Because the genome functions as mRNA, translation begins immediately at the 5′ end to produce the replicase polyproteins. ORF1a is translated into pp1a, and a proportion of ribosomes undergo programmed −1 ribosomal frameshifting at the ORF1a/ORF1b junction to continue translation into ORF1b, generating pp1ab (Bhatt et al., 2021; Kung et al., 2022). These polyproteins are proteolytically processed into non-structural proteins (nsps) that assemble into the replication–transcription complex (RTC) on rearranged intracellular membranes, which supports genome replication and transcription (Kung et al., 2022; V'kovski et al., 2021).

The RTC produces a full-length negative-strand RNA intermediate that serves as a template for new genomic RNA. In parallel, SARS-CoV-2 generates multiple subgenomic mRNAs (sgmRNAs) through discontinuous transcription. During negative-strand synthesis, the polymerase can pause at transcription-regulatory sequences (TRS) upstream of structural/accessory genes and switch templates to the 5′ leader TRS, forming leader–body junctions that yield negative-strand subgenomic templates, which are then copied into positive-strand sgmRNAs (Bentley et al., 2013; Kim et al., 2020; Long et al., 2021). Structural proteins (S, E, M, N) are translated and trafficked through the ER/ERGIC, where genomes packaged by N assemble with membrane proteins, and virions bud into secretory compartments for release by exocytosis (Kung et al., 2022; V'kovski et al., 2021). Because successful initiation of this replication depends on efficient spike-mediated membrane fusion, SARS-CoV-2 entry is strongly influenced by the host proteases that activate the spike.

1.6 SARS-CoV-2 variants (Alpha, Beta, Delta)

The SARS-CoV-2 virus has continually evolved through variants since its emergence, adapting to its environment (Peacock et al., 2021). The World Health Organisation (WHO) has categorised these variants into variants of interest (VOIs) and variants of concern (VOCs) for public awareness, as reported by Flores-Vega et al. (2022). Specifically, the variants of concern (VOCs) include:

Alpha variant (B.1.1.7)

The Alpha variant, designated B.1.1.7, emerged in the UK in late 2020 and quickly spread to multiple countries. This variant is characterised by several mutations in the spike (S) protein, including Y144, H69/V70 deletions and D1118H, T716I, P681H, A570D, N501Y, and S984A mutations (Borges et al., 2022). Notably, the spread of the Alpha variant varied between countries, particularly those closely connected to the UK. A study by Borges et al. (2022) analysed its prevalence in Portugal from late 2020 to early 2021, revealing that spike gene late detection (SGTL) and spike gene target failure (SGTF) could identify the B.1.1.7 lineage.

SGTF occurs when RT-PCR assays fail to amplify the S-gene target due to the H69/V70 deletion, while other viral gene targets (e.g., N or ORF1ab) remain detectable. This pattern emerged as an effective proxy for identifying B.1.1.7 in routine diagnostic settings. SGTL, by contrast, refers to delayed amplification of the S gene compared with other targets, also associated with S-gene mutations characteristic of the variant. Together, these signal disruptions provided an early epidemiological tool for tracking the lineage before widespread genomic sequencing capacity was available.

The variant's proportion was approximately 22% by the third week of 2021 and is expected to increase to 65% by the sixth week. However, effective physical distancing measures in the early weeks of 2021 slowed its rapid spread, keeping SGTL and SGTF rates below 50% by the seventh week (Borges et al., 2022).

Beta variant (B.1.351)

The Beta variant, B.1.351, was first detected in Botswana and South Africa in November 2021 (Tegally et al., 2021). This variant, as reported by the WHO in 2021, had over 35 genetic alterations in the spike protein. Concurrently, an increase in the B.1.1.529 (Omicron) variant was observed in South Africa, later identified as a variant of concern by the WHO. The Beta variant's spike protein features three mutations in the receptor-binding domain (RBD), specifically N501Y, E484K, and K417N, along with five additional alterations including A701V, R246I, D215G, D80A, and L18F (Tegally et al., 2021).

Delta Variant (B.1.617.2)

The Delta variant (B.1.617.2) shares a deletion in the non-coding N Kozak sequence with the Alpha variant and the recently identified Omicron variant (B.1.1.529). A nucleotide substitution at this site (28271A>T) alters the Kozak context immediately upstream of the N start codon, which plays a key role in regulating translation initiation efficiency. In the reference SARS-CoV-2 genome, this position contributes to a moderately strong Kozak consensus, whereas the replacement of adenine with thymine weakens the sequence, making it less similar to the optimal eukaryotic Kozak motif (gccRccAUGG). A weakened Kozak context generally reduces translation initiation (Kozak, 1986; Kozak, 2005), and current analyses indicate that the 28271A>T mutation is likely to decrease N-protein translation in variants carrying this substitution (Finkel et al., 2021). First identified in India in early 2021, the Delta variant rapidly became dominant worldwide (Yang & Shaman, 2021). It differs in the spike protein from the NL-02-2020 strain by mutations T19R, deletions at residues 157 and 158, D950N, E484K, T478K, L452R, R684L, and P681R. Harvey et al. (2021) noted that mutations such as N501Y, E484K, K417T and L18F arose independently in multiple variants through convergent evolution. The competitive advantage of Delta is thought to stem from increased ACE2

binding affinity and reduced antibody neutralisation, with the P681R mutation near the furin cleavage site potentially enhancing spike protein activation (Mlcochova et al., 2021).

1.7 The emergence and characteristics of the omicron variant (BA.1, BA.2, BA.4, BA.5)

The Omicron variant's emergence was unexpected, as it seemingly did not evolve from previously known SARS-CoV-2 variants in circulation, according to Eythorsson et al. (2022). Initially identified in Africa, the exact origin of Omicron remains unclear (Viana et al., 2022; Cele et al., 2022). It is suggested that the ancestral virus might have evolved over a prolonged period in patients with advanced immune suppression, leading to mutations associated with immune escape. Another hypothesis by Wei et al. (2021) proposes that Omicron could have originated in rodent reservoirs or other animals, considering specific unique mutations, Q493R and Q498R, characteristic of mouse adaptations. By early 2022, Omicron had spread to approximately 188 countries and became the dominant strain globally, accounting for 99.7% of sequences reported between February 23 and March 24, 2022 (WHO, 2022). Omicron is divided into several subvariants: BA.1, BA.1.1, BA.2, BA.4, BA.5, with BA.2 forming most cases. The BA.1 variant, often referred to as the original Omicron form, is identified by the S-gene target failure (SGTF), while BA.1.1 is a subvariant of BA.1 with an additional R346K mutation (Backer et al., 2022).

Interestingly, the BA.2 subvariant proportion, which does not exhibit SGTF, is increasing and becoming more prominent in countries like Singapore, Norway, India, and Denmark. This suggests a possible selective advantage over the BA.1 variant (Hodcroft, 2021). In Denmark, studies by Ito et al. (2022) showed that the reproduction number of BA.2 was approximately 1.25 times higher than that of BA.1. Bhattacharyya & Hanage (2022) predicted that the Omicron variant could infect over half of the world's population.

Guo et al. (2022) present a structural overview of the SARS-CoV-2 spike protein mutations found in the Omicron variant based on the SARS-CoV-2 spike protein (PDB: 7CWU_A), illustrated in Figure 3. This visualisation clearly highlights the large number of mutations and their location in the Omicron variant.

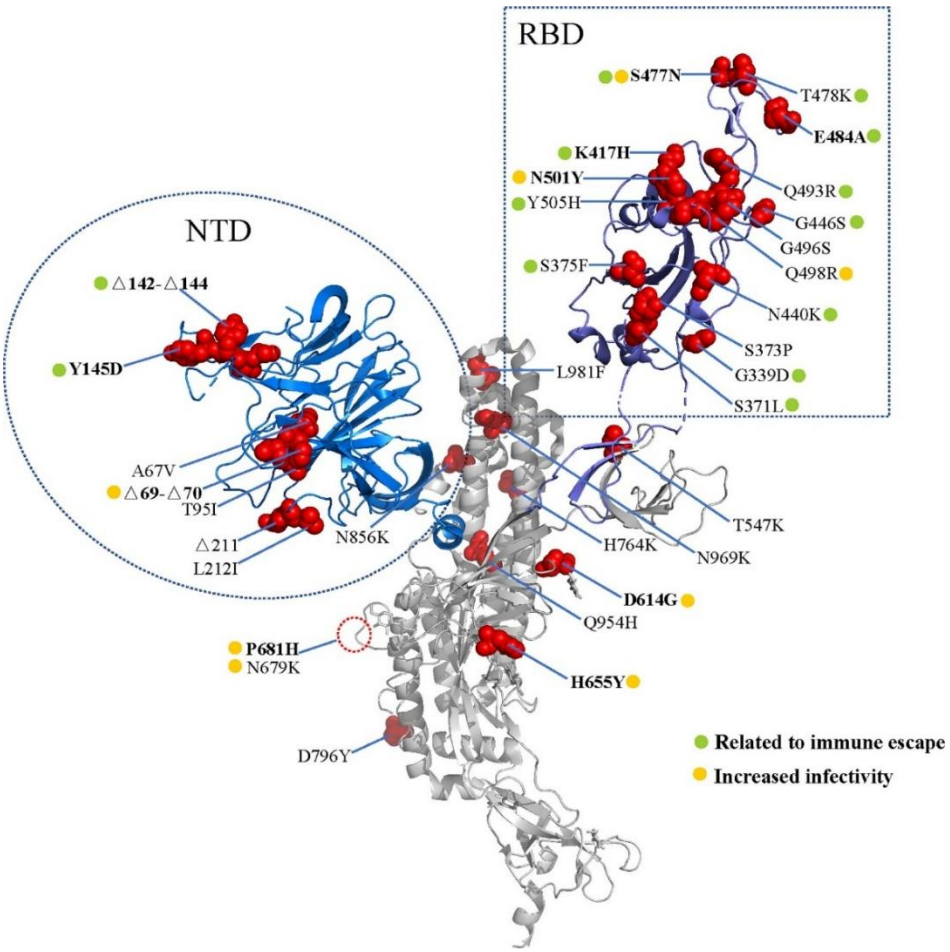

Figure 3: Mutations in the Omicron variant that cause spikes (Reproduced from Guo et al., 2022).

Red spheres highlight the specific mutation sites across the spike protein. The receptor-binding domain (RBD) and the N-terminal domain (NTD) are shown in purple and blue, respectively. Mutations are annotated to indicate their functional significance: green labels denote mutations associated with immune escape, while yellow labels indicate mutations linked to increased infectivity.

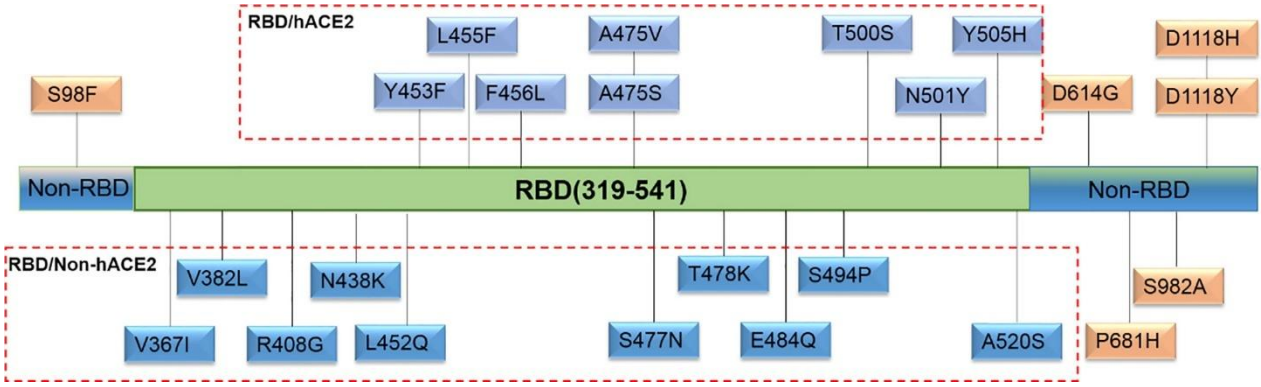

Figure 4: Schematic illustration of spike protein mutation in the SARS-CoV-2 genome.

Reproduced from Ding et al. (2021) analysed 24 S genes, which are spike mutations that occur both naturally and at high frequency from the GISAID database up to March 1, 2021. They identified 8 mutations in the RBD and hACE2 interaction region, 10 in the RBD region without hACE2 interaction, and six outside the RBD. These illustrations of spike protein mutations in the SARS-CoV-2 genome help clearly identify where each mutation occurs and provide insight into their potential functional effects.

1.8 Subtypes of the Omicron variant and their distinct characteristics

Omicron BA.1 and BA.1.1 The BA.1 lineage of the Omicron variant was first identified in Botswana, Africa, on November 11, 2021. Dominating Omicron cases globally in late 2021, BA.1 comprised over 97% of Omicron sequences. BA.1 predominantly utilises endocytosis for cell entry, unlike other variants that rely on cell fusion, and shows limited syncytia formation (fused cells). Notably, this variant has a reduced rate of cleaving the spike protein into its active S1/S2 form and does not depend on the TMPRSS2 protease for infection. The BA.1.1 subvariant and another BA.1.1 variant may be more responsible for the recent surge in cases than the BA.2 variant. A study on Syrian hamsters demonstrated that BA.1.1 infection resulted in less weight loss than the Delta variant and elicited an antibody response less effective against other variants (Mohandas et al., 2022).

Omicron BA.2 was first detected in South Africa on November 17, 2021, and was later identified in the United States in December 2021 (Fonager et al., 2022). Compared to BA.1, BA.2 exhibits a

higher effective reproduction number, increased fusogenicity, and greater pathogenicity. This subvariant also shows resistance to the immune response generated by BA.1 (Yamasoba et al., 2022).

The Omicron subvariants BA.4 and BA.5 were initially identified in late 2021, with BA.4 emerging around mid-December and BA.5 shortly thereafter in early January 2022 (Mühlemann et al., 2023; Wilks et al., 2023). These variants rapidly spread across various regions, notably dominating different epidemiological waves in countries such as Mexico during the fifth COVID-19 wave (Taboada et al., 2023). By March 2023, the European Centre for Disease Prevention and Control (ECDC) de-escalated BA.4 and BA.5 from its list of SARS-CoV-2 variants of concern as their prevalence declined. By early 2022, the variants BQ.1 and XBB also emerged, derived from the Omicron lineage and noted for their respective mutations and characteristics that distinguished them within the evolving SARS-CoV-2 landscape.

Each variant presents unique mutations that influence its infectivity and immune evasion capabilities. BA.4 and BA.5 share several mutations, notably the H69/V70 deletions and RBD substitutions such as L452R and F486V (Mühlemann et al., 2023; Wilks et al., 2023). These adaptations facilitate viral entry into host cells and enhance their ability to evade the immune responses generated by prior infections or vaccinations.

The XBB variant is characterised by mutations associated with increased immune resistance, including the spike N-terminal domain (NTD) deletion Y144del (Tamura et al., 2023). Notably, XBB is a recombinant Omicron lineage that arose from two BA.2-descendant parental lineages (BJ.1 and BM.1.1.1), creating a mosaic genome that combines genetic material from both lineages (Tamura et al., 2023; Scarpa et al., 2023). Recombination mapping indicates that the breakpoint lies within the spike receptor-binding domain (RBD), between genomic positions 22,897 and 22,941 (Wuhan-Hu-1 reference), corresponding to approximately amino acid positions 445–460 in spike, meaning that upstream and downstream segments of the spike gene are derived from different parents (Tamura et

al., 2023). The BQ.1 variant (a BA.5 descendant) similarly carries multiple spike substitutions linked to reduced neutralisation, demonstrating greater escape from neutralising antibodies relative to BA.5 (Tamura et al., 2023; Wang et al., 2023).

1.9 Shift to endosomal entry in Omicron variants

Omicron variants have shifted their preferred entry mechanism from TMPRSS2-mediated surface fusion to endosomal fusion, which does not depend on TMPRSS2 and instead relies on endosomal proteases such as cathepsins (Willett et al., 2022; Zhao et al., 2022). This shift is likely due to the reduced effectiveness of TMPRSS2 inhibitors against Omicron compared with Delta (Willett et al., 2022; Zhao et al., 2022). Importantly, TMPRSS2 expression is heterogeneously distributed along the respiratory tract: transcriptomic profiling indicates TMPRSS2 is expressed in epithelial populations across the nasal passages, conducting airways, and distal lung, including nasal epithelial cells, bronchial secretory/transient secretory and ciliated cell populations, and alveolar epithelial cells (including AT1/AT2) (Lukassen et al., 2020; Muus et al., 2021; Schuler et al., 2021; Sungnak et al., 2020). In contrast, cathepsin-mediated endosomal entry may be favored in tissues or cell types where endosomal proteases predominate; consistent with this, Willett et al. (2022) reported higher TMPRSS2 in lower-airway Calu-3 cells but higher cathepsin-L in primary human nasal epithelial cultures, supporting a protease landscape that can bias entry route and tissue tropism (Willett et al., 2022). Collectively, reduced reliance on TMPRSS2 and greater dependence on cathepsin-driven endosomal fusion may help explain Omicron's enhanced replication in the upper respiratory tract and comparatively reduced propensity for deep-lung infection (Willett et al., 2022; Zhao et al., 2022).

Differences between Omicron and other variants

Recent studies indicate that Omicron spreads faster but may cause less severe disease than the Delta variant. In South Africa, Omicron infections showed an 81% lower hospitalisation likelihood than non-Omicron infections (Wolter et al., 2022). Hospitalisation and mortality rates were significantly

lower during the Omicron wave than the Delta wave (Maslo et al., 2021). In the UK, Omicron infections were associated with a reduced likelihood of emergency care and hospitalisation (UK Health Security Agency, 2021). However, there was an increase in hospitalisations among infants during the Omicron wave (Torjesen, 2022).

Comparing BA.1 and BA.2 in South Africa, Wolter et al. (2022) found it challenging to determine if Omicron is less harmful due to prior immunity and its limited spread among older populations. Laboratory studies indicate that Omicron has lower replication rates in specific cell lines and a reduced infection rate compared to the Wuhan/D614G and Delta strains, suggesting milder symptoms in the lower respiratory tract. Syrian golden hamsters infected with Omicron showed less lung involvement and more pronounced effects in the nasal area than other variants (Sia et al., 2020; McMahan et al., 2022). These findings suggest that while Omicron may cause more infections in the upper respiratory tract, it is potentially less severe in the lower respiratory tract than previous SARS-CoV-2 variants.

Table 1: List of Variants of Concern (VOC) and the de-escalated variants mentioned in this paper (Inspired by GISAID EpiCoV database, WHO label, Pango lineages website, Simões & Rodríguez-Lázaro, 2022)

WHO label	Pango Lineage	Country first detected	Spike mutations of interest	Year and month first detected
Wild type (Wuhan)	Ancestral strain	China	Minimal because it represents the baseline sequence before major mutations emerged.	December 2019
α Alpha	B.1.1.7	United Kingdom	N501Y, D614G, P681H	September 2020
β Beta	B.1.351	South Africa	K417N, E484K, N501Y, D614G, A701V	September 2020
δ Delta	B.1.617.2	India	L452R, T478K, D614G, P681R	December 2020
o Omicron	BA.1	South Africa and Botswana	A67V, Δ69-70, T95I, G142D, Δ143-145, N211I, Δ212, ins215EPE, G339D, S371L, S373P, S375F, K417N, N440K, G446S, S477N, T478K, E484A, Q493R, G496S, Q498R, N501Y, Y505H, T547K, D614G, H655Y, N679K, P681H, N764K, D796Y, N856K, Q954H, N969K, L981F	November 2021
o Omicron	BA.2	South Africa	G142D, N211I, Δ212, V213G, G339D, S371F, S373P, S375F, T376A, D405N, R408S, K417N, N440K, S477N, T478K, E484A, Q493R, Q498R, N501Y, Y505H, D614G, H655Y, N679K, P681H, N764K, D796Y, Q954H, N969K	November 2021
o Omicron	BA.4	South Africa	L452R, F486V, R493Q	January 2022
o Omicron	BA.5	South Africa	L452R, F486V, R493Q	February 2022
o Omicron	BQ.1	n/a	K444T, N460K	n/a
o Omicron	XBB	n/a	N460K, F490S	n/a

1.10 Type I Interferons (IFNs) and their role in innate immunity

Type I interferons (IFNs; IFNα and IFNβ) are crucial mediators of innate immunity, particularly in antiviral defence. Upon secretion, type I IFNs induce hundreds of antiviral genes—collectively termed interferon-stimulated genes (ISGs)—that impede viral replication and enhance host cell antiviral defences (Wong & Chen, 2016; Acchioni et al., 2021). Canonically, IFNα/β binding to the heterodimeric type I IFN receptor (IFNAR1/IFNAR2) activates the associated kinases JAK1 and TYK2, triggering phosphorylation of STAT1 and STAT2. These STATs form the ISGF3 complex with IRF9, translocate to the nucleus, and bind interferon-stimulated response elements (ISREs) to drive ISG transcription and establish an antiviral state (Platanias, 2005; Au-Yeung et al., 2013; Fink & Grandvaux, 2013). Beyond direct antiviral effects, type I IFNs broadly shape innate and adaptive immunity by influencing the activation, migration, differentiation, and survival of immune subsets including T cells, B cells, dendritic cells (DCs), natural killer (NK) cells, monocytes, and macrophages (Le Bon et al., 2002; Ivashkiv & Donlin, 2014; McNab et al., 2015). Their antiviral efficacy is well established in vivo and in vitro (Hoagland et al., 2021; Zhou et al., 2020). For example, in infections with viruses such as Theiler's virus, Semliki Forest virus, vesicular stomatitis virus (VSV), vaccinia virus, and lymphocytic choriomeningitis virus (LCMV), mice lacking the interferon-α/β receptor (IFNAR) exhibit markedly impaired viral clearance (Müller et al., 1994).

Importantly, coronaviruses (CoVs) both trigger and antagonise this cascade at multiple steps. Several CoVs encode proteins that blunt IFN induction (upstream of secretion) and/or block IFNAR signalling (downstream of receptor engagement). In SARS-CoV and SARS-CoV-2, the accessory protein ORF6 potently inhibits type I IFN signalling by preventing phosphorylated STAT1/STAT2 nuclear translocation—thereby suppressing ISG induction even when IFN is present (Frieman et al., 2007; Miorin et al., 2020). In MERS-CoV, ORF4b can inhibit IRF3/IRF7-driven IFN-β production, dampening type I IFN induction and weakening subsequent IFNAR–JAK–STAT amplification (Yang et al., 2015). Collectively, these CoV strategies highlight how evasion of type I IFN induction and

disruption of IFNAR-dependent signalling converge to limit ISG expression, facilitating viral replication and spread despite an otherwise robust innate antiviral programme (Miorin et al., 2020; Yang et al., 2015; Frieman et al., 2007).

Upon viral infection, type I interferons (IFN-α/β) are produced following the recognition of viral RNA by pattern recognition receptors such as RIG-I and MDA5. Secreted IFNs bind to the interferon-α/β receptor (IFNAR) on infected and neighbouring cells, triggering activation of the Janus kinase–signal transducer and activator of transcription (JAK–STAT) pathway. Phosphorylated STAT1 and STAT2 form a complex with interferon regulatory factor 9 (IRF9), collectively known as ISGF3, which translocates to the nucleus to induce the transcription of hundreds of interferon-stimulated genes (ISGs) that establish an antiviral state (Schneider et al., 2014; McNab et al., 2015). Coronaviruses, including SARS-CoV-2, have evolved multiple strategies to antagonise type I IFN signalling, thereby dampening ISG induction and facilitating viral replication and immune evasion (Lei et al., 2020; Sa Ribero et al., 2020).

1.11 IFITM proteins

The interferon-induced transmembrane (IFITM) proteins (IFITM1, IFITM2 and IFITM3) are prominent interferon-stimulated genes (ISGs) that encode small membrane-associated proteins of the CD225/dispanin family and are widely conserved across vertebrates. Functionally, IFITM1/2/3 restrict infection by many enveloped viruses by inhibiting viral entry at an early stage, largely by altering the properties of host membranes at sites of fusion (Brass et al., 2009; Feeley et al., 2011). Their antiviral spectrum is strongly shaped by where they predominantly reside in the cell. IFITM1 is generally maintained at, or cycles through, the plasma membrane and early endocytic membranes, whereas IFITM2 and IFITM3 are more enriched in late endosomes/lysosomes (endolysosomal compartments), consistent with potent inhibition of viruses that require endosomal trafficking and low pH to fuse (Friedlová et al., 2022; Marceau et al., 2024; Yáñez et al., 2020). Mechanistically, this compartmentalisation is actively regulated: IFITM3 contains a canonical AP-2–recognised endocytic sorting motif (often described as a YEML/YxxΦ-type motif) that promotes internalisation and accumulation in endosomal compartments, supporting the idea that correct trafficking is integral to endosomal entry restriction (Friedlová et al., 2022).

IFITM proteins exhibit both constitutive and interferon-inducible expression, with levels varying across cell types and tissues. IFITM1 is predominantly localised to the plasma membrane, positioning it to restrict viral entry occurring at the cell surface, whereas IFITM2 and IFITM3 are primarily associated with endosomal and lysosomal compartments, where they can inhibit endosomal membrane fusion (Perreira et al., 2013; Bailey et al., 2014). Although IFITMs are strongly upregulated following interferon stimulation, basal expression has been reported in several epithelial tissues, including the respiratory tract, suggesting a role in intrinsic immunity even in the absence of overt interferon signalling (Wrensch et al., 2014). This compartment-specific localisation and context-dependent expression contribute to the variant- and pathway-specific effects of IFITMs observed during SARS-CoV-2 infection.

Importantly, IFITM expression is not confined to interferon-exposed states. Although IFITM1/2/3 are strongly induced downstream of interferon signalling, they can also be present at baseline and contribute to intrinsic antiviral readiness. In the original genome-wide functional identification of IFITMs as restriction factors, IFITM1/2/3 were shown to confer basal resistance to influenza A virus while also being inducible by type I and type II IFNs and contributing to interferon's virustatic effects (Brass et al., 2009). In vivo, murine Ifitm3 was reported to be constitutively expressed across multiple respiratory tissues, with induction particularly evident in lower airway epithelium following influenza infection, supporting a model in which parts of the airway maintain a "pre-armed" IFITM barrier that can be further amplified during infection (Bailey et al., 2012). Consistent with this, IFITM3 has also been described as constitutively expressed in human pulmonary endothelial cells, where it contributes to an early block to infection by seasonal influenza viruses (Sun et al., 2016).

Across the body, IFITM1/2/3 are broadly distributed rather than being restricted to a single organ system. Human transcriptomic summaries from the Human Protein Atlas (HPA) categorise IFITM1, IFITM2 and IFITM3 as having "low tissue specificity," consistent with widespread expression across diverse tissues. Nevertheless, abundance can vary by tissue and cellular composition, and strong induction can occur locally in inflamed or infected sites, such as the lower airway epithelium during influenza infection (Bailey et al., 2012). In contrast to the broadly expressed antiviral IFITMs, other family members show more specialised patterns: IFITM10 is described by HPA as "tissue enhanced" (including adrenal gland, bone marrow and retina), whereas IFITM5 (also known as BRIL) is bone-restricted and expressed almost exclusively in osteoblasts, reflecting divergent, non-antiviral specialisation within the IFITM family (Patoine et al., 2017).

1.12 Interaction between SARS-CoV-2 and IFITM proteins

Interferon-induced transmembrane proteins (IFITMs) play a crucial role in the host's defence against viral infections by impacting viral entry pathways. IFITMs exert antiviral effects primarily through the endocytic pathway, affecting viral entry in late endosomal compartments (Xie et al., 2020). These proteins inhibit viral entry by disrupting membrane fusion between the viral envelope and cellular membranes, thereby reducing the production of infectious virions or the infectivity of progeny virions (Zhao et al., 2019). IFITMs have been shown to impede viral entry by increasing cholesterol levels in the endosomal compartment, affecting the physical characteristics of cellular membranes and inhibiting virus-cell membrane fusion (Eckert et al., 2014). The precise molecular mechanisms underlying IFITM inhibition of SARS-CoV-2 viral entry are still under investigation, with studies suggesting that these proteins may influence viral entry by altering membrane fluidity and curvature, either promoting or interfering with the process (Li et al., 2013).

Although they have long been known as antiviral factors that restrict the entry of a broad range of enveloped viruses, emerging evidence has challenged this canonical view, particularly in the context of SARS-CoV-2. A study by Prelli Bozzo et al. (2021) revealed a surprising role for IFITMs, identifying them not as inhibitors but rather as co-factors that facilitate SARS-CoV-2 infection. Specifically, endogenous levels of IFITM2 were found to enhance viral entry into human cells, suggesting that the virus may exploit host IFITMs to improve its infectivity. In contrast, artificial overexpression of IFITM proteins was shown to inhibit infection, highlighting a striking duality in their function.

This is further supported by Nchioua et al. (2022), who demonstrated that IFITM2, when expressed at natural levels, promotes SARS-CoV-2 replication in human lung cells. These findings suggest that rather than being antiviral, IFITMs can be co-opted by SARS-CoV-2 to facilitate viral entry, depending on the expression level.

Xie et al. (2020) further investigated this phenomenon, finding that while overexpressed IFITM proteins inhibit SARS-CoV-2 entry, endogenous IFITM2 and IFITM3 support viral replication. Importantly, their study also indicated that overexpression of IFITMs could downregulate the surface expression of ACE2, the principal receptor for SARS-CoV-2, thereby blocking viral entry. These findings support that SARS-CoV-2 may hijack components of the IFITM-mediated antiviral pathway to enhance its entry efficiency, transforming a classical host defence mechanism into a viral advantage.

Adding further nuance, Shi et al. (2020) showed that the function of IFITM3 is strongly influenced by its subcellular localisation. While IFITM3 restricts viral entry through the endosomal route, it also enhances fusion at the plasma membrane. This opposite action is modulated by the presence of the serine protease TMPRSS2, which can shift the viral entry route and alter the function of IFITM expression. Their findings underscore the complexity of IFITM-virus interactions and highlight the importance of entry pathways in determining the antiviral or proviral roles of IFITMs.

IFITMs inhibit viral entry primarily by altering the biophysical properties of host membranes (e.g., increasing membrane rigidity and modifying lipid organisation), thereby impairing the ability of viral envelope glycoproteins (such as SARS-CoV-2 Spike) to undergo the structural rearrangements required for fusion between the viral envelope and the host membrane (Yu et al., 2015).Collectively, these studies agree on the multifaceted nature of IFITM proteins in SARS-CoV-2 infection; rather than serving solely as restriction factors, IFITMs, particularly IFITM2, could be exploited by the virus under physiological conditions to enhance infectivity. This contrasting role can be influenced by factors such as expression levels, subcellular localisation, and host protease activity.

Collectively, these studies demonstrate that IFITM proteins exert context-dependent effects on SARS-CoV-2 infection. Rather than functioning solely as restriction factors, IFITMs—particularly IFITM2—may be exploited by SARS-CoV-2 under physiological expression conditions to enhance

viral entry and replication. This dual behaviour appears to be influenced by multiple factors, including expression level, subcellular localisation, and host protease usage, all of which vary between cell types and viral variants. Consequently, the precise role of IFITMs during SARS-CoV-2 entry remains unresolved and may differ depending on both viral and host determinants.

1.13 Pseudoviruses

Pseudoviruses are replication-deficient viral particles engineered to express heterologous viral envelope proteins while retaining a non-pathogenic viral core (Xiang et al., 2022; Welch et al., 2016). This design enables the safe study of viral entry processes without the need to handle replication-competent viruses, making pseudoviruses a widely used tool in virology research. In the context of SARS-CoV-2, pseudotyped viruses (PVs) expressing spike proteins from different variants have been extensively employed to investigate viral entry mechanisms, antibody neutralisation, and the efficacy of entry inhibitors (Shang et al., 2020; Tsai et al., 2021).

A major advantage of pseudovirus systems is their favourable biosafety profile. Unlike live SARS-CoV-2, which requires biosafety level 3 (BSL-3) containment, pseudoviruses can typically be generated and handled in BSL-2 laboratories, increasing experimental accessibility and throughput (Nie et al., 2020; Neerukonda et al., 2021). This allows rapid comparative analysis of variant-specific entry properties while minimising risk to laboratory personnel.

Pseudoviruses can be engineered to incorporate reporter genes such as luciferase or green fluorescent protein, enabling quantitative measurement of viral entry efficiency in target cells (Tsai et al., 2021). These systems are particularly well suited for assessing spike-mediated entry across multiple variants and for evaluating how host factors influence early stages of infection.

Despite these advantages, pseudovirus assays model only a single round of viral entry and do not recapitulate later stages of the viral life cycle, including genome replication, immune evasion, and viral egress. Furthermore, differences in spike incorporation, cleavage efficiency, or virion architecture may influence assay outcomes compared with authentic virus (Chen & Zhang, 2021). Consequently, results derived from pseudovirus systems must be interpreted with these limitations in mind and are most informative when used to specifically interrogate entry-related mechanisms.

1.14 Lentiviruses

Lentiviruses are a genus of retroviruses characterised by their ability to integrate genetic material into the host genome, enabling stable and long-term transgene expression (Naldini et al., 1996; Cockrell & Kafri, 2007). Lentiviral vectors, commonly derived from human immunodeficiency virus-1 (HIV-1), have been extensively modified to remove pathogenic elements while retaining efficient gene delivery capabilities, making them valuable tools for both basic research and therapeutic applications (Zufferey et al., 1997; Milone & O'Doherty, 2018).

A key advantage of lentiviral systems is their ability to transduce both dividing and non-dividing cells, allowing broad applicability across diverse cell types, including epithelial and immune cells relevant to SARS-CoV-2 infection (Naldini et al., 1996; Kafri et al., 1997). Lentiviral vectors can also be pseudotyped with envelope proteins such as vesicular stomatitis virus G (VSV-G), enhancing vector stability and expanding cellular tropism (Burns et al., 1993; Morizono & Chen, 2014).

Importantly, laboratory-engineered lentiviral vectors are replication-incompetent and require separate packaging systems for particle production, substantially improving their safety profile and permitting use in BSL-2 facilities (Dull et al., 1998; Cockrell & Kafri, 2007). These properties make lentiviral vectors well suited for controlled overexpression studies, including the manipulation of host restriction factors such as IFITM proteins.

1.15 Research gap

Although IFITM proteins have been extensively studied as antiviral restriction factors, their precise role in SARS-CoV-2 infection remains unclear. Previous studies have reported inconsistent findings on whether IFITMs inhibit or facilitate viral entry, with outcomes varying with expression level, experimental system, and viral strain (Brass et al., 2009; Prelli Bozzo et al., 2021; Nchioua et al., 2022). Much of the existing literature has focused on a limited number of viruses, including influenza A virus and HIV-1, or on early SARS-related coronaviruses, leaving important gaps in understanding their relevance to SARS-CoV-2.

Furthermore, while the role of TMPRSS2 in SARS-CoV-2 entry is well characterised, the contributions of endosomal proteases and their interactions with IFITM proteins—particularly in the context of Omicron and its subvariants—remain incompletely defined (Hoffmann et al., 2020). Given the shift toward endosomal entry observed in Omicron variants, understanding how IFITM proteins influence variant-specific entry pathways is increasingly important.

Therefore, this study aims to investigate the role of IFITM1, IFITM2, and IFITM3 in SARS-CoV-2 entry using PVs systems and lentiviral-mediated gene expression. By comparing early and Omicron SARS-CoV-2 variants, this work seeks to clarify how IFITM proteins modulate viral entry in a variant-dependent manner and to address inconsistencies in the current literature.

1.16 Project Aims

The overall aim of this thesis is to investigate how interferon-induced transmembrane (IFITM) proteins influence SARS-CoV-2 entry, and whether their effects differ between early and later viral variants that preferentially use distinct entry pathways.

Specifically, this thesis addresses the following objectives:

1. To generate and validate a lentiviral system enabling exogenous expression of IFITM1, IFITM2, and IFITM3 in $A549^{ACE2}$ cells, and to quantify relative IFITM transcript expression following transduction.
2. To assess how IFITM1, IFITM2, and IFITM3 expression affects pseudotyped SARS-CoV-2 viral entry across a panel of variants, using luciferase reporter readouts normalised to matched no-IFITM controls.
3. To determine whether variant-specific entry phenotypes are consistent with differential reliance on cell-surface versus endosomal entry routes, by measuring entry in the presence of pathway inhibitors targeting TMPRSS2-dependent entry (camostat mesylate) and endosomal cathepsin-dependent entry (E64d).
4. To integrate the entry and inhibitor data to develop a mechanistic interpretation of how IFITM expression levels may restrict, have no effect, or potentially facilitate SARS-CoV-2 entry depending on variant biology and entry pathway usage.

These aims provide a framework for interpreting how IFITM proteins contribute to SARS-CoV-2 variant entry phenotypes and support future work exploring IFITM localisation and protein-level responses under more physiologically relevant conditions.

CHAPTER TWO: MATERIALS AND METHODS

2.1 Plasmids

The plasmids used in this study included the pCAGGs-gag/pol packaging construct, derived from the human immunodeficiency virus-1 (HIV-1) lentiviral vector (catalogue number: VC101743), and the pCSFLW firefly luciferase expression vector (catalogue number: TR30004). Envelope protein expression plasmids in the pcDNA3.1 backbone comprised VSV-G (Vesicular stomatitis virus glycoprotein G, pantropic envelope protein; catalogue number: RG216583), SARS-CoV-2 spike (catalogue number: VC102557), and spike variants corresponding to Wuhan, Alpha, Beta, Delta, BA.1, BA.2, and BA.4.

Plasmids were retrieved from storage at –20°C, and 50 ng of each plasmid was mixed with 30 µl of competent *E. coli* cells. The mixture was incubated on ice for 30 minutes, followed by heat shock at 42°C for 45 seconds, then immediately returned to ice for 5 minutes. Subsequently, 500 µl of 2×YT broth was added to each tube, which was then incubated on a shaker at 37°C, shaking at 250 rpm for 30 minutes. The transformation mixtures were plated onto 2×YT agar plates containing ampicillin and incubated overnight at 37°C.

The following day, plates were examined for bacterial colony formation. A single, well-isolated colony was picked using a sterile toothpick and inoculated into 3 ml of 2×YT broth supplemented with ampicillin (100 µg/ml). The culture was incubated at 37°C with shaking at 250 rpm for approximately 16 hours.

To prepare glycerol stocks, 0.5 ml of bacterial culture was mixed with 0.5 ml of sterile 50% glycerol solution. These stocks were stored at –80°C. The remaining bacterial cultures were centrifuged at 14,000 rpm for 5 minutes. The supernatant was discarded, and the cell pellet was stored at –20°C until further processing. Plasmid DNA was extracted using Midi and Mini-Prep kits from Jena

Bioscience (Germany) and the GeneJET Plasmid Miniprep Kits #K0481 and #K0482 from Thermo Scientific.

2.2 Cell lines

All tasks that required handling cells were conducted in the Biosafety Level 2 (BSL-2) laboratory following the health and safety guidelines of the University of Essex. Human embryonic kidney cell line 293 (HEK293T), Adenocarcinoma human alveolar basal epithelial cells (A549) stably expressing ACE2 ($A549^{ACE2}$) were used. The cell lines were preserved in liquid nitrogen and then thawed in a 37°C water bath prior to use. They were cultivated at 37°C in a humid environment with 5% CO_2, using different media types as detailed in Table 2.

Table 2: A list of all cell lines used and their respective growth medium. All cell lines were maintained at 37 °C in an incubator with 5% CO_2.

Cell Lines	**Growth media**
HEK293T	Dulbecco's Modified Eagle's medium (DMEM) 10% FBS 2 mM of L-Glutamine 1% of Pen-Strep
$A549^{ACE2}$	Ham's F-12K (Kaighn's) Medium 10% FBS 2 mM of L-Glutamine 1% of Pen-Strep Hygromycin B 200 µg/ml

2.3 Analysis of differential gene expression (RNA-seq analysis)

In this research, we utilised in-house data from human primary airway epithelial cells and immortalised MRC5 cells infected with various SARS-CoV-2 variants: B.1.1.7 (United Kingdom), B.1.351 (South Africa), and B.1.258 (IC19). The infection, RNA isolation, and RNA sequencing process were conducted by colleagues in the Giotis Lab.

The Giotis Lab conducted a study involving RNA-sequencing on human nasal airway epithelial cells infected with human coronaviruses (HCoV). The cells, sourced from Epithelix and representing a

mix from 14 donors, were maintained under specific conditions (5% CO_2, 37°C) and prepared for infection by cleaning with serum-free media. The infection involved exposing the cells to 200 µL of HCoV-229E and -OC43 strains, followed by incubation and washing steps.

RNA was isolated from these cells at 24 and 72 hours using Qiagen's RNeasy Mini Plus kit. Around 1 µg of RNA was utilised for sequencing library construction. Novogene handled the mRNA library preparation and sequencing. The raw sequencing data were analysed using Partek Flow software, focusing on quality control, alignment to the human genome (hg38), and quantification of gene expression. Gene expression analysis was done using the Ensembl Transcripts release 104 v2, with normalisation by the counts per million (CPM) method. Differentially expressed genes were identified using the DESeq2 package, focusing on those with a p-value less than 0.05, false discovery rate less than 0.05, and a fold change of either greater than or equal to 2 or less than or equal to -2.

This approach enables the explicit examination of the IFITM (Interferon-Induced Transmembrane) genes, which are recognised for their role in the body's immune response to viral infections. Through careful analysis of the data, it is possible to ascertain whether there is a notable increase in the expression (overexpression) of these genes following the infection of the cells with HCoV.

2.4 Alignment of protein sequences (phylogenetics)

The amino acid sequences of the S protein from various SARS-CoV-2 were obtained from the NCBI Gene Bank (https://www.ncbi.nlm.nih.gov/gene). These sequences were then aligned using the Clustal Omega tool available through EMBL-EBI (Clustal Omega < Multiple Sequence Alignment < EMBL-EBI). *See Appendix*

2.5 Bioinformatic analysis

Spike protein reference sequences for each SARS-CoV-2 variant (Wuhan, Alpha, Beta, Delta, and Omicron subvariants BA.1, BA.2, BA.4, BA.5, BQ.1, XBB) were retrieved from public databases. (Table 3) These amino acid sequences were analysed with BLASTp (NCBI) for alignment and similarity scoring. BLASTp (Basic Local Alignment Search Tool for proteins) compares protein sequences and identifies regions of similarity, reporting a percentage identity for the alignment. Each variant's spike was BLASTed against all others in a reciprocal manner to generate a full similarity matrix. See Appendix for BLAST/alignment, phylogenetics, and similarity matrices.

Table 3: List of variants used for bioinformatics and their spike protein accession number

VARIANTS	ACCESSION
Wuhan	QHD43416.1.
Beta	WDB12209.1
BQ.1	WEF88212.1
Delta	WDV60773.1
BA.4	UTE11510.1
BA.5	WED51419.1
BA.2	WEF79925.1
BA.2	WDY61995.1
Alpha	UYX70557.1
XBB	WED48949.1

Table 4 : Amino sequence used for Bioinformatics analysis

Name	Gen bank ID/ (NCBI)	Source
IFITM1	NP_003632.4	Giotis Lab
IFITM2	CAG46672.1	Giotis Lab
IFITM3	AFF60354.1	Giotis Lab

2.6 Production of pseudotypes virus (PV)

PVs were generated using HEK293T cells. These cells were sub-cultured in T25 flasks provided by Thermo Fisher Scientific, Waltham, MA, USA, and co-transfected once they reached over 60% confluence. For each flask, the co-transfection involved 700 ng of the p8.91 lentiviral packaging plasmid, 1100 ng of the pCSFLW firefly luciferase reporter plasmid, and 700 ng of the S-protein of interest (such as Wuhan, Alpha, etc.). The transfection complex was prepared using 150 µL of Opti-MEM™ (Thermo Fisher Scientific, Loughborough, UK) and incubated for 5 minutes. Subsequently, FuGENE®-HD (Catalogue number: E2311 Promega, Madison, WI, USA) was added at a FuGENE®-HD to DNA ratio of 3:1.

The transfection complex is then incubated at room temperature for 15 minutes and mixed by flicking the tube. During this incubation period, the DMEM media in the T25 flask are replaced. After the incubation, the transfection complex, which consists of the DNA mix and FuGENE®-HD, is added very slowly to the cells. Subsequently, the cells are returned to the incubator, which is maintained at 37°C and 5% CO_2.

The supernatant containing the PVs was collected from the cells at both 48 hours and 72 hours post-transfection. The supernatants from these two time points were combined and transferred into a 15 ml tube. This mixture was centrifuged at 1000 rpm for 5 minutes. Following this, the supernatant was carefully harvested using sterile 2.5 mL syringes and filtered through a 0.45 µm Acrodisc™ syringe filter with a Supor™ membrane, a product of Pall Life Sciences. The filtered supernatant was then stored at −80 °C for future use.

Table 5: Plasmid/spike protein of different SARS-CoV-2 variants used for PVs and LVs production

Plasmid	**Source**
pB117	Wendy Barclays group-R. Shattock
pVSVG	Wendy Barclays group-R. Shattock
pB1.351(Beta)	Wendy Barclays group-R. Shattock
pBA1 (Omicron 1)	Wendy Barclays group-R. Shattock
pBA2 (Omicron 2)	Wendy Barclays group-R. Shattock
pBA4	Wendy Barclays group-R. Shattock
pWuhan	Wendy Barclays group-R. Shattock
pDelta	Wendy Barclays group-R. Shattock
cathepsin L pCAGGS	Wendy Barclays group-R. Shattock
TMPRSS2 pCAGGS	Wendy Barclays group-R. Shattock
pcDNA3.1(ba5)	Giotis.Lab
pcDNA3.1(xbb)	Giotis.Lab
pcDNA3.1(xq1.1)	Giotis.Lab
Gag pol plasmid for pseudotypes	From Wendy, Barclays Group R. Shattock
pCSLW for pseudotypes	From Wendy, Barclays Group R. Shattock
pRIP Fluc RFP Lentivirus	M Dorner/Shoggins
gag-pol plasmid for lentiviral transduction	M Dorner

2.7 PV titration and luciferase assay/ luminescence

A549 cells engineered to express ACE2 were subcultured in T25 flasks, aiming for a 60-80% confluence at the time of transduction. The PVs supernatant was taken from the -80°C freezer. For the assay, 100 µl of the PVs supernatant stock was added to row A of a Nunc™ MicroWell™ 96-Well, Nunclon Delta-Treated, Flat-Bottom Microplate (Catalogue number: 136101). Serial dilutions were then performed down to row D, which contained 50 µl of complete media. Each dilution was thoroughly mixed by pipetting up and down at least 10 times, with pipette tips changed after each mixing. Although equal volumes of pseudovirus preparations were used across experimental conditions, functional titres were estimated by serial dilution and relative infectivity curves to assess comparative entry efficiency. Each dilution was inoculated with 4×10^4 target cells, seeded in a total volume of 50 µl per well.

After incubating for 48 hours at 37°C with 5% CO_2, the supernatants were carefully aspirated from each well and transferred to a white, non-reflective 96-well plate. A 50 µl mixture of Bright-Glo™ and

PBS was added in a 1:1 ratio in each well. This was followed by a 15-minute incubation, after which the plate was spun down using a plate spinner to mix the Bright-Glo™ with the supernatant thoroughly. Luminescence was measured using Promega's GloMax®-Multi Detection System.

All pseudoviruses (PVs) encode the luciferase reporter gene, which is expressed only after successful entry into the host cells. PV particles lacking viral envelope glycoproteins were used as a negative control to establish baseline background signals in the target cells. PVs transfected with VSVG were used as a positive control. In experiments that included the use of protease inhibitors, such as E-64d at 10 μM and camostat mesylate at concentrations of 50 and 100 μM, cells were pre-incubated with the inhibitor for 2 hours prior to further procedures.

2.8 Generation of IFITM-expressing lentiviral pseudo particles

On the day designated for transfection, the medium was switched to DMEM supplemented with 3% FBS. Lentiviral pseudoviruses were produced by co-transfecting 4×10^5 HEK293T cells, at 33% confluence in 6-well plates, with a specific set of plasmids. This experiment is inspired by Schoggins & Rice (2011). These included pTRIP.CMV.IVSb.ISG.ires.TagRFP proviral DNA (IFITM1, 2 and 3), HIV gag-pol, and Vesicular stomatitis virus glycoprotein (VSV-G), in a ratio of 1:0.8:0.2, respectively. 6 μl of Fugene (Roche) and 100 μl of Optimem (Gibco) were also added to the 2.0 μg of total DNA.

The supernatants were collected 48 hours post-transfection. The cells were washed with PBS, and then PBS was added for imaging using the EVOS system. The media was replaced, and the cells were returned to the incubator for a second harvest at 72 hours.

The supernatants from 48 and 72 hours were pooled and clarified by centrifugation. The 48-hour sample was temporarily stored at -80°C for a day.

The samples were centrifuged at 1000 rpm for 5 minutes to clear them. The clarified supernatant was then treated with 20 mM Hepes (from a 1M stock solution) to stabilise the virus and prevent lysis,

and 4 µg/ml polybrene (from a 50 mg/mL stock) to enhance viral entry into cells. Finally, the prepared pseudoviral stock was stored at -80°C for future use.

2.9 Assessment of camostat mesylate cytotoxicity in A549^{ACE2} cells

On the day designated for cell seeding, A549^{ACE2} cells were harvested from stock cultures using trypsin-EDTA and centrifugation to pellet the cells. Cells were resuspended in complete F-12K medium and counted using an automated counter to ensure accurate seeding density. A total of 1×10^5 cells were seeded in each well of a 12-well tissue culture plate in 1 mL of complete medium. The plates were gently swirled to ensure uniform cell distribution, then incubated overnight at 37°C with 5% CO_2 to allow adherence and achieve approximately 70–80% confluence.

The following day, camostat mesylate (Cat no: HY13512) working solutions were freshly prepared in complete F-12K medium. Serial dilutions ranging from 10 µM to 100 µM were generated, and a vehicle control containing the solvent alone (e.g., DMSO) at the equivalent concentration used in the highest drug condition was included.

Culture media were carefully aspirated from each well, and 3 mL of the respective camostat mesylate dilutions or control media were added in triplicate to the designated wells. The plates were returned to the incubator and maintained at 37°C with 5% CO_2. Treatment durations ranged from 24 to 72 hours, based on experimental design. Cell morphology and viability were monitored periodically using the Incucyte Live-Cell Analysis System to assess potential cytotoxic effects of camostat mesylate exposure across time points.

2.10 Assessment of E64d cytotoxicity in A549^{ACE2} cells

On the day prior to treatment, A549^{ACE2} cells were harvested using trypsin-EDTA, centrifuged, and resuspended in complete DMEM medium. Cells were counted using an automated counter and seeded at a density of 1×10^5 cells per well in 1 mL of complete medium into 12-well tissue culture plates. Plates were gently agitated to ensure uniform distribution and placed in a humidified 37°C incubator with 5% CO_2 for overnight adherence and growth to approximately 70–80% confluence.

On the day of treatment, E64d (a cysteine protease inhibitor) was diluted in complete K12-K medium to prepare working concentrations ranging from 10 μM to 100 μM. A vehicle control group containing the same concentration of DMSO as in the highest E64d condition was included.

Existing media were aspirated carefully to avoid disturbing the adherent monolayer. Then, 3 mL of each E64d dilution or corresponding vehicle control was added to the designated wells in triplicate for each concentration. Plates were returned to the incubator and maintained at 37°C with 5% CO_2 for 24 to 72 hours, as dictated by the experimental timeline.

Live-cell monitoring was performed using the Incucyte imaging system at regular intervals throughout the treatment period. Changes in cell confluence, morphology, and potential cytotoxic effects were recorded and analysed to evaluate the tolerability of E64d at various concentrations.

2.11 Isolating RNA using TRIzol reagent

On the day designated for RNA extraction, $A549^{ACE2}$ cells were lysed directly in their culture vessels using TRIzol Reagent (Thermo Fisher Scientific). A volume of 1 mL TRIzol was applied per 10 cm^2 of surface area, followed by repeated pipetting to ensure thorough cell disruption and nucleoprotein complex dissociation. Lysates were transferred to RNase-free 1.5 mL microcentrifuge tubes. Samples were incubated at room temperature for 5 minutes to facilitate complete dissociation. 0.2 mL of chloroform was added per 1 mL of TRIzol used for phase separation. Tubes were capped securely, shaken vigorously by hand for 15 seconds, and incubated at room temperature for 2–3 minutes. Phase separation was achieved by centrifugation at 12,000 × g for 15 minutes at 4°C.

Post-centrifugation, three distinct layers were observed: a lower red organic phase, an interphase, and a clear aqueous phase containing the RNA. The aqueous layer, comprising approximately 60% of the total volume, was carefully transferred to a fresh RNase-free microcentrifuge tube, taking care to avoid disturbing the interphase.RNA was precipitated by adding 0.5 mL of isopropanol per 1 mL of TRIzol. The mixture was incubated at room temperature for 10 minutes and centrifuged at 12,000 × g for 10 minutes at 4°C. A visible, gel-like RNA pellet formed at the bottom of the tube.

For washing, the supernatant was gently removed, and the pellet was resuspended in 1 mL of 75% ethanol (prepared in RNase-free water) per 1 mL of TRIzol originally used. Samples were briefly vortexed and centrifuged at 7,500 × g for 5 minutes at 4°C. The ethanol was carefully aspirated without disturbing the pellet. The RNA pellet was then air-dried for 5–10 minutes at room temperature, avoiding complete desiccation to facilitate downstream solubilisation. Pellets were dissolved in RNase-free water by pipetting and incubated at 55–60°C for 10 minutes to ensure full resuspension.

RNA yield and purity were determined spectrophotometrically, and RNA integrity was assessed by electrophoresis on a denaturing agarose gel or using a Bioanalyzer system. All steps were performed

using RNase-free reagents and consumables to prevent degradation. Phase lock gel tubes were optionally employed to improve phase separation.

2.12 Reverse transcription of RNA

The RNA isolated was thawed on ice for reverse transcription to generate complementary viral DNA. The QuantiTect Reverse Transcription Kit (QIAGEN) was used following the manufacturer's instructions. For each 100 ng of RNA, 2 µL of Genomic DNA Wipeout Buffer was added, and RNase-free water was used to bring the total volume to 14 µL for the genomic DNA elimination step. This mixture was incubated at 42 °C for 2 minutes, then immediately placed on ice. Next, an RT master mix was prepared, consisting of 1 µl Quantiscript Reverse Transcriptase, 1 µL RT Primer Mix, and 4 µl Quantiscript RT Buffer. A volume of 6 µL of this master mix was added to each RNA sample, resulting in a final volume of 20 µL. Reverse transcription was carried out using the Prime Thermal Cycler by TECHNE by incubating the reaction at 42 °C for 30 minutes, followed by enzyme inactivation at 95 °C for 3 minutes. The resulting cDNA was either used immediately for real-time PCR (RT-PCR) or stored at −20 °C for later use.

2.13 Real-Time Quantitative Reverse Transcription PCR (qRT-PCR)

qRT-PCR was performed using the CFX Opus 96 Real Time PCR system by BIO-RAD, in duplicate reactions in a 96-well plate. cDNA aliquots and primers (as listed in Table 6) were thawed on ice before use. Each reaction mixture consisted of 2 µl of cDNA, 5 µl of PowerUp SYBR Green Master Mix (Applied Biosystems, UK), 0.3 µl of forward primer (10 µM), 0.3 µl of reverse primer (10 µM), and 2.4 µl of nuclease-free water (ddH_2O), resulting in a final volume of 10 µl per well.

After adding the primer mix, a PCR sealing film was applied to the plate, then briefly centrifuged. After the RNA was added, the plate was centrifuged again to ensure proper mixing. The qRT-PCR cycling conditions included initial activation of Uracil-DNA glycosylases (UDG) at 50°C for 2 minutes, followed by polymerase activation at 95°C for 2 minutes. This was followed by 40

amplification cycles consisting of denaturation at 95°C for 15 seconds and annealing at 60°C for 1 minute.

Cycle threshold (Ct) values were obtained and normalised to the mean Ct values of the reference genes GAPDH for each sample. Relative fold changes in gene expression were calculated using the $2^{\wedge-\Delta\Delta Ct}$ method described by Pfaffl (2001), with expression levels compared to those of mock-treated cells. All data are presented as mean values ± standard deviation (SD)

Table 6: Primers used for qRT-PCR

Gene	Forward primer (5'- 3')	Reverse primer (5'-3')	Source
IFITM1	GGG CAT CCT CAT GAC CAT TGG A	GGC TAC TAG TAA CCC CGT TTT TCC TG	Giotis Lab
IFITM2	GTC ACC ATG AAC CAC ATT GTG CAA AC	CCC CCA GCA TAG CCA CTT CC	Giotis Lab
IFITM3	ACC ATG AAT CAC ACT GTC CAA ACC TT	CCA GCA CAG CCA CCT CG	Giotis Lab
GAPDH	CCG CGT GGT GCA TTT GGC CG	CTCCTTGGATGCC ATGTGGAC	Giotis Lab

2.14 Statistical analyses of one-way ANOVA and two-way ANOVA

All statistical analyses were conducted using GraphPad Prism version 10.6.2. Unless otherwise specified, each experiment was performed with at least two to three independent replicates. Data were first assessed for normality, and where appropriate, one-way ANOVA was used to evaluate statistical significance between groups.

2.15 Analysis of RNA-seq data

In this study, in-house data from human primary airway epithelial (HAE) cells infected with various SARS-CoV-2 variants were analysed. The variants used are B.1.258 (IC19), Alpha (B.1.1.7), Beta (B.1.351), Delta (B.1.617.2), BA.1 and BA.5. RNA isolation and sequencing were carried out by

other members of the Giotis Lab. Prior to infection, HAE cultures were washed with serum-free media to remove mucus and debris. Cells were infected with 200 µL of virus-containing supernatant listed above and incubated at 33°C for 1 hour. Following infection, cells were harvested at 24 hours and 72 hours for RNA isolation using the RNeasy Mini Plus kit. Approximately 1 µg of total RNA from each sample was used to construct sequencing libraries. mRNA libraries were prepared using poly-A enrichment, and high-throughput sequencing was performed by Novogene. The resulting raw sequencing data (FASTQ files) were imported into Partek Flow software (v11.0.24.0301) for downstream analysis. Reads were aligned using the STAR aligner, and differential gene expression was calculated using the DESeq2 algorithm.

2.16 Figure production

Figures were prepared using Adobe Photoshop and Procreate. Figure 2 (SARS-CoV-2 viral entry pathway) was redrawn and refined for clarity, and Figure 6 (dendrogram illustrating the emergence of Omicron subvariants from the ancestral strain) was created using these software tools. Figure 5 was created Biorender https://app.biorender.com/

CHAPTER THREE: Results - analysis of SARS-CoV-2 variants, bioinformatics, and the role of camostat mesylate and E64

3.1 Introduction

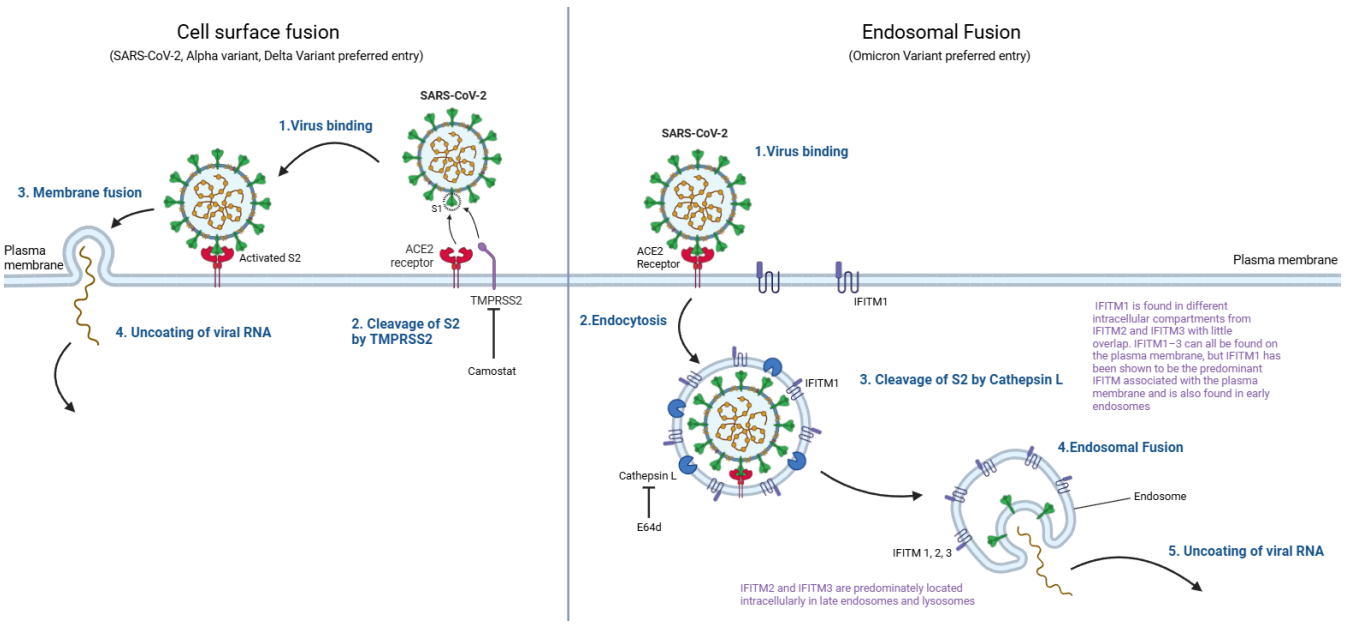

Figure 5: Entry Route of SARS-CoV-2: Involvement of Interferon-Inducible Transmembrane Proteins (IFITMs)

This illustration depicts the entry mechanism of SARS-CoV-2, the virus responsible for COVID-19, focusing on the role of Interferon-Inducible Transmembrane Proteins (IFITMs). The structure is created using Biorender https://app.biorender.com/ to visually summarise the multifaceted viral entry process and the cellular barriers influenced by IFITMs.

The emergence of SARS-CoV-2 variants has necessitated a deeper understanding of their biological behaviour, transmission dynamics, and cellular entry mechanisms. Coronaviruses, including SARS-CoV-2, can utilise multiple entry routes to infect host cells, primarily through either endosomal or plasma membrane pathways (Hoffmann et al., 2020; Jackson et al., 2021) (Figure 5).

The endosomal pathway involves activation of the viral spike protein by endosomal proteases such as cathepsin L (Zhou et al., 2015). However, the plasma membrane pathway relies mainly on serine proteases like TMPRSS2, facilitating more rapid viral entry into host cells and bypassing endocytic

processing (Zhao et al., 2021; Benlarbi et al., 2022). Recent studies have presented evidence suggesting that SARS-CoV-2, particularly the Omicron variant, may favour one pathway. Some investigations indicate that Omicron efficiently utilises the TMPRSS2-mediated plasma membrane entry route (Benlarbi et al., 2022; Siwak et al., 2024), while other findings suggest a reliance on cathepsin-mediated endosomal entry under certain conditions (Shi et al., 2024).

Understanding these divergent entry routes is critical, as this knowledge may inform therapeutic strategies. Two notable protease inhibitors, camostat mesylate and E64D, have been identified for their potential to block SARS-CoV-2 entry via these respective pathways. camostat mesylate is recognised for inhibiting TMPRSS2, thereby preventing spike-mediated fusion at the plasma membrane (McKee et al., 2020; Zhao et al., 2021). E64D, conversely, is known to block cathepsin L and can hinder viral entry through the endosomal route (Zhou et al., 2015; Bakillah et al., 2022). While clinical trials attempting to repurpose these inhibitors for COVID-19 treatment have yielded limited success, they remain invaluable tools in preclinical research focused on understanding viral entry dynamics (Zhao et al., 2021; Sun et al., 2021).

The chapter investigates different SARS-CoV-2 variants using bioinformatics tools to compare spike glycoprotein sequences, assess their similarity and evolutionary relationships, and see how sequence differences influence viral entry and immune evasion. Along with in vitro experiments using spiked PVs to understand how the virus enters and evaluate how well camostat mesylate and E64D can inhibit this process.

3.2 Bioinformatic comparisons of different variants' spike

This analysis aimed to compare the spike glycoprotein sequences of key SARS-CoV-2 variants to quantify their similarity and determine their evolutionary relationships. By examining the amino acid differences among variants, we can assess the molecular changes that the spike protein has undergone from the original Wuhan strain (Wuhan Hu-1) to Variants of Concern (VOCs) such as Alpha, Beta, Delta, and the later Omicron lineages (Li et al., 2020; Nie et al., 2020). This understanding of sequence differences provides vital context for evaluating phenotypic changes related to viral entry and immune evasion strategies employed by these variants.

Table 7: Matrix table of Variants compared based on amino acid (Blastp)

	Wuhan	***Alpha***	***Beta***	***Delta***	***BA.1***	***BA.2***	***BA.4***	***BA.5***	***BQ.1***	***XBB***
Wuhan		*99.21%*	*99.21%*	*99.21%*	*96.94%*	*97.56%*	*97.25%*	*97.25%*	*97.17%*	*96.70%*
Alpha	*99.21%*		*98.74%*	*98.66%*	*97.09%*	*97.25%*	*97.25%*	*97.25%*	*97.17%*	*96.54%*
Beta	*99.21%*	*98.74%*		*98.59%*	*96.71%*	*97.33%*	*97.01%*	*97.01%*	*96.94%*	*96.47%*
Delta	*99.21%*	*98.66%*	*98.59%*		*96.55%*	*97.25%*	*97.09%*	*97.09%*	*97.01%*	*96.39%*
BA.1	*96.94%*	*97.09%*	*96.71%*	*96.55%*		*97.88%*	*97.72%*	*97.72%*	*97.64%*	*97.10%*
BA.2	*97.56%*	*97.25%*	*97.33%*	*97.25%*	*97.88%*		*99.53%*	*99.53%*	*99.45%*	*98.82%*
BA.4	*97.25%*	*97.25%*	*97.01%*	*97.09%*	*97.72%*	*99.53%*		*99.84%*	*99.76%*	*98.58%*
BA.5	*97.25%*	*97.25%*	*97.01%*	*97.09%*	*97.72%*	*99.53%*	*99.84%*		*99.76%*	*98.58%*
BQ.1	*97.17%*	*97.17%*	*96.94%*	*97.01%*	*97.64%*	*99.45%*	*99.76%*	*99.76%*		*98.66%*
XBB	*96.70%*	*96.54%*	*96.47%*	*96.39%*	*97.10%*	*98.82%*	*98.58%*	*98.58%*	*98.66%*	

Research has indicated that specific mutations in the spike protein can significantly influence viral infectivity and the virus's ability to evade immune responses (Nie et al., 2020; Starr et al., 2020). For example, key substitution in the spike protein's receptor-binding domain (RBD) can enhance binding affinity to the ACE2 receptor, thus facilitating greater entry efficiency (Chaintoutis et al., 2021). Furthermore, the evolutionary trajectory of SARS-CoV-2 variants has been documented through phylogenetic analyses, illustrating how these mutations correlate with the global spread of the virus and the emergence of distinct lineages (Li et al., 2022).

Spike protein reference sequences for each SARS-CoV-2 variant (Wuhan, Alpha, Beta, Delta, and Omicron subvariants BA.1, BA.2, BA.4, BA.5, BQ.1, XBB) were retrieved from public databases. These amino acid sequences were analysed with BLASTp (NCBI) for alignment and similarity scoring. BLASTp (Basic Local Alignment Search Tool for proteins) compares protein sequences and identifies regions of similarity, reporting a per cent identity value for the alignment. Each variant's spike was BLASTed against all others in a reciprocal manner to generate a full similarity matrix (Table 7). This approach provided a quantitative measure of how similar each spike protein is to every other. In addition, multiple sequence alignment was performed using tools like Clustal Omega to align all spike sequences simultaneously (See Appendix).

Such comparisons allow researchers to determine conserved regions that may be critical for protein functionality, interactions, and resistance to various pressures, such as viral infections or mutations. By identifying these conserved sequences, we can infer similarities and differences that may relate to protein behaviour, pathogenicity, and environmental adaptability.

In conclusion, integrating amino acid sequence comparisons through software tools such as BLASTp enables researchers to delve deeper into the evolutionary implications of protein variants. By focusing on crucial areas like the spike protein, the assessment provides critical insights into the

functional consequences of genetic variations, which are essential for informed decisions in medical and biotechnological applications.

The aligned sequences were used to construct a phylogenetic tree (dendrogram) (Figure 7) where the branch lengths reflect the percentage amino acid differences based on Table 7. This provides a clear view of evolutionary relationships among the variants used in this study. And to compare with the existing dendrogram (adapted) from the CDC (Figure 6)

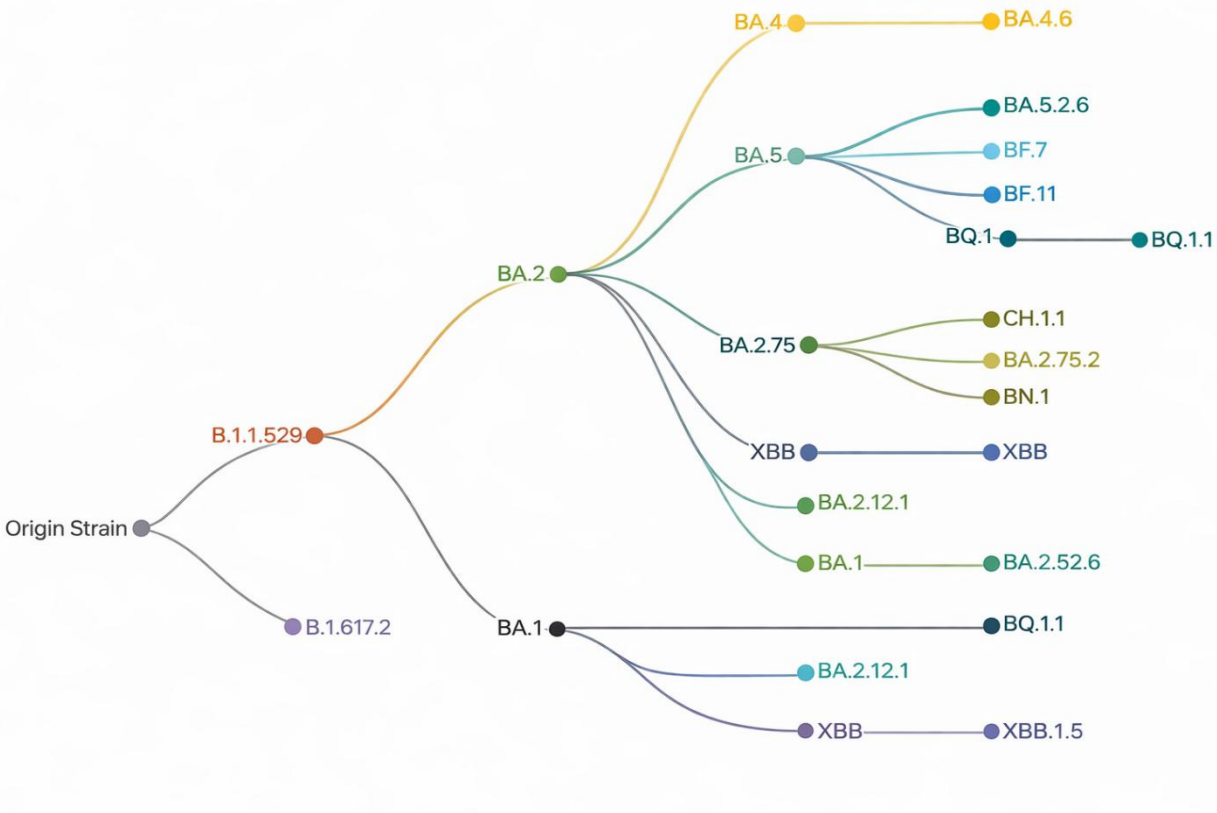

Figure 6: Dendrogram showing how omicron subvariants emerged from the original strain

Schematic representation of the evolutionary progression of SARS-CoV-2 variants from the ancestral origin strain. Early lineages (B.1.1.529 and B.1.617.2) give rise to the Omicron lineage (BA.1 and BA.2), from which multiple sublineages emerged, including BA.4, BA.5, BA.2.75, BA.2.12.1, XBB, and their respective descendants (e.g., BA.4.6, BF.7, BF.11, BQ.1.1, CH.1.1, BN.1, and XBB.1.5). Branches illustrate evolutionary divergence, and colours differentiate distinct lineages and sublineages for clarity. Figure adapted and inspired by materials from the Centres for Disease Control and Prevention (CDC).

3.3 Phylogenetic relationships

A phylogenetic dendrogram based on the spike protein alignments was constructed to visualise the relationships implied by the sequence similarities (Figure 7).

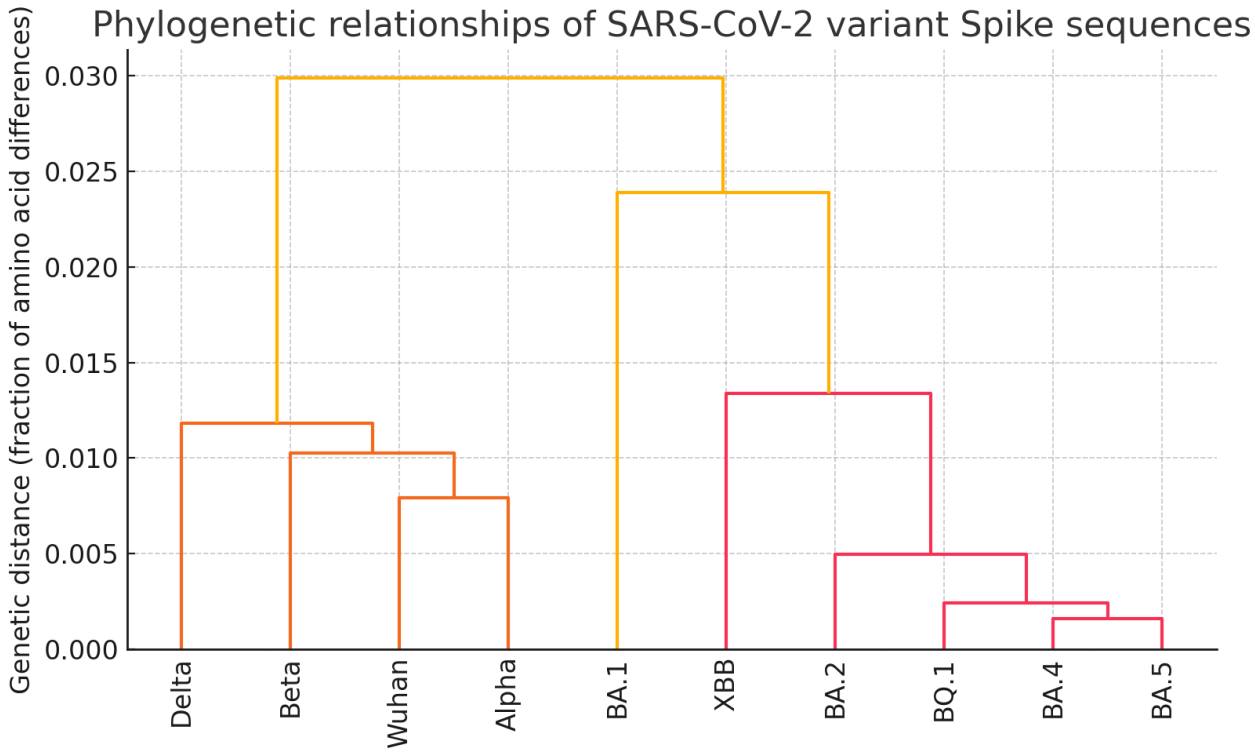

Figure 7: Phylogenetic dendrogram of SARS-CoV-2 variant Spike sequences.

Dendrogram showing clustering of spike protein sequences from Wuhan, Alpha, Beta, Delta, BA.1, BA.2, BA.4, BA.5, BQ.1, and XBB. Branch lengths represent genetic distance (fraction of amino-acid differences), with shorter distances indicating greater sequence similarity.

The tree clusters variants by genetic distance (percentage of amino acid differences in spike). It illustrates two well-separated groups: the early variants (original Wuhan, Alpha, Beta, Delta) versus the Omicron-era variants. The four early variants cluster tightly together (left side of Figure 7 with short branch lengths), reflecting their high spike similarity (only ~1% divergence). In contrast, all Omicron-related variants form a distinct branch apart from those earlier variants, consistent with Omicron's status as a divergent VOC. BA.1 is seen branching off earlier (longer orange branch),

indicating it is genetically distinct from BA.2 and its descendants. This matches the lower percent identities observed between BA.1 and other Omicron subvariants (97.1–97.88%).

Within the Omicron clade (right side of Figure 7), the BA.2-derived subvariants (BA.2, BA.4, BA.5, BQ.1, XBB) group extremely closely, with minimal branch lengths separating them. This indicates that BA.4, BA.5, BQ.1, and XBB share a very recent common ancestor with BA.2 – indeed, BA.4 and BA.5 are so close that they appear almost as a single node, in line with reports that their spike genes are identical or differ by only a couple residues. The subvariant BQ.1 clusters with BA.5, reinforcing that BQ.1 evolved from the BA.5 lineage. XBB also clusters within the BA.2/BA.5 group, though at a slightly longer branch, which is expected given XBB's recombinant origin (combining two BA.2 sub-lineages).

In summary, the phylogenetic analysis suggests that while Alpha, Beta, and Delta all stem from the primary Wuhan lineage with incremental changes, the Omicron variants represent a highly divergent lineage. All Omicron subvariants share a common ancestor distinct from the earlier VOCs, with BA.1 splitting off first and the BA.2-derived cluster (including BA.4/5, BQ.1, XBB) evolving later. This evolutionary trajectory, inferred from spike protein sequences, aligns with the epidemiological emergence of Omicron sub-lineages in late 2021 and 2022. The clear separation between Omicron and pre-Omicron variants in the tree underscores the substantial genetic evolution of Omicron variants. Such phylogenetic insights provide a framework for interpreting differences in virus behaviour. For example, a more divergent spike (as seen in Omicron) can entail altered receptor binding or antibody evasion, topics further explored in subsequent experiments. The sequence-based relationships established here form the foundation for understanding how these variants might differ in functional assays and susceptibility to host factors.

3.4 Detection of luciferase activity of spiked PVs entry in A549^{ACE2}.

To investigate the efficiency of viral entry of different SARS-CoV-2 variants into A549 lung cells modified to express the ACE2 receptor, it is crucial to understand the role of ACE2 in viral entry and the comparative infectivity of the tested variants. The ACE2 receptor serves as the primary entry point for SARS-CoV-2 into human cells (Harvey et al., 2021). This study utilised spike-pseudotyped lentiviruses (LVs), each bearing the spike glycoprotein of a single SARS-CoV-2 variant (Wuhan, Alpha, Beta, Delta, BA.1, BA.2, BA.4, BA.5, XBB, and BQ.1), alongside a negative control (Δ-env) lacking envelope glycoproteins. The vesicular stomatitis virus glycoprotein (VSV-G) was included as a positive control due to its well-established high entry efficiency in viral transduction assays (Muik et al., 2022).

Prior to performing the comparative entry assays, each pseudovirus stock was functionally titrated on A549^{ACE2} cells to ensure that comparable viral inputs were used. A fixed starting volume of each PV stock was serially diluted across a 96-well plate containing equal numbers of A549^{ACE2} cells. After 48 hours, luciferase activity was measured using Bright-Glo substrate and a plate luminometer, yielding relative light unit (RLU) readings proportional to successful viral entry and reporter expression. Titres were expressed as RLU per millilitre (log10), and the dilution producing a robust signal within the linear range of detection was selected as the working input for each pseudovirus. This titration ensured that subsequent entry assays compared functionally equivalent infection levels across different spike variants, rather than equal raw volumes of virus stock.

Relative Luminescence Units (RLU) provide a quantitative measure of luminescence output and are widely used in virological and biochemical assays. An increase in RLU for a given pseudovirus indicates enhanced viral entry efficiency, which may reflect a greater ability of the spike protein to mediate attachment or fusion with host cell membranes. The negative control served as a baseline for comparison with other variants. Data presented in Figure 8 demonstrate that the Delta variant ($p < 0.0001$) and Beta exhibited significantly higher RLU values than the negative control, suggesting

enhanced entry capability into $A549^{ACE2}$ cells. Among the Omicron subvariants, BA.1 displayed the lowest entry efficiency, whereas BA.2 and BA.4 showed a modest increase, suggesting subtle improvements in their ability to engage ACE2 or facilitate membrane fusion. The VSV-G positive control produced the highest RLU, validating the dynamic range and sensitivity of the assay ($p < 0.0001$).

While this titration-based normalisation provides functional comparability, it has inherent limitations. The luciferase signal reflects successful viral transduction rather than absolute particle number; therefore, equivalent RLU does not necessarily indicate equal numbers of virions or identical spike incorporation. Moreover, the luciferase readout integrates multiple post-entry processes, such as reverse transcription, integration, and reporter gene expression, so it cannot exclusively represent membrane fusion or entry. Biological differences between spike variants may also influence the kinetics of these downstream events, complicating the interpretation of RLU as a strict measure of entry efficiency.

To address these limitations and strengthen data interpretation, future experiments could complement luciferase-based titration with physical quantification of viral input, such as measurement of capsid protein p24 by ELISA, reverse transcriptase activity assays, or quantification of viral genomes by RT-qPCR. Verification of spike incorporation into pseudovirions through Western blotting would further control for production variability. Additionally, incorporating an entry-proximal assay (e.g., BlaM-Vpr–based fusion assay or early reverse transcription product detection) would help isolate the entry step from later replication events. Together, these refinements would enable more definitive conclusions regarding the true differences in entry efficiency among SARS-CoV-2 variants.

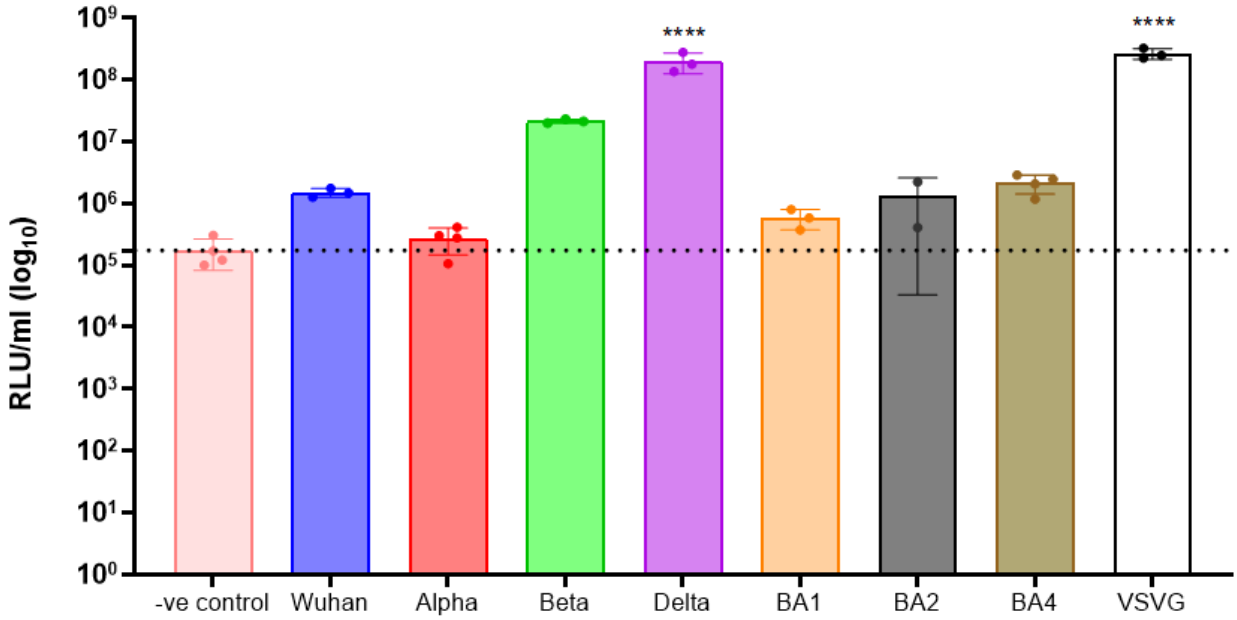

Figure 8: Detection of luciferase activity of spiked PVs entry in A549ACE2

*Cells were transduced with spike-pseudotyped lentiviral particles bearing SARS-CoV-2 variants (Wuhan, Alpha, Beta, Delta) and Omicron subvariants (BA.1, BA.2, BA.4), alongside a VSV-G–PV used as a positive control. Viral entry was quantified by measuring relative luminescence units per millilitre (RLU/ml) and is presented on a logarithmic scale (log_{10}). Data represent the mean ± standard deviation (SD) from n = 4 independent experiments. All spike-PVs demonstrated the ability to enter cells, with the Delta variant showing significantly higher entry efficiency compared to the negative control. Statistical significance was assessed using one-way ANOVA followed by Dunnett's multiple comparisons test (**** $P < 0.0001$, compared with -ve control). Omicron subvariants exhibited variable entry efficiencies, with BA.4 showing lower entry than BA.2 but higher entry than BA.1 under these experimental conditions. The VSV-PV showed the highest entry efficiency.*

3.5 Assessing the cell toxicity of camostat mesylate

After confirming that my viral entry assays using pseudotypes were functional across different SARS-CoV-2 variants, the next crucial step was to evaluate the cytotoxicity of camostat mesylate, the serine protease inhibitor used in my experiments. Understanding the impact of camostat mesylate on cell viability was essential to ensure that any observed effects on viral entry were not due to toxicity but rather its intended inhibition mechanism.

To evaluate the cytotoxicity of camostat mesylate, a cell viability assay was performed using the Incucyte live-cell imaging system. Cells were treated with a range of camostat mesylate

concentrations (10 µM, 25 µM, 50 µM, and 100 µM), along with a control of DMSO at a concentration equivalent to that present in the 100 µM camostat mesylate treatment condition.

As illustrated in Figure 9, treatment with lower camostat mesylate concentrations (10 µM and 25 µM) did not exhibit any observable cytotoxic effects. Cell confluence in these conditions increased rapidly, reaching approximately 100%, and remained stable over the 72-hour observation period. These results were comparable to those observed in the DMSO control group, indicating that low concentrations of camostat mesylate do not impair cell proliferation or viability.

However, increasing concentrations revealed a dose-dependent cytotoxic effect. While 50 µM demonstrated a slower initial increase in cellular confluence compared to lower doses, cells still reached around 95% confluence by 36 hours and maintained stability thereafter. This indicated acceptable toxicity levels that would not interfere with viral entry measurements. In contrast, 100 µM showed marked cytotoxicity, with confluence remaining below 80% and increasing only gradually over time.

To guide my selection of camostat mesylate concentrations for subsequent viral entry experiments, I consulted relevant literature that used camostat mesylate in similar cellular contexts involving SARS-CoV-2. Chang et al. (2022) demonstrated that camostat mesylate significantly inhibited SARS-CoV-2 infection without causing cell toxicity and that the half maximal inhibitory concentration (IC_{50}) for ACE2plusC3 cells was 59.98 µM. On the other hand. Li et al. (2022) used 10 µM, where the cell viability was close to 100%, and the higher concentration reduced it slightly for A549-A cells. Based on these findings, and that 75 µM and 100 µM did not reach 100% in my experiment, they were excluded from the selection. I chose to proceed with 50 µM camostat mesylate. This concentration offered an optimal balance: it was high enough to ensure robust protease inhibition without introducing significant cytotoxicity that could confound viral entry results.

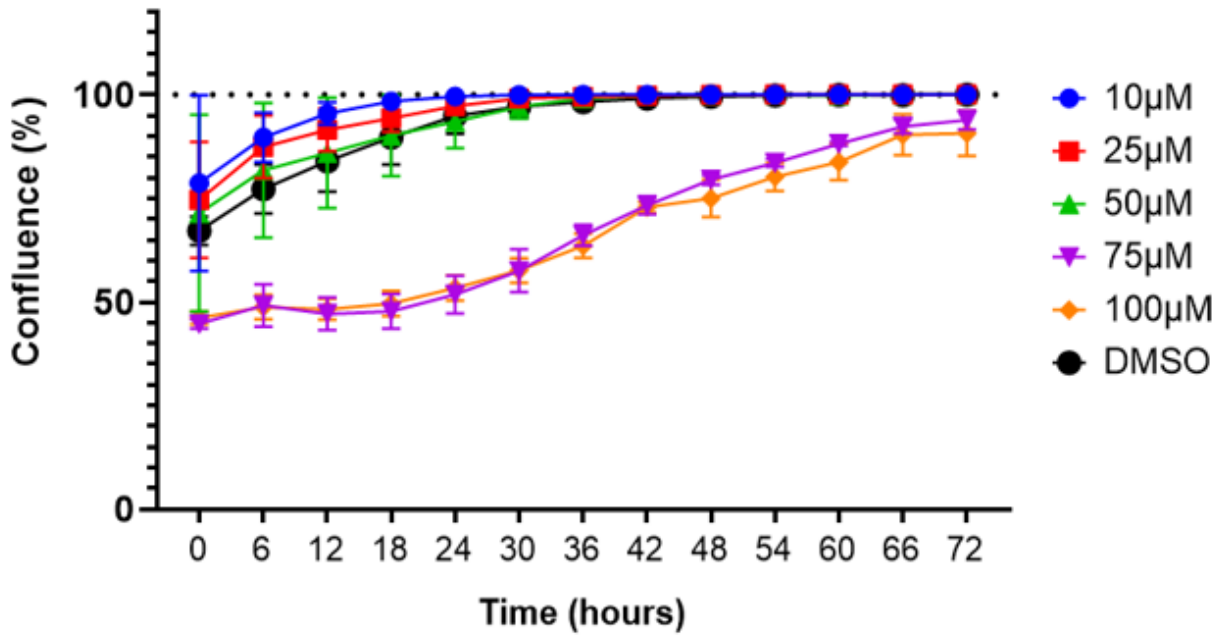

Figure 9: camostat mesylate cytotoxicity effects on A549ACE2 cell confluence over 72 hours

Cells were treated with increasing concentrations of camostat mesylate *(10 µM, 25 µM, 50 µM, and 100 µM) or DMSO as a vehicle control (equivalent to the DMSO content in the 100 µM* camostat mesylate *condition). Cell confluence was monitored in real-time using the Incucyte live-cell imaging system over 72 hours. The y-axis represents confluence, which is the percentage of the surface area of the well covered by live, adherent cells. A higher confluence value indicates greater cell viability and proliferation. Data are presented as the mean ± standard deviation (SD) from n = 2 independent experiments. Treatment with 10 µM and 25 µM* camostat mesylate *did not significantly impair cell proliferation, with confluence rapidly reaching near 100% and plateauing similarly to the DMSO control. In contrast, higher concentrations (50 µM and 100 µM) showed a dose-dependent reduction in cell confluence, indicative of potential cytotoxic effects.*

3.6 Protease inhibitors, such as camostat mesylate, reduce the cell entry of early variants of SARS-CoV-2

In my investigation of the role of TMPRSS2 in the cellular entry of SARS-CoV-2, I utilised $A549^{ACE2}$ cells treated with camostat mesylate, a well-characterised serine protease inhibitor. This treatment inhibits TMPRSS2 activity, which is required for cleavage of the viral spike protein and facilitates entry via the cell-surface fusion pathway (Hoffmann et al., 2020). The Wuhan strain was used as a reference variant to assess the inhibitory efficacy of camostat mesylate, as it represents one of the earliest circulating SARS-CoV-2 strains (Jocher et al., 2022). Viral entry was quantified using luciferase activity and expressed as relative luminescence units (RLU%). All values were normalised to the untreated control condition for each pseudovirus, which was set to 100%.

My experimental results (Figure 10) showed that the Wuhan strain, as well as the Beta and Delta variants, exhibited significant inhibition following camostat mesylate treatment. The magnitude of inhibition observed for these variants is consistent with previous reports, indicating their reliance on TMPRSS2-mediated entry (Gunst et al., 2021).

In contrast, when assessing Omicron subvariants BA.2, BA.4, and BA.5 ($P < 0.0001$), a marked reduction in inhibition was observed. Notably, camostat mesylate treatment was associated with a relative increase in measured viral entry for these subvariants compared with untreated conditions. This indicates that blocking TMPRSS2 activity does not restrict entry of these variants and that entry is enhanced under TMPRSS2-inhibited conditions.

This pattern was consistent across all Omicron subvariants tested and contrasts with the inhibition profile observed for earlier variants. Collectively, these results demonstrate that while camostat mesylate effectively reduces entry of early SARS-CoV-2 variants, it does not inhibit, and is associated with increased entry of, Omicron subvariants BA.2–BA.5 in $A549^{ACE2}$ cells.

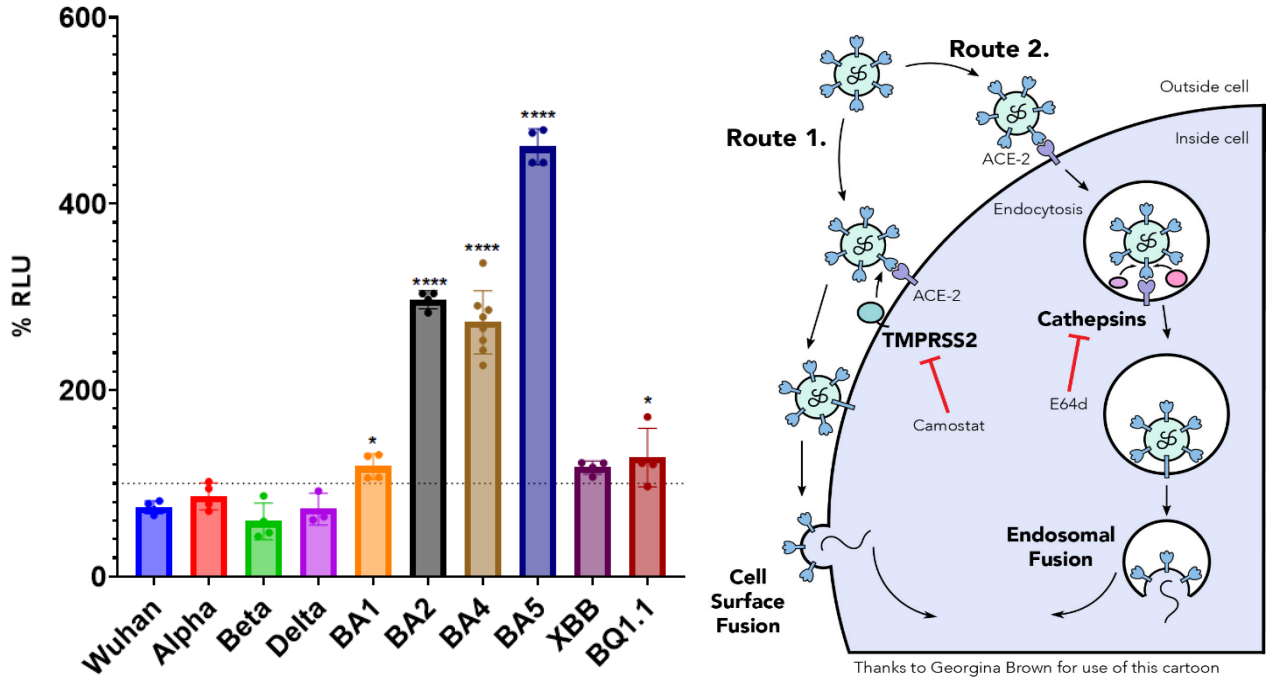

Figure 10: Efficacy of camostat mesylate (50 µM) in inhibiting SARS-CoV-2 variant entry into A549^{ACE2} cells.

The inhibitory effect of camostat mesylate (50 µM) on the entry of various SARS-CoV-2 variants was assessed in A549 cells overexpressing ACE2. Viral entry was quantified using a luciferase-based pseudovirus assay, and results are presented as relative light units (RLU), normalised to untreated controls. The tested variants include the original Wuhan strain and major variants of concern: Alpha, Beta, Delta, BA.1, BA.2, BA.4, BA.5, XBB, and BQ.1.1. Data are presented as the mean ± standard deviation (SD) from n = 3 independent experiments. One-way ANOVA, Dunnett's multiple comparisons test was performed to measure statistical significance (=P<0.05, **** = P <0.0001) between Wuhan and BA.1, BA.2 and BA.5*

3.7 Assessing the cell toxicity of E64d

Next, I proceeded to evaluate the cytotoxicity of E64d, an inhibitor that plays a crucial role in blocking endosomal protease activity (Bestle et al., 2020). It was imperative to ensure that E64d was well-tolerated by the $A549^{ACE2}$ cells to avoid confounding effects of cytotoxicity on the experimental outcomes. $A549^{ACE2}$ cells were treated with escalating concentrations of E64d (10 μM, 25 μM, 50 μM, 75 μM, and 100 μM), alongside DMSO as a vehicle control (equivalent to the DMSO content in the 100 μM E64d condition, and cellular confluence was monitored over 72 hours using the IncuCyte live-cell imaging system (Figure 11).

The data revealed that at all concentrations (10 μM, 25 μM, 50 μM, 75 μM, and 100 μM), cells exhibited high viability, effectively reaching and maintaining nearly 100% confluence. DMSO was used as the vehicle control. Although cells treated with DMSO showed a slower initial increase in confluence compared to other conditions, they still reached 100% confluence by 54 hours. This indicates that E64d, at concentrations up to 100 μM, does not impair cell growth or exhibit cytotoxicity in the cell line used. Therefore, it is unlikely to interfere with future experiments involving this cell line.

To determine an appropriate concentration of E64d for subsequent viral entry assays, I reviewed existing literature involving similar experiments involving SARS-CoV-2 pseudovirus. Although no studies were found that specifically used $A549^{ACE2}$ cells, relevant insights were drawn from related models. For instance, Ou et al. (2020) employed 30 μM E64d in HEK293/hACE2 cells, while Zhao et al. (2021) used 20 μM in Huh7 cells. Taking these findings into account, I set out to use a conservative concentration of 10 μM E64d for all forthcoming experiments. This dosage was chosen to ensure minimal cytotoxicity or any potential adverse effects on cell viability.

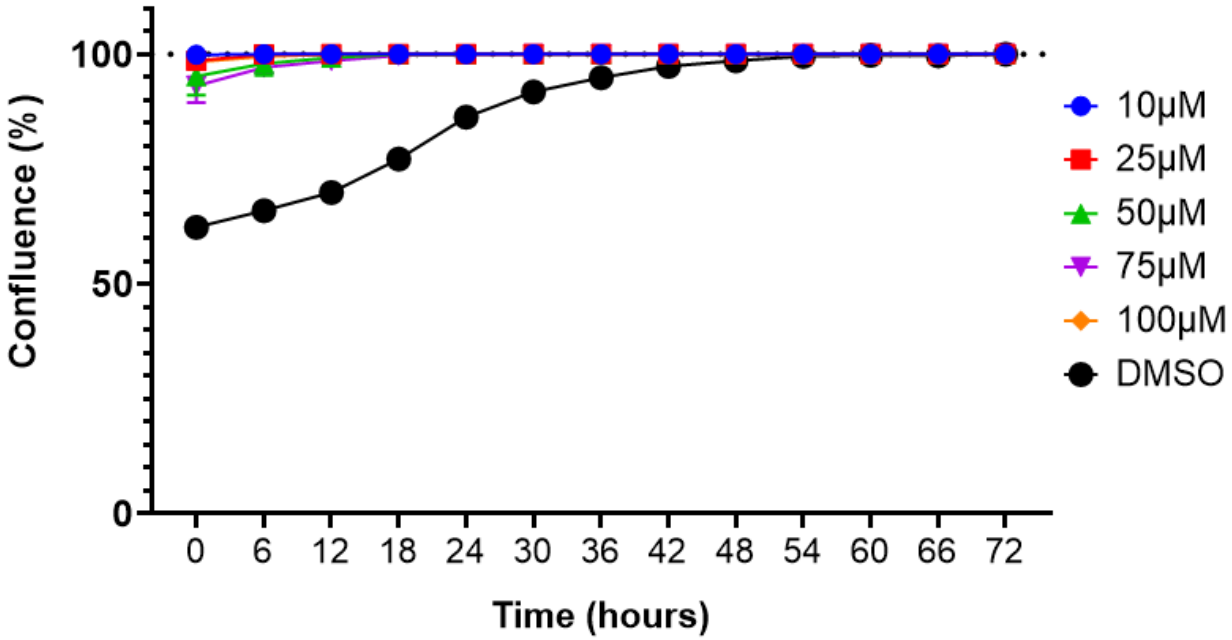

Figure 11: Cytotoxicity evaluation of E64d in A549^{ACE2} cells.

A549^{ACE2} *cells were treated with various concentrations of E64d (10, 25, 50, 75, and 100 μM) and DMSO (control) for 72 hours. Cell viability was monitored using the IncuCyte live-cell imaging system, and confluence percentages were recorded over time. The y-axis represents confluence, the percentage of the surface area of the well covered by live, adherent cells. A higher confluence value indicates greater cell viability and proliferation. Data are presented as the mean ± standard deviation (SD) from n = 3 independent biological replicates.*

3.8 Protease inhibitors E64d reduce the cell entry of Omicron variants of SARS-CoV-2

To investigate the role of cathepsin L in SARS-CoV-2 entry, we treated A549 cells overexpressing the ACE2 receptor with 10 μM Aloxistatin (E64d), a broad-spectrum cysteine protease inhibitor known for its efficacy in blocking cathepsin L within the endosomal entry pathway (Curreli et al., 2020; Padmanabhan et al., 2020). This route is critical for viral entry, as cathepsins facilitate cleavage and activation of the spike protein, enabling fusion between the viral envelope and host cell membrane (Glowacka et al., 2011; Padmanabhan et al., 2020).

I employed pseudoviruses (PVs) expressing the spike (S) protein from various SARS-CoV-2 variants, alongside vesicular stomatitis virus glycoprotein (VSV-G) as a positive control, to assess entry efficiency. The experimental results revealed a differential impact of E64d on viral entry, as illustrated in Figure 12. The Beta strain showed the highest viral entry in the presence of E64d. This suggests that Beta is relatively resistant to inhibition of the cathepsin-dependent endosomal route in this cell system and may rely more strongly on protease activation pathways that are less affected by E64d (e.g., cell-surface activation rather than endosomal cathepsin L cleavage). In addition, because E64d inhibits multiple endosomal cysteine proteases, it may reduce non-productive proteolysis or lysosomal degradation of incoming pseudovirions, thereby increasing the fraction of particles that remain intact long enough to enter via alternative, E64d-insensitive routes. Therefore, the increase in Beta viral entry (RLU%) likely reflects a shift in the balance between productive entry and endosomal degradation/processing rather than true enhancement of cathepsin L–dependent entry (Glowacka et al., 2011; Padmanabhan et al., 2020).

This was followed by the Wuhan and Delta variants, supporting the idea that these early lineages predominantly utilise TMPRSS2-dependent pathways for cell entry (Hoffmann et al., 2020; Meng et al., 2022; Peacock et al., 2022). In contrast, the more recent BA.2 and BA.4 Omicron subvariants showed markedly reduced entry ($P < 0.0001$) following E64d treatment, as indicated by significantly lower entry levels. This finding is consistent with a strong dependence on endosomal protease

activity for efficient entry in these subvariants, such that blocking cysteine proteases with E64d has a greater inhibitory effect. Overall, these data support the model that early variants are comparatively less dependent on cathepsin-mediated endosomal activation, whereas Omicron subvariants show greater sensitivity to disruption of the endosomal pathway (Hoffmann et al., 2020; Meng et al., 2022; Peacock et al., 2022).

The schematic in Figure 12 illustrates the two principal entry routes for SARS-CoV-2: a) direct fusion at the cell surface via TMPRSS2 (Route 1), and b) endosomal fusion dependent on cathepsins (Route 2). The targeted inhibition of the endosomal route by E64d reinforces our observations that variants with greater reliance on cathepsin-dependent activation are more susceptible to E64d, whereas variants favouring TMPRSS2-mediated entry may exhibit relative resistance and, in some cases, an apparent increase in signal if endosomal degradation is reduced (Glowacka et al., 2011; Chen et al., 2021). These findings highlight the importance of dissecting the interactions between SARS-CoV-2 variants and host proteases, particularly when considering therapeutic strategies that target viral entry mechanisms. Taken together, these entry and inhibitor data indicate that variant-dependent protease usage is strongly shaped by cellular context in $A549^{ACE2}$ cells. Building on these findings, Chapter 4 examines whether host restriction factors (IFITM1, IFITM2, and IFITM3) further modulate spike-mediated entry across early and Omicron variants.

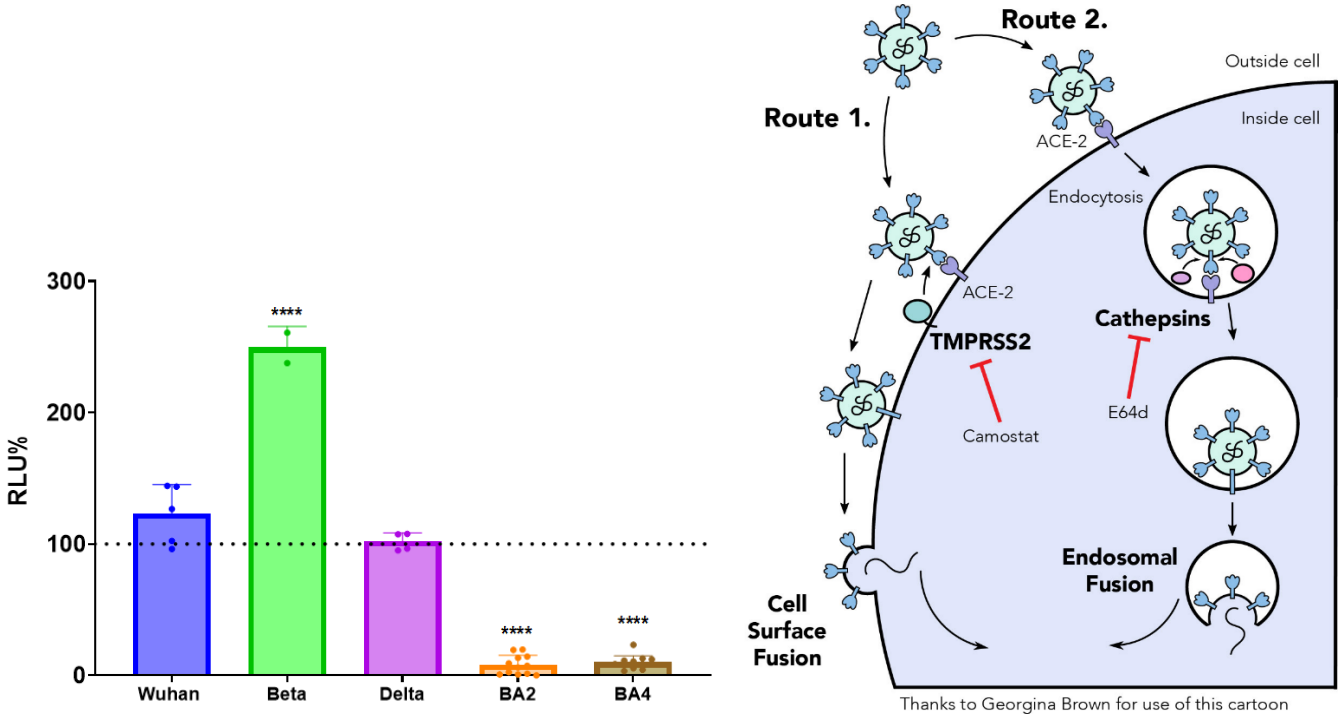

Figure 12: Efficacy of E64d in inhibiting the entry of different SARS-CoV-2 variants into A549^{ACE2} cells at 10 μM

*The graph presents the efficacy of E64d in inhibiting different pseudoviruses (PVs) expressing the spike (S) protein from various SARS-CoV-2 variants, measured in % RLU (Relative Light Units). The variants compared include the original Wuhan strain and the Beta, Delta, BA.2, and BA.4 variants. One-way ANOVA, Dunnett's multiple comparisons test was performed to measure statistical significance (**** = P <0.0001) between Wuhan and Beta, BA.2 and BA.4 Data are presented as the mean ± standard deviation (SD) from n = 3 independent biological replicates.*

CHAPTER FOUR: Result – Role of IFITMs in SARS-CoV-2 entry mechanisms

4.1 Rationale for investigating IFITMs

Interferon-induced transmembrane proteins (IFITMs) are critical host-derived restriction factors that regulate viral entry into host cells. Initially characterised as antiviral proteins, IFITMs inhibit infection primarily by interfering with the fusion of viral and host cell membranes, thereby limiting the delivery of viral genomes into the cytosol (Smith et al., 2014; Marie-Pierre Confort et al., 2023). IFITM1, IFITM2, and IFITM3 in particular have been shown to restrict a wide range of enveloped viruses, including HIV and influenza virus, highlighting their broad antiviral potential (Qian et al., 2015; Yu et al., 2015).

Mechanistic studies demonstrate that IFITMs do not exert a uniform antiviral effect but instead modulate their activity according to the viral entry route and cellular context. In this sense, IFITMs "adapt their function" by exerting antiviral activity at distinct cellular membranes depending on where viral fusion occurs. IFITM1 is predominantly localised at the plasma membrane, whereas IFITM2 and IFITM3 are mainly enriched in endosomal compartments, positioning them to differentially influence surface-mediated or endosomal viral entry pathways, respectively (Shi et al., 2021; Koch et al., 2021). This compartment-specific localisation allows IFITMs to selectively restrict viruses that rely on particular entry mechanisms (Marie-Pierre Confort et al., 2023; Zhao et al., 2018).

This functional adaptability is particularly relevant in the context of SARS-CoV-2 infection, where viral entry can occur either at the plasma membrane or via endocytosis. Early SARS-CoV-2 variants predominantly utilised TMPRSS2-dependent plasma membrane fusion, whereas the Omicron variant displays a greater reliance on endosomal entry pathways (Hoffmann et al., 2020; Koch et al., 2021). The presence or absence of entry cofactors such as TMPRSS2 therefore indirectly determines which IFITM family members are most influential during infection. In this context, the versatility of

IFITMs reflects their ability to exert distinct effects depending on host protease availability and the dominant viral entry route, rather than acting as static or universally restrictive proteins (Unali et al., 2023).

At the molecular level, IFITMs restrict viral entry by altering membrane properties, including membrane fluidity and curvature, which impairs hemifusion and subsequent fusion pore formation (Desai et al., 2014; Wang et al., 2024). IFITM3, for example, inhibits the progression from hemifusion to full fusion within endosomes, thereby preventing viral genome release (Desai et al., 2014). Beyond simple receptor-level interference, IFITMs interact with multiple host and viral factors involved in membrane fusion dynamics, protease-dependent spike activation, and intracellular trafficking. These interactions underscore a multifaceted mode of action in which IFITMs influence viral propagation through coordinated effects on membrane architecture and entry-associated host machinery, rather than by blocking receptor engagement alone.

Importantly, IFITM proteins function not only as passive physical barriers but also as active modulators of membrane fusion processes, reinforcing their central role in innate antiviral defence. In addition to their established antiviral activity, IFITMs have been implicated in broader immunological functions, including roles in adaptive immunity and cancer biology (Wang et al., 2024).

The effectiveness of IFITM-mediated restriction is strongly influenced by cellular context, expression level, and viral adaptation. Several studies have shown that the impact of IFITMs varies between cell types, and that certain viruses have evolved mechanisms to evade or exploit IFITM activity, highlighting the complexity of IFITM–virus interactions (Smith et al., 2014). These findings emphasise the need for a more nuanced understanding of IFITM function when considering their role in antiviral defence and therapeutic targeting.

Further investigation through integrating Omicron-specific analyses with targeted experimental assays will clarify how IFITMs shape variant-dependent entry pathways. Notably, recent studies have demonstrated that IFITM proteins can be required for efficient SARS-CoV-2 replication in human lung epithelial cells, challenging the traditional view of IFITMs as exclusively antiviral factors (Xu et al., 2022; Prelli Bozzo et al., 2021). This apparent contradiction is supported by evidence that IFITM3 restricts endosomal entry while simultaneously enhancing plasma membrane fusion under certain conditions, potentially facilitating infection (Shi et al., 2020; Prelli Bozzo et al., 2021).

This chapter, therefore, aims to resolve these discrepancies by providing a comprehensive analysis of IFITM expression and function using RNA sequencing, bioinformatics, and in vitro experimental validation. Elucidating these mechanisms is critical, as distinct SARS-CoV-2 variants may differentially exploit IFITMs to enhance viral fitness and pathogenicity.

4.2 RNA-sequencing and Partek flow analysis

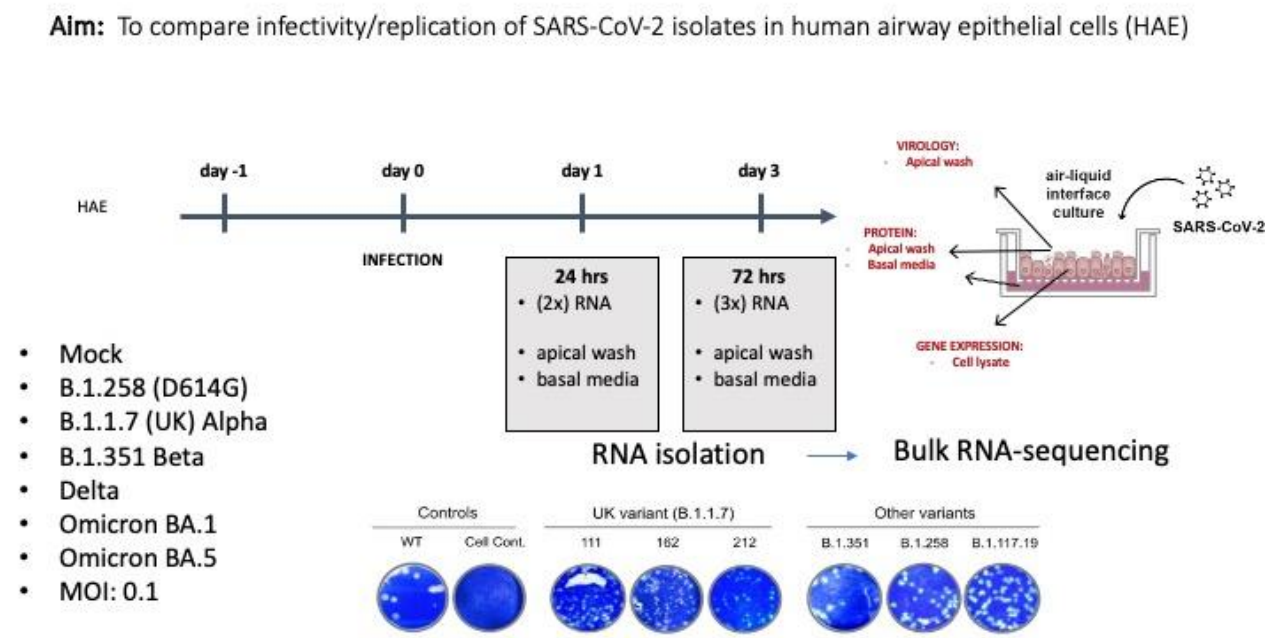

Figure 13:Infection and RNA sequencing of air–liquid interface human nasal airway epithelial cells (HAE) Reproduced from Giothis's Lab.

Prior to infection, HAE cultures were washed with serum-free media to remove mucus and debris. Cells were infected with 200 µL of virus-containing supernatant and incubated at 33°C for 1 hour. Following infection, cells were harvested at 24 hours and 72 hours for RNA isolation using the RNeasy Mini Plus kit. Approximately 1 µg of total RNA from each sample was used for the construction of sequencing libraries. mRNA library preparation (poly-A enrichment) and high-throughput sequencing were performed by Novogene. Sequencing data (FASTQ raw files) were subsequently imported into Partek Flow for downstream analysis.

To investigate the host response to SARS-CoV-2 infection (Figure 13), our laboratory previously utilised human nasal airway epithelial (HAE) cells exposed to the virus at an air–liquid interface, followed by RNA sequencing analysis via Partek Flow software. I reanalysed existing RNA-seq data from other members of the group. The full dataset is deposited in the GEO database and is available under GEO accession GSE237576.

My analysis (Figure 14) demonstrates increased expression of interferon-induced transmembrane proteins (IFITM1, IFITM2, and IFITM3) in human airway epithelial (HAE) cells following infection with SARS-CoV-2 variants. IFITM expression increased in a time-dependent manner between 24 h

and 72 h post-infection, with the magnitude of induction varying between viral variants. Overall, all variants showed higher IFITM expression at the later time point; however, Delta and Omicron sublineages exhibited the greatest increases between 24 h and 72 h, with differences reaching statistical significance (* = $P < 0.05$; ** = $P < 0.01$; *** = $P < 0.001$; **** = $P < 0.0001$). This indicates that SARS-CoV-2 variants differ in their capacity to induce IFITM expression in airway epithelial cells.

While the observed upregulation of IFITM proteins aligns with their established role as components of the innate immune response, increased expression alone does not definitively demonstrate antiviral activity. IFITMs are classically described as restriction factors that inhibit viral entry by altering membrane properties and preventing membrane fusion; however, their role during SARS-CoV-2 infection appears to be more complex and context dependent (Shi et al., 2020; Prelli Bozzo et al., 2021). Emerging evidence suggests that, under certain physiological conditions, IFITM expression may be tolerated or exploited by SARS-CoV-2, particularly during endosomal entry, raising the possibility that IFITM upregulation reflects a host response that is insufficient to fully restrict viral replication (Prelli Bozzo et al., 2021; Shi et al., 2020).

Consequently, increased IFITM expression does not necessarily equate to reduced viral replication. Definitive assessment of antiviral function would require correlation of IFITM expression levels with direct virological readouts, such as viral RNA burden or infectious virus production. In the absence of these measurements, it remains unclear whether elevated IFITM expression represents effective viral restriction or an ongoing host response to persistent infection. This highlights the importance of integrating host gene expression analyses with functional virological assays to accurately interpret the role of IFITMs during SARS-CoV-2 infection.

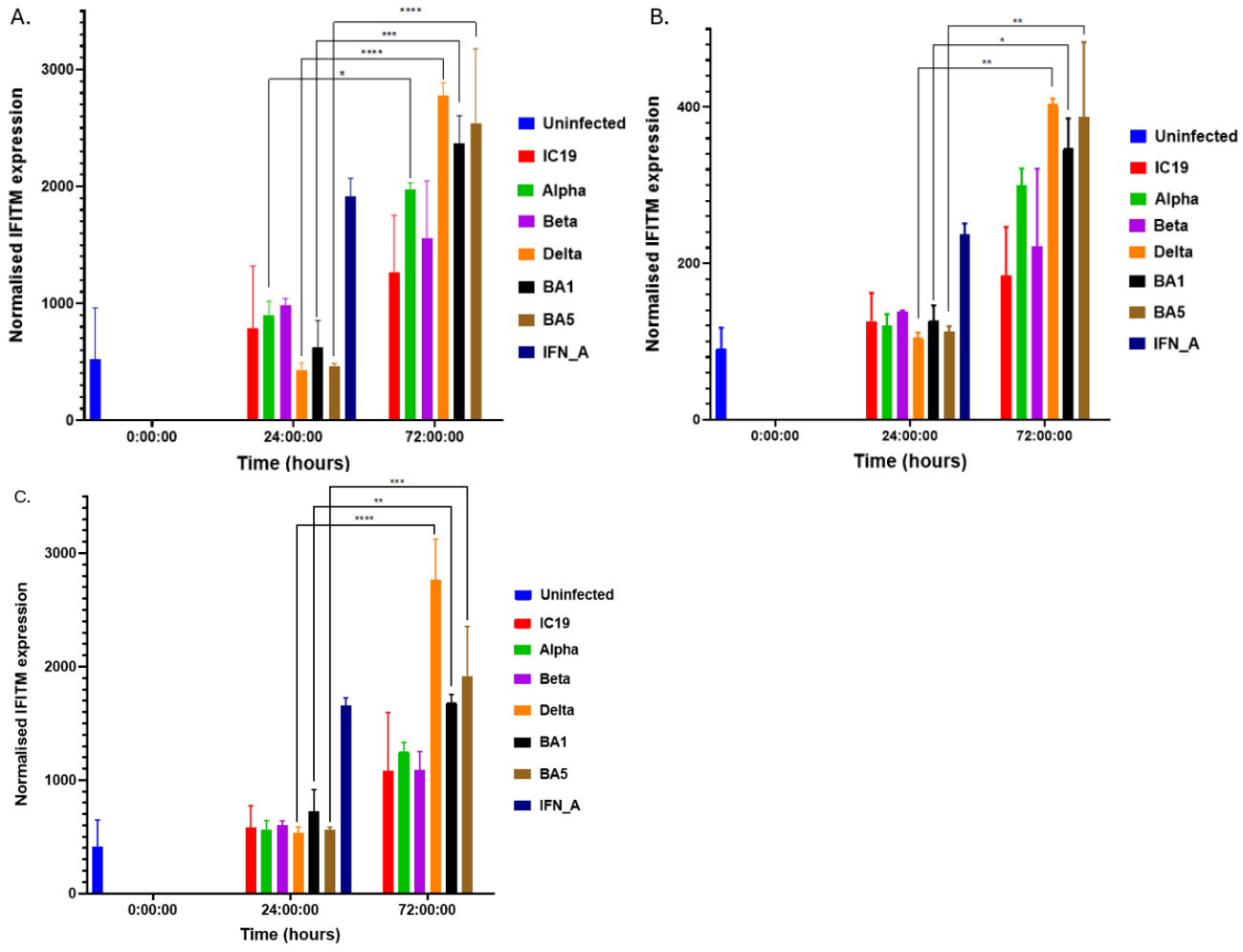

Figure 14: Increased expression of IFITMs by some SARS-CoV-2 variants.

Normalised IFITM1,2,3 expression in human primary airway epithelial cells cultured at an air–liquid interface following infection with SARS-CoV-2 variants (IC19, Beta, Alpha, Delta, BA.1 and BA.5). Cells were infected at a multiplicity of infection (MOI) of 0.1 and harvested at 24 h and 72 h post-infection; uninfected cells served as the baseline control. (A) IFITM 1, (B) IFITM 2, (C) IFITM 3. IFITMs expression was quantified by RNA sequencing and values are presented as mean ± SD from n=2 independent experiments. Data processing and visualisation were performed in GraphPad Prism. Two-way ANOVA with Šídák's multiple comparisons test (24 h vs 72 h within each variant) (= P < 0.05; ** = P < 0.01; *** = P < 0.001; **** = P < 0.0001)*

4.3 Comparison of IFITM amino acid sequences

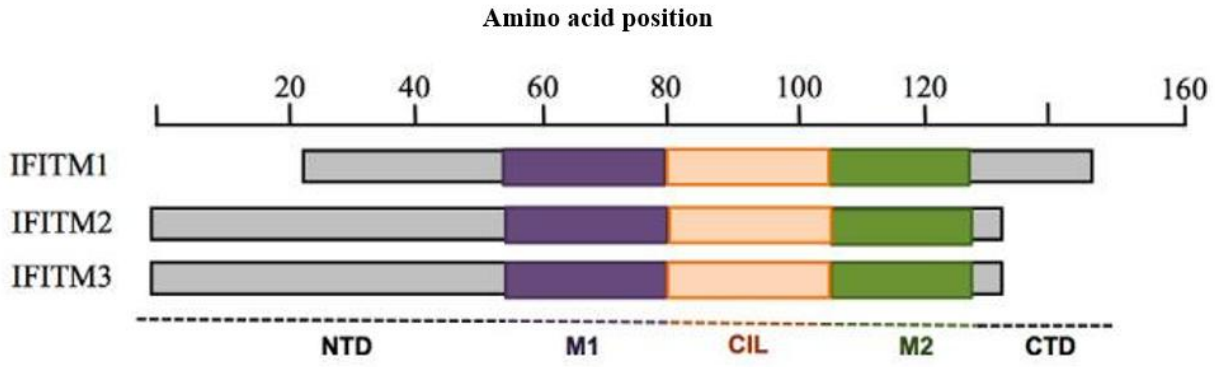

Figure 15. Schematic representation of human IFITM family members.

Domain organisation of IFITM1, IFITM2, and IFITM3, highlighting conserved and divergent regions. IFITM1 differs from IFITM2 and IFITM3 by a 21-amino-acid truncation at the N-terminus and a 13-amino-acid extension at the C-terminus. All three proteins share conserved membrane-associated domains (M1 and M2) and a central intracellular loop (CIL), while divergence at the terminal regions may contribute to differences in subcellular localisation and antiviral function. Inspired by Narayana et al. (2015)

Given the differential induction of IFITMs at the transcript level, we next examined whether structural differences between IFITMs might explain their functional divergence. To assess the degree of similarity among IFITM family members, I compared the amino acid sequences of IFITM1, IFITM2, and IFITM3 using reference sequences from NCBI and GenBank. The analysis (Table 11) revealed that IFITM2 and IFITM3 share the highest sequence identity (92.37%), indicating a close evolutionary relationship and suggesting substantial functional overlap. In contrast, IFITM1 exhibits lower sequence identity with IFITM3 (83.02%) and IFITM2 (80.19%), consistent with greater divergence within this family member. All pairwise comparisons (Table 8-10) yielded extremely low E-values (ranging from 3e−61 to 4e−92), confirming the statistical significance of the alignments.

To place these sequence differences into a structural context, the domain organisation of human IFITM1, IFITM2, and IFITM3 is illustrated in Figure 15. All three proteins share a conserved core architecture comprising an N-terminal domain (NTD), two membrane-associated regions (M1 and M2), and a central intracellular loop (CIL), supporting a shared core antiviral mechanism. Consistent with the sequence identity analysis, IFITM2 and IFITM3 display highly similar domain lengths and organisation, whereas IFITM1 shows distinct terminal variation, characterised by N-terminal truncation and C-terminal extension relative to the other family members.

Beyond these structural differences, variability within the terminal regions is biologically significant. IFITM3 contains an N-terminal tyrosine-based endocytic sorting signal (the 20-YEML-23 YxxΦ motif) that promotes AP-2–dependent internalisation and trafficking to endolysosomal compartments, which is important for restricting viruses that enter via pH-dependent endosomal fusion (Jia et al., 2014). IFITM3 localisation and activity are further shaped by post-translational modification of N-terminal residues (including lysines), with phosphorylation of Tyr20 influencing both endocytosis and ubiquitination—supporting the idea that these modifications regulate IFITM3 trafficking and turnover rather than simply "driving" late endosomal localisation (Chesarino et al., 2014). In contrast, IFITM1 lacks the IFITM3-type endocytic sorting motif and is more commonly enriched at the plasma membrane, whereas IFITM2 shows overlapping/intermediate distribution depending on cell context (Narayana et al., 2015; Smith et al., 2019). Consistent with these localisation differences, IFITM3 is often more effective against viruses that fuse within endosomal compartments, while IFITM1 more strongly inhibits viruses that fuse at or near the cell surface (Narayana et al., 2015; Smith et al., 2019).

Collectively, these findings indicate that divergence within the IFITM family is not simply the result of evolutionary drift but reflects functional specialisation driven by differences in terminal regions and domain organisation. Such variations likely influence protein localisation, post-translational regulation, and interactions with host or viral factors, thereby shaping the antiviral specificity of

individual IFITM proteins. This integrated sequence and structural analysis provides a framework for understanding how closely related IFITM family members exert distinct yet complementary roles in antiviral defence.

Table 8:Amino acid of IFITMS compared to IFITM1(NCBI Reference Sequence: NP_003632.4)

	REFERENCE (GENBANK)	***E VALUE***	***PERCENT %***	***LENGTH***
IFITM3	*AFF60354.1*	*9e-63*	*83.02%*	*133*
IFITM2	*CAG46672.1*	*3e-61*	*80.19%*	*132*

Table 9:Amino acid of IFITMS compared to IFITM2 (CAG46672.1)

	REFERENCE	***E VALUE***	***PERCENT %***	***LENGTH***
IFITM3	*AFF60354.1 (Genbank)*	*4e-92*	*92.37%*	*133*
IFITM1	*NP_003632.4 (NCBI)*	*3e-61*	*80.19%*	*125*

Table 10:Amino acid of IFITMS compared to IFITM3 (AFF60354.1)

	REFERENCE	***E VALUE***	***PERCENT %***	***LENGTH***
IFITM2	*CAG46672.1 (Genbank)*	*4e-92*	*92.37%*	*133*
IFITM1	*NP_003632.4 (NCBI)*	*9e-63*	*83.02%*	*125*

Table 11: Matrix table of the Amino acid of IFITMS compared

	IFITM1	***IFITM2***	***IFITM3***
IFITM1	*/*	*80.19%*	*83.02%*
IFITM2	*80.19%*	*/*	*92.37%*
IFITM3	*83.02%*	*92.37%*	*/*

4.4 Efficient transduction of HEK293T Cells with lentiviral vectors encoding IFITM proteins

Lentiviral vectors were used to overexpress IFITM1, IFITM2, and IFITM3 in $A549^{ACE2}$ cells to assess the contribution of each IFITM to SARS-CoV-2 variant entry. To verify the efficiency of the lentiviral vectors prior to downstream entry assays, HEK293T cells were transduced with lentiviruses encoding IFITM1, IFITM2, or IFITM3 and co-expressing red fluorescent protein (RFP) as a reporter. Transduction efficiency was assessed by fluorescence microscopy at 48 and 72 h post-transduction.

Cells transduced with the empty lentiviral vector showed minimal background fluorescence at both time points, confirming negligible signal from the vector backbone and providing a negative control. In contrast, cells transduced with IFITM-expressing constructs displayed robust RFP fluorescence, indicating successful gene delivery and expression. IFITM1 produced strong RFP fluorescence at both 48 and 72 h, with a slightly more diffuse distribution at 72 h. IFITM2-transduced cells also showed clear and consistent RFP expression at both time points, supporting efficient transduction. IFITM3 produced the most intense RFP signal under these conditions.

A lentiviral vector expressing firefly luciferase (Fluc) alongside RFP was included as a positive control and showed strong, widespread fluorescence at both time points. Together, these observations confirm that the lentiviral preparations were functional and capable of mediating high levels of transgene expression in HEK293T cells, supporting their suitability for subsequent experiments.

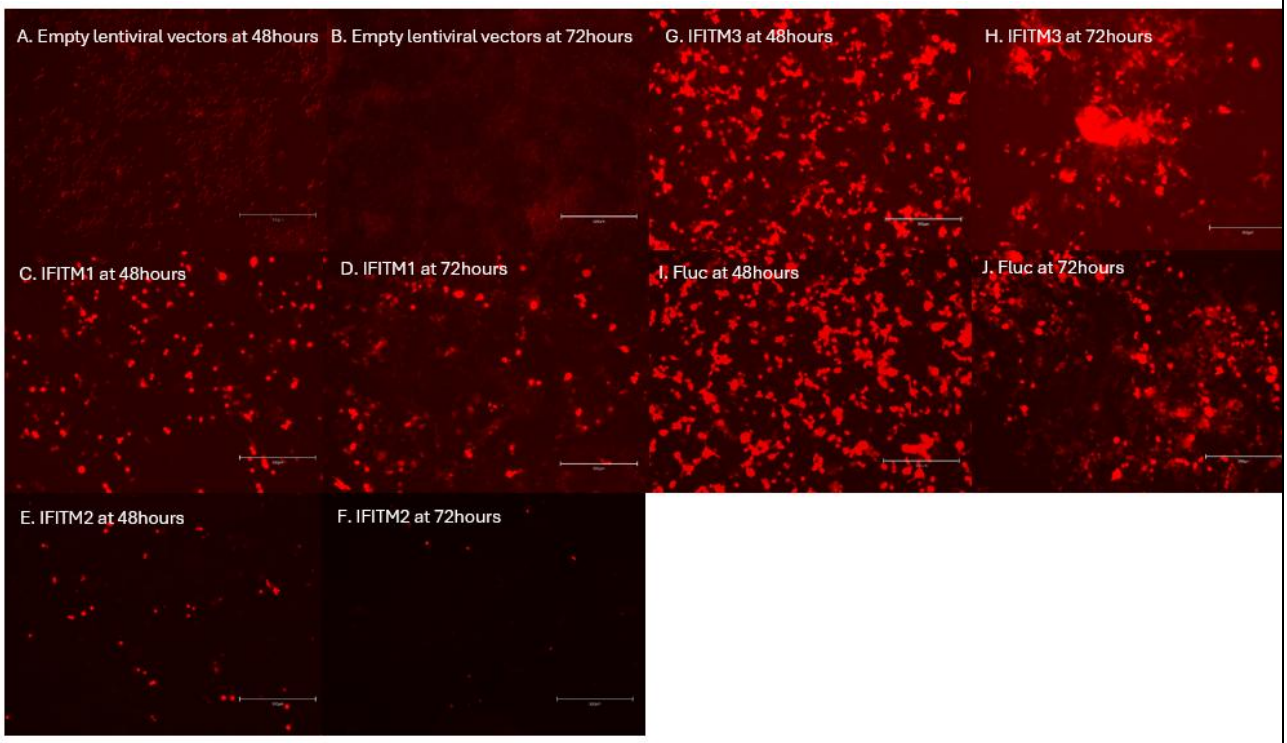

Figure 16: Visualisation of Lentiviral Vectors Encoding IFITM Proteins in HEK293T Cells Using EVOS Imaging at 10× Magnification.

HEK293T cells were transduced with lentiviral vectors encoding interferon-induced transmembrane proteins (IFITMs) and a red fluorescent protein (RFP) reporter gene. Transduction efficiency was assessed at 48- and 72-hours post-transfection by detecting RFP expression using the EVOS Cell Imaging System under 10× magnification. EVOS allows multiplex fluorescence imaging across four distinct channels, enabling precise detection of RFP expression. (A, C, E, G, I) Images captured at 48 hours. (B, D, F, H, J) Corresponding images captured at 72 hours post-transduction. Scale bar length = 300 µm.

4.5 Optimisation of IFITM expression ratios in A549^{ACE2} Cells

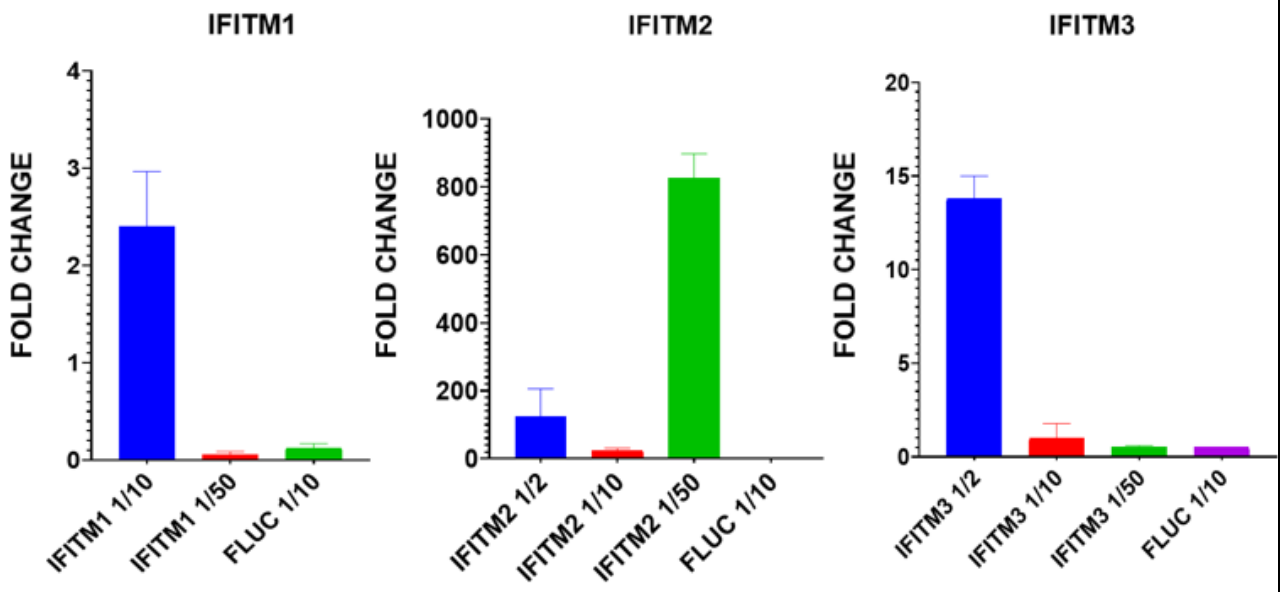

Figure 17: Lentivirus Titration determination of IFITMs expression.

Lentiviral titration to determine IFITM expression levels. Cells were transduced with lentiviral vectors encoding IFITM1, IFITM2, or IFITM3 at the indicated virus dilutions (IFITM1: 1/10 and 1/50; IFITM2: 1/2, 1/10, and 1/50; IFITM3: 1/2, 1/10, and 1/50). Expression is shown as fold change (y-axis) for each condition, with separate panels for IFITM1 (left), IFITM2 (middle), and IFITM3 (right). Data are presented as the mean ± standard deviation (SD) from n = 2 independent biological replicates

.

To determine the optimal conditions for IFITM expression, A549 cells stably expressing ACE2 were transduced with lentiviral constructs encoding IFITM1, IFITM2, or IFITM3 using a range of vector-to-cell transduction ratios, defined as the ratio of lentiviral particles carrying the IFITM constructs relative to the number of target cells at the time of infection (Kutner et al., 2009; Naldini, 2015). This parameter influences the likelihood that each cell is infected by the lentivirus and therefore affects both the number of cells transduced and the strength of transgene expression. Expression analysis was performed 48 hours post-transduction, a time point selected to allow sufficient lentiviral integration and stabilisation of transgene expression while minimising transient early effects associated with viral entry (Kutner et al., 2009). IFITM expression was quantified by RT-qPCR and is presented as relative IFITM mRNA expression, calculated as fold change compared to a control (FLUC). The data shown in Figure 17, therefore, represent changes in mRNA levels, rather than

fluorescence intensity, protein expression, or the proportion of cells expressing the transgene, and reflect the average expression across the whole cell population.

Lentiviral transduction does not infect all cells in the population, so the fold change values represent an average of both transduced and non-transduced cells. As a result, expression levels in successfully transduced cells are likely underestimated. However, because all conditions were treated in the same way, comparisons between different transduction ratios remain valid. This limitation could be addressed in future experiments by enriching for transduced cells or by confirming IFITM expression at the protein level. As IFITMs are membrane-associated proteins, Western blotting or flow cytometry would provide stronger evidence that increased mRNA expression results in functional protein expression (Perreira et al., 2013; Bailey et al., 2014).

For IFITM1, the 1/10 transduction ratio produced the highest expression level, resulting in an approximate 2.4-fold increase above baseline, whereas the 1/50 condition yielded negligible expression. Accordingly, the 1/10 ratio was selected as the optimal condition for IFITM1 expression. In contrast, IFITM2 expression was most pronounced at the 1/50 transduction ratio, reaching approximately 850-fold above baseline, indicating a strong dependence on vector input for efficient expression. This ratio was therefore selected for subsequent experiments. IFITM3 expression displayed a distinct profile, with maximal induction observed at the 1/2 ratio, yielding an approximate 14.5-fold increase. Expression was substantially reduced at the lower transduction ratios, indicating that higher vector input is required to achieve robust IFITM3 expression.

In summary, these results demonstrate that optimal IFITM expression in $A549^{ACE2}$ cells is achieved using distinct transduction ratios for each IFITM family member, with IFITM1 optimally expressed at a 1/10 ratio, IFITM2 at a 1/50 ratio, and IFITM3 at a 1/2 ratio. These optimised conditions were therefore selected for all subsequent experiments investigating the functional roles of IFITMs in antiviral responses.

4.6 Differential sensitivity of SARS-CoV-2 variants to IFITM1-mediated restriction in A549^{ACE2} cells

To evaluate the effect of IFITM1 expression on viral entry across different SARS-CoV-2 variants, relative luminescence units (RLU) were measured in A549^{ACE2} cells transduced with IFITM1-expressing lentivirus and infected with pseudoviruses bearing spike proteins from multiple SARS-CoV-2 variants. Results are presented as relative luminescence units (RLU%), calculated by normalising each sample to the corresponding pseudovirus (PV) in the absence of IFITM1 (no-IFITM1 control). In this assay, the baseline is defined as 100% viral entry in the no-IFITM control condition. Values below baseline (<100%) indicate reduced viral entry relative to the control, consistent with inhibition/restriction, whereas values at baseline (~100%) indicate little or no effect. Values above baseline (>100%) indicate increased viral entry relative to the control, consistent with enhanced entry (or a lack of restriction).

The Wuhan variant showed the greatest susceptibility to IFITM1-mediated restriction. Alpha displayed a moderate decrease in entry (RLU% ~60%), which was statistically significant ($P < 0.001$). In contrast, Beta, Delta, BA.1, and BA.2 exhibited markedly reduced RLU% values (~45–60%), consistent with stronger IFITM1-mediated restriction, and these differences were highly significant ($P < 0.0001$). BA.4 and BA.5 remained close to baseline (approximately ≥90%), indicating reduced susceptibility to IFITM1 and relative resistance to inhibition. XBB maintained a comparatively high entry (~70%) but was still significantly reduced relative to the control ($P < 0.01$), whereas BQ1.1 showed intermediate susceptibility (~60%) with a significant reduction ($P < 0.001$).

Overall, these data indicate that the impact of IFITM1 on SARS-CoV-2 entry varies with variant, with earlier variants (notably Beta, Delta, BA.1, and BA.2) being most sensitive, while later Omicron subvariants (particularly BA.4 and BA.5) are substantially less sensitive.

The subcellular localisation of IFITMs was not directly assessed in this model, representing a limitation of the study. This is relevant because the antiviral activity of interferon-induced transmembrane proteins (IFITMs) is strongly dependent on their cellular distribution. IFITMs are predominantly associated with the plasma membrane, where they are generally linked to restricting viral entry, whereas altered trafficking or mislocalisation can attenuate antiviral activity or, in certain contexts, promote viral fusion (Bailey et al., 2014; Shi et al., 2017).

Subcellular localisation of IFITMs can be assessed using immunofluorescence staining followed by confocal microscopy and colocalisation analysis with compartment-specific markers (e.g., EEA1 for early endosomes, Rab7 for late endosomes, or LAMP1 for lysosomes) (Meischel et al., 2021). Complementary biochemical approaches, such as cell-surface biotinylation to quantify plasma membrane–exposed pools and subcellular fractionation followed by immunoblotting to distinguish membrane compartments, can provide quantitative validation of IFITM distribution (Weston et al., 2014).

As IFITMs were overexpressed via lentiviral transduction in this study, non-physiological expression levels may have influenced their intracellular trafficking. Consequently, the observed differences in relative luminescence units (RLU%) between SARS-CoV-2 variants may reflect not only intrinsic viral resistance to IFITM1-mediated restriction, but also variant-specific utilisation of entry pathways that are differentially sensitive to IFITM1 depending on its localisation. Without direct confirmation of IFITMs subcellular distribution, mechanistic interpretations linking IFITMs expression levels to antiviral function should therefore be made with caution (Shi et al., 2017; Zhao et al., 2020).

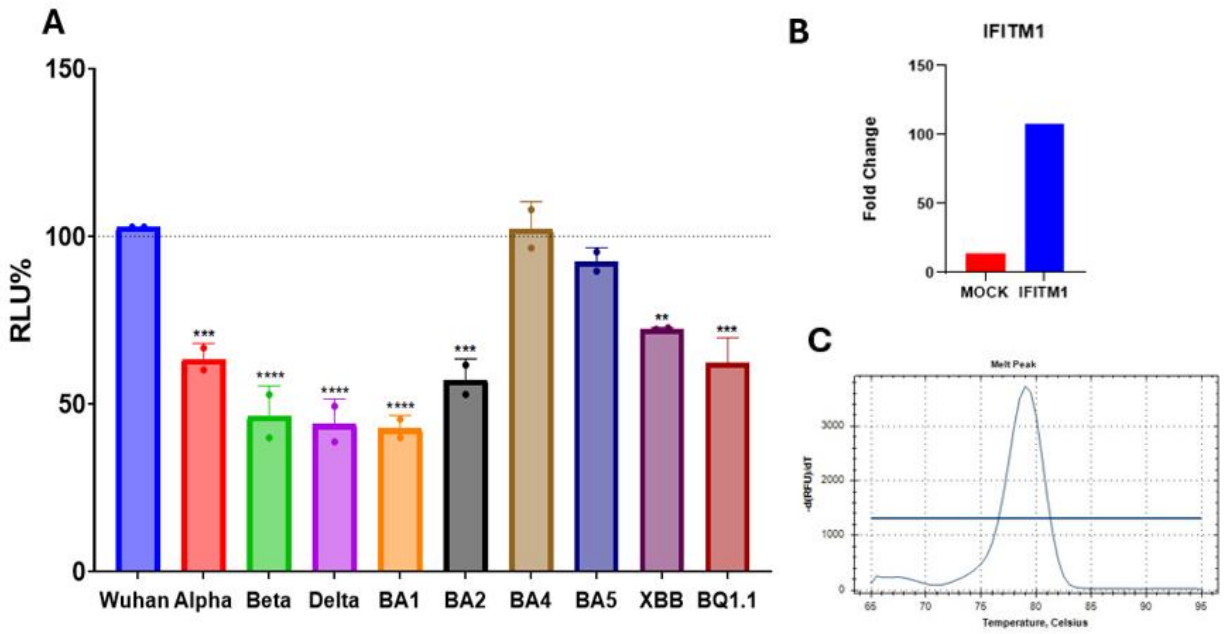

Figure 18: Expression of interferon (IFN)-induced transmembrane protein 1 (IFITM1) in cells infected with different SARS-CoV-2 variants and quantitative analysis of its expression.

(A) Shows the quantitative analysis of IFITM1-mediated restriction of viral entry in A549^{ACE2} *cells expressing IFITM1, following infection with SARS-CoV-2 variants including Wuhan, Alpha, Beta, Delta, BA.1, BA.2, BA.4, BA.5, XBB, and BQ1.1. Relative luminescence units (RLU%) were measured, calculated, and Data are presented as the mean ± standard deviation (SD) from 2 independent experiments. One-way ANOVA Dunnett's multiple comparisons test was performed to measure statistical significance (** P < 0.01,*** P < 0.001,**** P < 0.0001) between Wuhan and Beta, Delta, and BA1. (B) depicts the relative expression levels of IFITM1 mRNA under the same experimental conditions. Fold change was determined by quantitative PCR (qPCR), with expression normalised to the housekeeping gene (GAPDH). Data represent the mean ± standard deviation (SD) from n = 2 independent experiments. Additionally, a melt peak analysis of IFITM1 gene amplification (C) was performed via qPCR to assess specificity, with the melt curve showing a single peak, confirming specific target amplification*

4.7 Effect of IFITM2 expression on viral entry across SARS-CoV-2 variants

Next, to investigate the impact of IFITM2 expression on viral entry, relative luminescence units (RLU) were quantified across a panel of SARS-CoV-2 variants, with RLU% used to represent viral entry efficiency. The ancestral Wuhan strain and the Alpha variant both exhibited high RLU% values, averaging approximately 75–78%, suggesting that IFITM2 expression had minimal impact on the entry of these early viral lineages. Similarly, the Omicron subvariants BA.5, XBB, and BQ.1.1 showed elevated RLU% values exceeding 75%, indicating that these later-emerging variants retained strong entry capacity despite IFITM2 expression.

In contrast, other variants demonstrated significantly reduced entry efficiency in the presence of IFITM2. The Delta variant showed the most substantial reduction in RLU%, with an average value near 30%, representing a statistically significant difference compared to the Wuhan reference ($p = 0.0006$). The BA.1 subvariant also displayed a marked decrease in RLU%, falling below 40% and achieving statistical significance ($p = 0.0017$). BA.4 exhibited a moderate yet statistically significant reduction in viral entry, with RLU% values around 50% ($p = 0.0265$). These data suggest that IFITM2 exerts a more substantial inhibitory effect on specific variants.

The Beta variant and BA.2 showed intermediate reductions in RLU%, but these changes did not reach statistical significance. Although BA.2 exhibited somewhat reduced RLU% compared to Wuhan, the lack of relevance suggests a more modest impact of IFITM2 on this subvariant.

Together, these findings demonstrate that IFITM2 imposes differential restriction on SARS-CoV-2 variants, with pronounced inhibitory effects on Delta, BA.1, and BA.4, while having minimal influence on Wuhan, Alpha, BA.5, XBB, and BQ.1.1. This variation in sensitivity highlights the dynamic evolution of viral entry pathways and potential adaptation to evade host restriction factors like IFITM2.

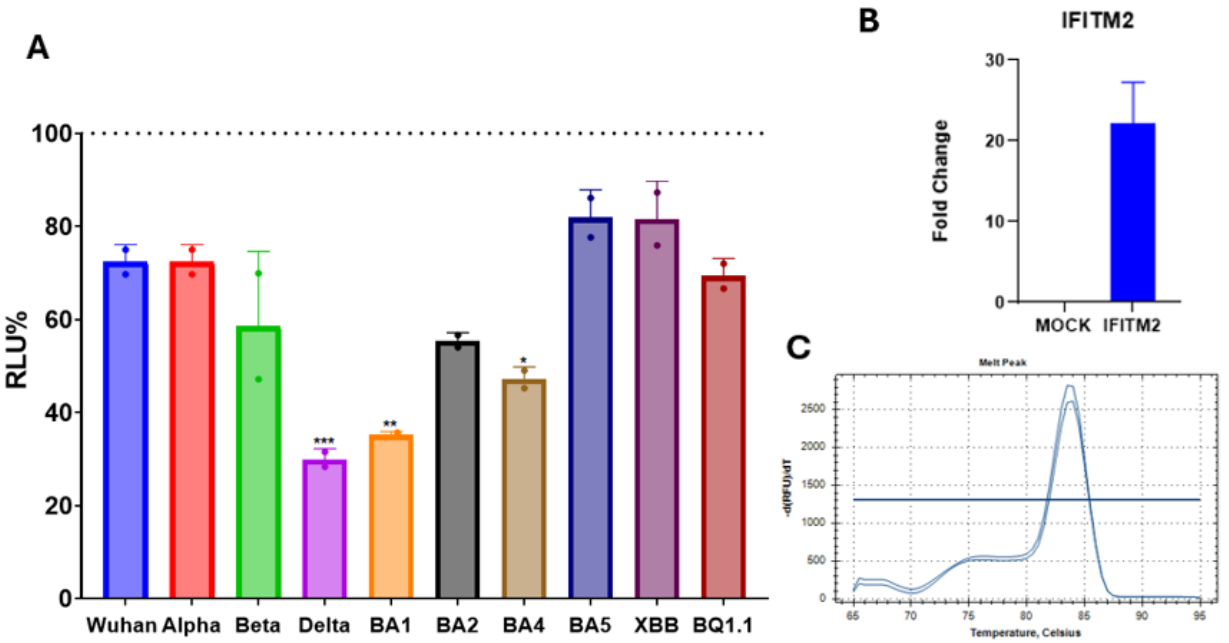

Figure 19: Expression of interferon (IFN)-induced transmembrane protein 2 (IFITM2) in viral variant-infected cells and quantitative analysis of its expression.

*(A)Quantitative analysis of IFITM2-mediated restriction of viral entry in cells infected with different SARS-CoV-2 variants. Luciferase were measured in A549 $^{ACE2+IFITM2}$ (*A549^{ACE2} *cell line expressing IFITM2) after infection with Wuhan, Alpha, Beta, Delta, BA.1, BA.2, BA.4, BA.5, XBB, and BQ1.1 variants. Moreover, the Data from luciferase readings were used to calculate the % viral entry level. Data are presented as the mean ± standard deviation (SD) from n = 3 independent experiments. One-way ANOVA Dunnett's multiple comparisons test was performed to measure statistical significance ,with significant differences observed between Wuhan and Delta (***P = 0.0006), Wuhan and BA.1 (**P = 0.0017), and Wuhan and BA.4 (*P = 0.0265). (B)Relative expression levels of IFITM2 mRNA in experimental conditions. Fold change was determined by quantitative PCR (qPCR), with IFITM1 expression normalised to a housekeeping gene (GapDH). Data represent the mean ± standard deviation (SD) from n = 2 independent experiments. (C)Melt peak analysis of IFITM2 gene amplification. Quantitative PCR (qPCR) was performed to verify the specificity of the amplification, with the melt curve showing a single peak indicating specific target amplification.*

4.8 IFITM3 expression does not significantly reduce viral entry efficiency.

The role of IFITM3 in SARS-CoV-2 spike-mediated entry was assessed by infecting IFITM3-expressing cells with pseudoviruses bearing spike proteins from multiple SARS-CoV-2 variants. Viral entry was quantified using a luciferase-based assay and expressed as relative luminescence units (RLU%), normalised to the corresponding pseudovirus control lacking IFITM expression (set to 100% entry). Values below 100% indicate reduced entry relative to the control, whereas values above 100% indicate increased entry.

Across all variants tested, IFITM3 expression did not significantly reduce viral entry (One-way ANOVA; Dunnett's multiple comparisons test was used to assess statistical significance). Although mean RLU% values tended to fall below 100%, the reductions were small and variable and showed substantial overlap with the no-IFITM control. Collectively, these data indicate that IFITM3 does not exert a consistent inhibitory effect on spike-mediated entry in this cellular model and has a negligible impact on variant entry efficiency under the conditions tested.

Overall, overexpression of IFITM1 and IFITM2 reduced entry across multiple variants, whereas IFITM3 showed no detectable effect under the conditions tested. Chapter 5 integrates these findings with known variant entry routes to interpret how protease availability and IFITM context may shape the observed phenotypes.

.

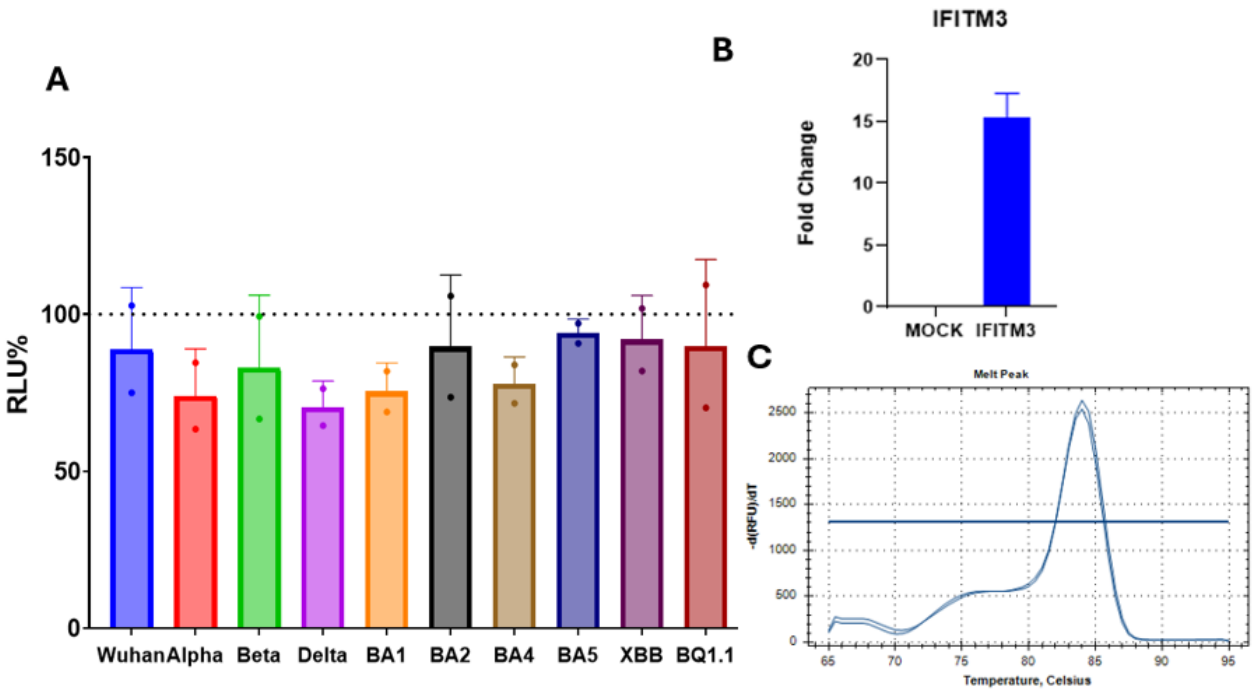

Figure 20: Expression of interferon (IFN)-induced transmembrane protein 3 (IFITM3) in viral variant-infected cells and quantitative analysis of its expression.

(A)Quantitative analysis of IFITM3-mediated restriction of viral entry in cells infected with different SARS-CoV-2 variants. Relative luminescence units (RLU%) were measured in the $A549^{ACE2}$ *cell line expressing IFITM3 after infection with Wuhan, Alpha, Beta, Delta, BA.1, BA.2, BA.4, BA.5, XBB, and BQ1.1 variants. Data are presented as the mean ± standard deviation (SD) from n = 2 independent experiments. (B)Relative expression levels of IFITM1 mRNA in experimental conditions. Fold change was determined by quantitative PCR (qPCR), with IFITM3 expression normalised to a housekeeping gene (GapDH). Data represent the mean ± standard deviation (SD) from n = 2 independent experiments. (C)Melt peak analysis of IFITM3 gene amplification. Quantitative PCR (qPCR) was performed to verify the specificity of the amplification, with the melt curve showing a single peak indicating specific target amplification.*

CHAPTER FIVE: DISCUSSION

5.1 Addressing technical challenges and approaches

Before interpreting the biological implications of inhibitor sensitivity and IFITM overexpression, several technical considerations about pseudovirus production and the A549ACE2 model are important for contextualising the entry phenotypes observed in this study.

PV production is a valuable method for studying viruses without the constraints of infection, making it a popular choice in viral research (Yang et al., 2020). This technique produces replication-defective PVs, allowing safe handling in BSL-2 laboratories commonly found in universities. Generating PVs typically involves transfecting packaging cells with specific viral proteins, a reporter, and a packaging system, such as HIV-1 (Yang et al., 2020). By utilising PVs, researchers can investigate various aspects of viral behaviour, including cell entry mechanisms, in a controlled and cost-effective manner (Bentley et al., 2015; Carnell et al., 2015). PVs were generated by transfection of packaging cells with selected surface viral proteins, a reporter system, and a packaging mechanism based on HIV-1(Di Genova et al., 2021; Schoggins & Rice, 2011). The concentration of pseudoviruses (PVs) in the target cells was determined by quantifying the expression of the reporter gene through a luciferase assay.

The initial challenge involved the low transduction titres of some pseudoviruses (PVs) produced. To address this and enhance the PV titre values, adjustments were made in the transfection conditions to improve the yield. This included modifying the transfection protocol for HEK293T cells from an 80% confluence level to 60%. This change meant fewer dead cells were at 48 hours by the time of collection, and a higher yield of PVs was obtained at 72 hours. Additionally, new plasmids were transformed to replace the initial batch, which had low concentrations, further contributing to improved PV production.

Another challenge involved the $A549^{ACE2}$ cells, which were growing at a slow pace and occasionally perishing. Several strategies were attempted to address this, including cultivating a new batch of cells, more frequent media changes, splitting the cells at a lower ratio, and increasing the concentration of hygromycin B. However, these measures were unsuccessful. The breakthrough came with adjusting the FBS concentration from 10% to 15% and switching to a passage 2 $A549^{ACE2}$ cell line, which effectively resolved the issue of cell health.

Moreover, to investigate the preferred entry pathways of different variants – endosomal fusion or cell surface entry – protease inhibitors such as camostat mesylate and E64d were employed, along with lung cells genetically modified to overexpress ACE2 stably. This approach was designed to discern the specific entry mechanisms favoured by various viral variants. However, this approach may impact the reliability of the results, given that the $A549^{ACE2}$ cells express very low levels of TMPRSS2, a critical factor in understanding the entry mechanisms of the virus (Hoffmann et al., 2020).

5.2 Unravelling the variants preferred pathway

The entry mechanisms of SARS-CoV-2 variants, including Wuhan, Alpha, Beta, Delta, and Omicron, have been extensively characterised. Omicron shows reduced TMPRSS2 usage and a shift towards endosomal entry, whereas Delta more efficiently utilises TMPRSS2-mediated fusion at the plasma membrane (Meng et al., 2022; Willett et al., 2022). Clinically, Delta has been associated with higher recovery of infectious virus (and lower Ct values) than Alpha in both vaccinated and unvaccinated individuals, which may contribute to increased transmissibility and disease severity (Luo et al., 2022). Furthermore, variants including Alpha, Beta, Delta, and Omicron exhibit greater environmental stability than the Wuhan strain, with Omicron showing the longest persistence in the Hirose et al. dataset (Hirose et al., 2022).

In this study, viral entry was quantified by measuring luciferase activity following pseudovirus (PV) infection of A549 cells overexpressing ACE2 (Figure 8). The Delta variant generated significantly higher luminescence signals than other variants ($P < 0.0001$), indicating enhanced entry efficiency in this experimental system.

To examine the role of TMPRSS2-mediated surface fusion, cells were treated with camostat mesylate (Figure 10), a serine protease inhibitor that blocks TMPRSS2 activity. Early variants, including Wuhan, Alpha, Beta, and Delta, showed significant reductions in entry following camostat treatment, supporting their reliance on TMPRSS2-dependent fusion. In contrast, Omicron subvariants BA.2, BA.4 and BA.5 showed significantly increased entry relative to untreated controls ($P < 0.0001$), with BA.5 displaying the highest levels. This increase is unlikely to reflect enhanced infectivity, but rather a shift in the utilisation of entry pathways. As Omicron subvariants preferentially depend on endosomal cathepsin-mediated activation, inhibition of TMPRSS2 may

reduce competition between surface and endosomal routes, thereby favouring endosomal fusion and increasing measured luciferase activity under TMPRSS2-inhibited conditions.

The role of endosomal cysteine proteases was evaluated using E64d (Figure 12), a cell-permeable inhibitor commonly used to block cathepsin-mediated endosomal entry (including cathepsins B and L). Omicron subvariants BA.2 and BA.4 exhibited significantly reduced entry following E64d treatment ($P < 0.0001$), consistent with greater reliance on cathepsin-dependent spike activation in endosomal compartments. In contrast, earlier variants showed comparatively limited sensitivity, indicating reduced dependence on the endosomal route under these experimental conditions. Notably, the Beta variant showed increased entry in the presence of E64d relative to untreated controls. This enhancement may reflect altered pathway utilisation (e.g., a relative shift towards protease pathways less affected by E64d) and/or reduced non-productive endosomal processing, rather than increased cathepsin-dependent entry.

In summary, these findings indicate that SARS-CoV-2 variants differ in their dependence on host proteases for entry. Camostat mesylate preferentially restricts variants that utilise TMPRSS2-mediated surface fusion, whereas E64d preferentially impairs Omicron subvariants that rely more heavily on cathepsin-mediated endosomal activation. Together, these inhibitor-specific responses highlight the flexibility of entry pathway utilisation across SARS-CoV-2 variants and the virus's capacity to shift between surface and endosomal routes depending on spike properties and cellular context.

5.3 Differential effects of IFITM proteins on SARS-CoV-2 entry across viral variants

Interferon-induced transmembrane proteins (IFITMs) are widely recognised for their antiviral activity against enveloped viruses by restricting membrane fusion and thereby limiting viral entry into host cells. IFITM1, IFITM2, and IFITM3 are classically viewed as intrinsic restriction factors that contribute to broad-spectrum antiviral defence. However, this framework has been revised by evidence showing that IFITMs can also promote infection in a context-dependent manner, including during SARS-CoV-2 infection.

Prelli Bozzo et al. (2021) reported that IFITMs act as cofactors for efficient SARS-CoV-2 infection at endogenous expression levels in human lung cells, with IFITM2 often exerting the strongest proviral effect. In the same study, artificial overexpression of IFITMs inhibited SARS-CoV-2 entry, supporting the idea that SARS-CoV-2 can interact with and potentially hijack IFITM proteins, depending on expression levels and cellular context. This is consistent with findings from Nchioua et al. (2022), who showed that depletion of endogenous IFITM2 markedly reduced productive infection of multiple SARS-CoV-2 variants of concern in human lung cells, supporting a cofactor role for IFITM2 during infection.

These observations align with the pseudovirus entry data in this study (Figures 18 and 19), in which IFITM1 overexpression in $A549^{ACE2}$ cells significantly reduced entry for most spike-pseudotyped variants, with limited or no reduction observed for pseudotypes bearing Wuhan, BA.4, or BA.5 spike proteins. IFITM2 overexpression also reduced entry across the variant panel, with particularly strong restriction observed for variants such as Delta and early Omicron lineages (BA.1, BA.2, BA.4). In parallel, RNA-seq analysis in infected HAE cells (Figure 14) showed variant- and time-dependent differences in IFITM1/2/3 induction, highlighting that IFITM expression is dynamically regulated during infection and varies by variant.

Further support for the expression-level "duality" comes from Xie et al. (2023), who demonstrated that endogenous IFITM2 and/or IFITM3 can support efficient replication of SARS-CoV-1/2, whereas IFITM overexpression inhibits infection, in part through effects on host factors and trafficking. In addition, Shi et al. showed that IFITM3 function can diverge depending on entry route and cellular context: mutations affecting IFITM3 endocytosis and conditions that favour plasma-membrane fusion (e.g., increased TMPRSS2-driven entry) can attenuate restriction and, in some settings, convert IFITM3 from an inhibitor into an enhancer of SARS-CoV-2 infection.

In this study, IFITM3 overexpression in $A549^{ACE2}$ cells did not produce a statistically significant change in spike-pseudotyped SARS-CoV-2 entry for any tested variant. Although small shifts in mean RLU% were observed, the effects were inconsistent and not significant, indicating a negligible impact of IFITM3 on entry under these experimental conditions. This suggests that any restrictive or facilitative effects of IFITM3 reported elsewhere may depend on factors not captured in this model, such as endogenous expression levels, subcellular localisation, or the balance between endosomal and TMPRSS2-mediated entry routes.

Overall, the data support variant-dependent sensitivity to IFITM-mediated modulation of entry. IFITM1 and IFITM2 overexpression reduced entry for most, whereas IFITM3 overexpression had no detectable effect in this system, consistent with the broader literature showing that IFITM function is highly context dependent.

5.4 Limitations and future work

Several methodological limitations should be considered when interpreting these data, and they directly inform priorities for future work. For the qPCR analyses, reference gene suitability was selected based on prior work in the laboratory and on comparisons with datasets generated by other lab members, providing internal consistency. However, reference gene stability was not formally evaluated using established algorithms such as geNorm or NormFinder (Andersen et al., 2004; Vandesompele et al., 2002). Because infection and interferon signalling can influence the expression of commonly used housekeeping genes, systematic stability testing would increase confidence in the normalised IFITM expression profiles (Sundaram et al., 2019).

Although pseudovirus (PV) stocks were generated and titrated, equal functional titres were not explicitly normalised across all experiments. Variation in infectious units between PV preparations can influence measured entry efficiency and contribute to inter-experimental variability. Future experiments should standardise PV input using infectious units (IU/mL) (and, where useful, particle-associated measures as supporting metrics) to strengthen quantitative comparability across conditions (Bentley et al., 2015).

IFITM expression was not assessed at the protein level under the experimental conditions used, limiting interpretation of whether changes in mRNA abundance reflect altered protein levels. Since IFITMs are subject to post-transcriptional and post-translational regulation, future work should include protein-level validation using Western blotting, flow cytometry, or immunofluorescence to relate IFITM abundance more directly to entry phenotypes (Friedlová et al., 2022). In parallel, the subcellular localisation of IFITMs following lentiviral transduction was not examined, despite localisation being a key determinant of IFITM function; IFITM1 is more commonly associated with the plasma membrane, whereas IFITM2 and IFITM3 are enriched in intracellular/endosomal compartments (Narayana et al., 2015; Weston et al., 2014). Overexpression can perturb trafficking and promote mislocalisation, so confocal microscopy with compartment-specific markers and

colocalisation analysis would help confirm that each IFITM is positioned appropriately to exert its expected effects (Weston et al., 2014).

The use of SARS-CoV-2 spike–pseudotyped viruses also constrains interpretation. While PVs provide a robust and safer system for quantifying spike-mediated entry, they do not capture post-entry stages of the viral life cycle such as genome replication, assembly, release, and immune evasion. Consequently, conclusions from this study are restricted to entry-related processes, and complementary experiments using replication-competent virus would be valuable to determine whether IFITMs influence infection beyond entry (Bentley et al., 2015; Thimmiraju et al., 2024). Additionally, the reliance on exogenous overexpression of IFITMs may not reflect endogenous expression levels achieved during natural infection. Future studies should therefore assess viral entry and (where relevant) replication under more physiological IFITM induction, such as type I/III interferon stimulation, and test causality by targeted depletion of individual IFITMs using siRNA or CRISPR–Cas9 approaches (Nchioua et al., 2022; Prelli Bozzo et al., 2021; Xie et al., 2023). These strategies would help distinguish physiological IFITM activity from overexpression-associated artefacts.

Several additional experimental directions would strengthen mechanistic resolution and relevance to variant evolution. First, a broader panel of currently circulating Omicron subvariants should be evaluated to determine whether ongoing spike diversification alters susceptibility to IFITM-mediated effects. Second, repeating entry assays in cells co-expressing ACE2 and TMPRSS2 would clarify how TMPRSS2-driven surface fusion modifies IFITM phenotypes, particularly given evidence that TMPRSS2 can shift IFITM3 behaviour in a context-dependent manner (Shi et al., 2021). Third, incorporating physiologically relevant airway models would improve translational relevance: primary nasal epithelial cultures capture the upper-airway environment of early infection and comparative datasets report variant-specific differences in replication dynamics across nasal versus lower-airway systems (Tanneti et al., 2024). Finally, pairing luciferase entry assays with flow

cytometry and protein-level measurements would provide a stronger framework to connect IFITM abundance, localisation, and experimental manipulation with entry outcomes and, where appropriate, viral RNA or infectious virus outputs (Friedlová et al., 2022).

5.5 Conclusion

Camostat mesylate was used to inhibit TMPRSS2 and reduce plasma-membrane fusion. In the $A549^{ACE2}$ model, which expresses low endogenous TMPRSS2, the Delta pseudovirus retained higher residual entry than Omicron in the presence of camostat. This suggests that, under these conditions, Delta entry is less constrained by TMPRSS2 inhibition and may rely more heavily on TMPRSS2-independent routes, including endosomal entry (Hoffmann et al., 2020; Meng et al., 2022). These data highlight a key interpretive point: cellular protease availability—particularly low TMPRSS2 expression—can substantially shape apparent variant entry efficiency and the observed magnitude of inhibitor effects in vitro (Hoffmann et al., 2020; Meng et al., 2022).

Conversely, E64d was used to inhibit endosomal cysteine proteases involved in cathepsin-mediated spike activation, thereby impairing the endosomal entry route. Sensitivity patterns were consistent with a meaningful contribution of cathepsin-dependent entry to SARS-CoV-2 infection, with variants more reliant on endosomal processing showing greater reductions following E64d treatment (Cannalire et al., 2020; Zhao et al., 2021). Taken together, these pharmacological findings support the concept that SARS-CoV-2 variants differ in their relative use of TMPRSS2-mediated surface fusion versus cathepsin-mediated endosomal activation, and that this balance is strongly influenced by cellular context (Hoffmann et al., 2020; Meng et al., 2022).

As SARS-CoV-2 continues to diversify, defining how variants engage host entry factors—including interferon-induced transmembrane (IFITM) proteins—remains important. In this experimental system, exogenous expression of IFITM1 and IFITM2 reduced spike-pseudotyped viral entry across multiple variants, consistent with restriction activity under overexpression conditions (Friedlová et

al., 2022; Shi et al., 2021). In contrast, IFITM3 overexpression did not significantly alter entry for any variant tested, indicating no detectable restrictive effect in this model. This pattern aligns with the wider literature showing that IFITM activity is highly context dependent: endogenous IFITMs (notably IFITM2) can support efficient SARS-CoV-2 infection in some human lung cell models, whereas artificial overexpression can inhibit entry (Nchioua et al., 2022; Prelli Bozzo et al., 2021; Xie et al., 2023).

These findings also define clear directions for future work. Validation in physiologically relevant airway models and with replication-competent virus will be required to determine whether the entry phenotypes observed here translate to full infection outcomes. In addition, testing in ACE2/TMPRSS2 co-expressing systems would clarify how TMPRSS2 availability modulates inhibitor responses and IFITM effects, particularly for IFITM3, which has been reported to show entry-route-dependent phenotypes (Meng et al., 2022; Shi et al., 2021). More broadly, host-directed approaches that enhance innate antiviral programmes—such as interferon-based strategies that induce multiple interferon-stimulated genes, including IFITMs—remain of interest, although efficacy is likely to depend on timing, dose, and inflammatory risk (Jhuti et al., 2022). Overall, resolving how entry pathways and restriction factor phenotypes vary by variant and cellular context will strengthen mechanistic understanding of SARS-CoV-2 pathogenesis and support antiviral strategies that are more resilient to viral evolution (Meng et al., 2022; Prelli Bozzo et al., 2021).

REFERENCES

Acchioni, C., Palermo, E., Sandini, S., Acchioni, M., Hiscott, J., & Sgarbanti, M. (2021). Fighting HIV-1 Persistence: At the Crossroads of "Shoc-K and B-Lock". Pathogens (Basel, Switzerland), 10(11), 1517. https://doi.org/10.3390/pathogens10111517

Allan, E. & Yates, R. (2015). Redundancy between cysteine cathepsins in murine experimental autoimmune encephalomyelitis. Plos One, 10(6), e0128945. https://doi.org/10.1371/journal.pone.0128945

Andersen, C. L., Jensen, J. L., & Ørntoft, T. F. (2004). Normalization of Real-Time Quantitative Reverse Transcription-PCR Data: A Model-Based Variance Estimation Approach to Identify Genes Suited for Normalization, Applied to Bladder and Colon Cancer Data Sets. Cancer Research, 64(15), 5245–5250. https://doi.org/10.1158/0008-5472.can-04-0496

Au-Yeung, N., Mandhana, R., & Horvath, C. M. (2013). Transcriptional regulation by STAT1 and STAT2 in the interferon JAK-STAT pathway. JAK-STAT, 2(3), e23931. https://doi.org/10.4161/jkst.23931

Baby, K., Vithalkar, M. P., Dastidar, S. G., Mukhopadhyay, C., Hamdy, R., Soliman, S. S. M., & Nayak, Y. (2025). Exploring TMPRSS2 Drug Target to Combat Influenza and Coronavirus Infection. Scientifica, 2025(1). https://doi.org/10.1155/sci5/3687892

Backer, J. A., Eggink, D., Andeweg, S. P., Veldhuijzen, I. K., van Maarseveen, N., Vermaas, K., Vlaemynck, B., Schepers, R., van den Hof, S., Reusken, C. B., & Wallinga, J. (2022). Shorter serial intervals in SARS-CoV-2 cases with Omicron BA.1 variant compared with Delta variant, the Netherlands, 13 to 26 December 2021. Eurosurveillance, 27(6), 2200042. https://doi.org/10.2807/1560-7917.ES.2022.27.6.2200042

Bai, C., Zhong, Q., & Gao, G. F. (2021). Overview of SARS-CoV-2 genome-encoded proteins. Science China Life Sciences, 65(2). https://doi.org/10.1007/s11427-021-1964-4

Bailey, C. C., Huang, I-Chueh., Kam, C., & Farzan, M. (2012). Ifitm3 Limits the Severity of Acute Influenza in Mice. PLoS Pathogens, 8(9), e1002909. https://doi.org/10.1371/journal.ppat.1002909

Bailey, C. C., Zhong, G., Huang, I. C., & Farzan, M. (2014). IFITM-family proteins: The cell's first line of antiviral defense. Annual Review of Virology, 1(1), 261-283. https://doi.org/10.1146/annurev-virology-031413-085537

Bakillah, A., Hejji, F. A., Almasaud, A., Jami, H. A., Hawwari, A., Qarni, A. A., Iqbal, J., & Alharbi, N. K. (2022). Lipid Raft Integrity and Cellular Cholesterol Homeostasis Are Critical for SARS-CoV-2 Entry into Cells. Nutrients, 14(16), 3417. https://doi.org/10.3390/nu14163417

Benlarbi, M., Laroche, G., Fink, C., Fu, K., Mulloy, R. P., Phan, A., Ariana, A., Stewart, C. M., Prévost, J., Beaudoin-Bussières, G., Daniel, R., Bo, Y., El Ferri, O., Yockell-Lelièvre, J., Stanford, W. L., Giguère, P. M., Mubareka, S., Finzi, A., Dekaban, G. A., Dikeakos, J. D., Côté, M. (2022). Identification and differential usage of a host metalloproteinase entry pathway by SARS-CoV-2 Delta and Omicron. iScience, 25(11), 105316. https://doi.org/10.1016/j.isci.2022.105316

Bentley, E. M., Mather, S. T., & Temperton, N. J. (2015). The use of pseudotypes to study viruses, virus sero-epidemiology and vaccination. Vaccine, 33(26), 2955–2962. https://doi.org/10.1016/j.vaccine.2015.04.071

Bentley, K., Sarah May Keep, Armesto, M., & Britton, P. (2013). Identification of a Noncanonically Transcribed Subgenomic mRNA of Infectious Bronchitis Virus and Other Gammacoronaviruses. Journal of Virology, 87(4), 2128–2136. https://doi.org/10.1128/jvi.02967-12

Bestle, D., Heindl, M. R., Limburg, H., Van Lam van, T., Pilgram, O., Moulton, H., Stein, D. A., Hardes, K., Eickmann, M., Dolnik, O., Rohde, C., Klenk, H. D., Garten, W., Steinmetzer, T., &

Böttcher-Friebertshäuser, E. (2020). TMPRSS2 and furin are both essential for proteolytic activation of SARS-CoV-2 in human airway cells. Life science alliance, 3(9), e202000786. https://doi.org/10.26508/lsa.202000786

Bhatt, P. R., Scaiola, A., Loughran, G., Leibundgut, M., Kratzel, A., Meurs, R., Dreos, R., O'Connor, K. M., McMillan, A., Bode, J. W., Thiel, V., Gatfield, D., Atkins, J. F., & Ban, N. (2021). Structural basis of ribosomal frameshifting during translation of the SARS-CoV-2 RNA genome. Science, 372(6548), 1306–1313. https://doi.org/10.1126/science.abf3546

Bhattacharyya, R. P., & Hanage, W. P. (2022). Challenges in Inferring Intrinsic Severity of the SARS-CoV-2 Omicron Variant. The New England journal of medicine, 386(7), e14. https://doi.org/10.1056/NEJMp2119682

Borges, V., Isidro, J., Trovão, N. S., Duarte, S., Cortes-Martins, H., Martiniano, H., Gordo, I., Leite, R., Vieira, L., Portuguese network for SARS-CoV-2 genomics (Consortium), Guiomar, R., & Gomes, J. P. (2022). SARS-CoV-2 introductions and early dynamics of the epidemic in Portugal. Communications medicine, 2, 10. https://doi.org/10.1038/s43856-022-00072-0

Brass, A. L., Huang, I.-C., Benita, Y., John, S. P., Krishnan, M. N., Feeley, E. M., Ryan, B. J., Weyer, J. L., van der Weyden, L., Fikrig, E., Adams, D. J., Xavier, R. J., Farzan, M., & Elledge, S. J. (2009). The IFITM proteins mediate cellular resistance to influenza A H1N1 virus, West Nile virus, and dengue virus. Cell, 139(7), 1243–1254. https://doi.org/10.1016/j.cell.2009.12.017

Burns, J. C., Friedmann, T., Driever, W., Burrascano, M., & Yee, J. K. (1993). Vesicular stomatitis virus G glycoprotein pseudotyped retroviral vectors: concentration to very high titer and efficient gene transfer into mammalian and nonmammalian cells. Proceedings of the National Academy of Sciences, 90(17), 8033-8037. https://doi.org/10.1073/pnas.90.17.8033

Cannalire, R., Stefanelli, I., Cerchia, C., Beccari, A. R., Pelliccia, S., & Summa, V. (2020). SARS-CoV-2 Entry Inhibitors: Small Molecules and Peptides Targeting Virus or Host Cells. International Journal of Molecular Sciences, 21(16), 5707. https://doi.org/10.3390/ijms21165707

Carnell, G. W., Ferrara, F., Grehan, K., Thompson, C. P., & Temperton, N. J. (2015). Pseudotype-Based Neutralization Assays for Influenza: A Systematic Analysis. Frontiers in Immunology, 6. https://doi.org/10.3389/fimmu.2015.00161

Cele, S., Jackson, L., Khoury, D. S., Khan, K., Moyo-Gwete, T., Tegally, H., San, J. E., Cromer, D., Scheepers, C., Amoako, D. G., Karim, F., Bernstein, M., Lustig, G., Archary, D., Smith, M., Ganga, Y., Jule, Z., Reedoy, K., Hwa, S.-H., & Giandhari, J. (2022). Omicron extensively but incompletely escapes Pfizer BNT162b2 neutralization. Nature, 602(7898), 1–3. https://doi.org/10.1038/s41586-021-04387-1

Chaintoutis, S. C., Thomou, Z., Mouchtaropoulou, E., Tsiolas, G., Chassalevris, T., Stylianaki, I., Lagou, M., Michailidou, S., Moutou, E., Koenen, J. J. H., Dijkshoorn, J. W., Paraskevis, D., Poutahidis, T., Siarkou, V. I., Sypsa, V., Argiriou, A., Fortomaris, P., & Dovas, C. I. (2021). Outbreaks of SARS-CoV-2 in naturally infected mink farms: Impact, transmission dynamics, genetic patterns, and environmental contamination. PLOS Pathogens, 17(9), e1009883. https://doi.org/10.1371/journal.ppat.1009883

Chang, C.-W., Parsi, K. M., Somasundaran, M., Vanderleeden, E., Liu, P., Cruz, J., Cousineau, A., Finberg, R. W., & Kurt-Jones, E. A. (2022). A Newly Engineered A549 Cell Line Expressing ACE2 and TMPRSS2 Is Highly Permissive to SARS-CoV-2, Including the Delta and Omicron Variants. Viruses, 14(7), 1369. https://doi.org/10.3390/v14071369

Chen, Y., Lear, T. B., Evankovich, J. W., Larsen, M. B., Lin, B., Alfaras, I., Kennerdell, J. R., Salminen, L., Camarco, D. P., Lockwood, K. C., Tuncer, F., Liu, J., Myerburg, M. M., McDyer, J. F., Liu, Y., Finkel, T., & Chen, B. B. (2021). A high-throughput screen for TMPRSS2 expression

identifies FDA-approved compounds that can limit SARS-CoV-2 entry. Nature communications, 12(1), 3907. https://doi.org/10.1038/s41467-021-24156-y

Chesarino, N. M., McMichael, T. M., Hach, J. C., & Yount, J. S. (2014). Phosphorylation of the antiviral protein interferon-inducible transmembrane protein 3 (IFITM3) dually regulates its endocytosis and ubiquitination. Journal of Biological Chemistry, 289(17), 11986-11992. https://doi.org/10.1074/jbc.M114.557694

Cockrell, A. S., & Kafri, T. (2007). Gene delivery by lentivirus vectors. Molecular Biotechnology, 36(3), 184-204. https://doi.org/10.1007/s12033-007-0010-8

Curreli, F., Victor, S. M. B., Ahmed, S., Drelich, A., Tong, X., Tseng, C.-T. K., Hillyer, C. D., & Debnath, A. K. (2020). Stapled Peptides Based on Human Angiotensin-Converting Enzyme 2 (ACE2) Potently Inhibit SARS-CoV-2 Infection In Vitro. MBio, 11(6). https://doi.org/10.1128/mBio.02451-20

Desai, T. M., Marin, M., Chin, C. R., Savidis, G., Brass, A. L., & Melikyan, G. B. (2014). IFITM3 restricts influenza A virus entry by blocking the formation of fusion pores following virus-endosome hemifusion. PLoS pathogens, 10(4), e1004048. https://doi.org/10.1371/journal.ppat.1004048

Di Genova, C., Sampson, A., Scott, S., Cantoni, D., Mayora-Neto, M., Bentley, E., Mattiuzzo, G., Wright, E., Derveni, M., Auld, B., Ferrara, B. T., Harrison, D., Said, M., Selim, A., Thompson, E., Thompson, C., Carnell, G., & Temperton, N. (2021). Production, titration, neutralisation, storage and lyophilisation of severe acute respiratory syndrome coronavirus 2 (SARS-CoV-2) lentiviral pseudotypes. Bio-protocol, 11(21), e4236. https://doi.org/10.21769/BioProtoc.4236

Ding, C., He, J., Zhang, X., Jiang, C., Sun, Y., Zhang, Y., Chen, Q., He, H., Li, W., Xie, J., Liu, Z., & Gao, Y. (2021). Crucial Mutations of Spike Protein on SARS-CoV-2 Evolved to Variant Strains Escaping Neutralization of Convalescent Plasmas and RBD-Specific Monoclonal Antibodies. Frontiers in Immunology, 12. https://doi.org/10.3389/fimmu.2021.693775

Dull, T., Zufferey, R., Kelly, M., Mandel, R. J., Nguyen, M., Trono, D., & Naldini, L. (1998). A Third-Generation Lentivirus Vector with a Conditional Packaging System. Journal of Virology, 72(11), 8463-8471. https://doi.org/10.1128/jvi.72.11.8463-8471.1998

Eckert, N., Wrensch, F., Gärtner, S., Palanisamy, N., Goedecke, U., Jäger, N., Pöhlmann, S., & Winkler, M. (2014). Influenza A virus encoding secreted Gaussia luciferase as useful tool to analyze viral replication and its inhibition by antiviral compounds and cellular proteins. PloS one, 9(5), e97695. https://doi.org/10.1371/journal.pone.0097695

Eythorsson, E., Runolfsdottir, H. L., Ingvarsson, R. F., Sigurdsson, M. I., & Palsson, R. (2022). Rate of SARS-CoV-2 Reinfection During an Omicron Wave in Iceland. JAMA Network Open, 5(8), e2225320-e2225320. https://doi.org/10.1001/jamanetworkopen.2022.25320

Feeley, E. M., Sims, J. S., John, S. P., Chin, C. R., Pertel, T., Chen, L.-M., Gaiha, G. D., Ryan, B. J., Donis, R. O., Elledge, S. J., & Brass, A. L. (2011). IFITM3 Inhibits Influenza A Virus Infection by Preventing Cytosolic Entry. PLoS Pathogens, 7(10), e1002337. https://doi.org/10.1371/journal.ppat.1002337

Fehr, A. R., & Perlman, S. (2015). Coronaviruses: an overview of their replication and pathogenesis. Methods in molecular biology (Clifton, N.J.), 1282, 1–23. https://doi.org/10.1007/978-1-4939-2438-7_1

Fink, K., & Grandvaux, N. (2013). STAT2 and IRF9: Beyond ISGF3. JAK-STAT, 2(4), e27521. https://doi.org/10.4161/jkst.27521

Finkel, Y., Mizrahi, O., Nachshon, A., Weingarten-Gabbay, S., Morgenstern, D., Yahalom-Ronen, Y., Tamir, H., Achdout, H., Stein, D., Israeli, O., Beth-Din, A., Melamed, S., Weiss, S., Israely, T., Paran, N., Schwartz, M., & Stern-Ginossar, N. (2020). The coding capacity of SARS-CoV-2. Nature, 1–6. https://doi.org/10.1038/s41586-020-2739-1

Fonager, J., Bennedbæk, M., Bager, P., Wohlfahrt, J., Ellegaard, K. M., Ingham, A. C., Edslev, S. M., Stegger, M., Sieber, R. N., Lassauniere, R., Fomsgaard, A., Lillebaek, T., Svarrer, C. W., Møller, F. T., Møller, C. H., Legarth, R., Sydenham, T. V., Steinke, K., Paulsen, S. J., Castruita, J. A. S., Rasmussen, M. (2022). Molecular epidemiology of the SARS-CoV-2 variant Omicron BA.2 sub-lineage in Denmark, 29 November 2021 to 2 January 2022. Euro surveillance : bulletin Europeen sur les maladies transmissibles = European communicable disease bulletin, 27(10), 2200181. https://doi.org/10.2807/1560-7917.ES.2022.27.10.2200181

Friedlová Nela, Filip Zavadil Kokáš, Hupp, T. R., Bořivoj Vojtěšek, & Nekulová, M. (2022). IFITM protein regulation and functions: Far beyond the fight against viruses. Frontiers in Immunology, 13. https://doi.org/10.3389/fimmu.2022.1042368

Frieman, M., Yount, B., Heise, M., Kopecky-Bromberg, S. A., Palese, P., & Baric, R. S. (2007). Severe acute respiratory syndrome coronavirus ORF6 antagonizes STAT1 function by sequestering nuclear import factors on the rough endoplasmic reticulum/Golgi membrane. Journal of Virology, 81(18), 9812-9824. https://doi.org/10.1128/JVI.01012-07

Giulia Unali, Crivicich, G., Pagani, I., Monah Abou Alezz, Filippo Folchini, Valeri, E., Vittoria Matafora, Reisz, J. A., Giordano, A., Cuccovillo, I., Butta, G. M., Donnici, L., D'Alessandro, A., Raffaele De Francesco, Manganaro, L., Davide Cittaro, Merelli, I., Petrillo, C., Bachi, Á., & Vicenzi, E. (2023). Interferon-inducible phospholipids govern IFITM3-dependent endosomal antiviral immunity. The EMBO Journal, 42(10). https://doi.org/10.15252/embj.2022112234

Glowacka, I., Bertram, S., Müller, M. A., Allen, P., Soilleux, E., Pfefferle, S., Steffen, I., Tsegaye, T. S., He, Y., Gnirss, K., Niemeyer, D., Schneider, H., Drosten, C., & Pöhlmann, S. (2011). Evidence that TMPRSS2 activates the severe acute respiratory syndrome coronavirus spike protein for membrane fusion and reduces viral control by the humoral immune response. Journal of virology, 85(9), 4122-4134. https://doi.org/10.1128/JVI.02232-10

Gunst, J. D., Staerke, N. B., Pahus, M. H., Kristensen, L. H., Bodilsen, J., Lohse, N., Dalgaard, L. S., Brønnum, D., Fröbert, O., Hønge, B., Johansen, I. S., Monrad, I., Erikstrup, C., Rosendal, R., Vilstrup, E., Mariager, T., Bove, D. G., Offersen, R., Shakar, S., Cajander, S., Søgaard, O. S. (2021). Efficacy of the TMPRSS2 inhibitor camostat mesilate in patients hospitalized with Covid-19-a double-blind randomized controlled trial. EClinicalMedicine, 35, 100849. https://doi.org/10.1016/j.eclinm.2021.100849

Guo, Y., Han, J., Zhang, Y., He, J., Yu, W., Zhang, X., Wu, J., Zhang, S., Kong, Y., Guo, Y., Lin, Y., & Zhang, J. (2022). SARS-CoV-2 Omicron Variant: Epidemiological Features, Biological Characteristics, and Clinical Significance. Frontiers in Immunology, 13. https://doi.org/10.3389/fimmu.2022.877101

Gupta R. (2022). SARS-CoV-2 Omicron spike mediated immune escape and tropism shift. Research square, rs.3.rs-1191837. https://doi.org/10.21203/rs.3.rs-1191837/v1

Harvey, W. T., Carabelli, A. M., Jackson, B., Gupta, R. K., Thomson, E. C., Harrison, E. M., Ludden, C., Reeve, R., Rambaut, A., Peacock, S. J., & Robertson, D. L. (2021). SARS-CoV-2 variants, spike mutations and immune escape. Nature Reviews Microbiology, 19(7), 409-424. https://doi.org/10.1038/s41579-021-00573-0

Hirose, R., Itoh, Y., Ikegaya, H., Miyazaki, H., Watanabe, N., Yoshida, T., Bandou, R., Daidoji, T., & Nakaya, T. (2022). Differences in environmental stability among SARS-CoV-2 variants of concern: Both Omicron BA.1 and BA.2 have higher stability. Clinical Microbiology and Infection. https://doi.org/10.1016/j.cmi.2022.05.020

Hoagland, D. A., Møller, R., Uhl, S. A., Oishi, K., Frere, J., Golynker, I., Horiuchi, S., Panis, M., Blanco-Melo, D., Sachs, D., Arkun, K., Lim, J. K., & tenOever, B. R. (2021). Leveraging the antiviral type I interferon system as a first line of defense against SARS-CoV-2 pathogenicity. Immunity, 54(3), 557–570.e5. https://doi.org/10.1016/j.immuni.2021.01.017

Hoffmann, M., Kleine-Weber, H., & Pöhlmann, S. (2020). A Multibasic Cleavage Site in the Spike Protein of SARS-CoV-2 Is Essential for Infection of Human Lung Cells. Molecular cell, 78(4), 779-784.e5. https://doi.org/10.1016/j.molcel.2020.04.022

Hoffmann, M., Kleine-Weber, H., Schroeder, S., Krüger, N., Herrler, T., Erichsen, S., Schiergens, T. S., Herrler, G., Wu, N.-H., Nitsche, A., Müller, M. A., Drosten, C., & Pöhlmann, S. (2020). SARS-CoV-2 cell entry depends on ACE2 and TMPRSS2 and is blocked by a clinically proven protease inhibitor. Cell, 181(2), 271–280.e8. https://doi.org/10.1016/j.cell.2020.02.052

Huai Luo, C., Paul Morris, C., Sachithanandham, J., Amadi, A., Gaston, D. C., Li, M., Swanson, N. J., Schwartz, M., Klein, E. Y., Pekosz, A., & Mostafa, H. H. (2022). Infection With the Severe Acute Respiratory Syndrome Coronavirus 2 (SARS-CoV-2) Delta Variant Is Associated With Higher Recovery of Infectious Virus Compared to the Alpha Variant in Both Unvaccinated and Vaccinated Individuals. Clinical infectious diseases : an official publication of the Infectious Diseases Society of America, 75(1), e715–e725. https://doi.org/10.1093/cid/ciab986

Irham, L. M., Chou, W.-H., Calkins, M. J., Adikusuma, W., Hsieh, S.-L., & Chang, W.-C. (2020). Genetic variants that influence SARS-CoV-2 receptor TMPRSS2 expression among population cohorts from multiple continents. Biochemical and Biophysical Research Communications, 529(2), 263-269. https://doi.org/10.1016/j.bbrc.2020.05.179

Ito, K., Piantham, C., & Nishiura, H. (2022). Relative instantaneous reproduction number of Omicron SARS-CoV-2 variant with respect to the Delta variant in Denmark. Journal of medical virology, 94(5), 2265-2268. https://doi.org/10.1002/jmv.27560

Ivashkiv, L. B., & Donlin, L. T. (2013). Regulation of type I interferon responses. Nature Reviews Immunology, 14(1), 36-49. https://doi.org/10.1038/nri3581

Iwata-Yoshikawa, N., Okamura, T., Shimizu, Y., Hasegawa, H., Takeda, M., & Nagata, N. (2019). Tmprss2 contributes to virus spread and immunopathology in the airways of murine models after coronavirus infection. Journal of Virology, 93(6). https://doi.org/10.1128/jvi.01815-18

Jackson, C. B., Farzan, M., Chen, B., & Choe, H. (2021). Mechanisms of SARS-CoV-2 Entry into Cells. Nature Reviews Molecular Cell Biology, 23(1), 1–18. https://doi.org/10.1038/s41580-021-00418-x

Jahirul Islam, M., Nawal Islam, N., Siddik Alom, M., Kabir, M., & Halim, M. A. (2023). A review on structural, non-structural, and accessory proteins of SARS-CoV-2: Highlighting drug target sites. Immunobiology, 228(1), 152302. https://doi.org/10.1016/j.imbio.2022.152302

Jhuti, D., Rawat, A., Guo, C. M., Wilson, L. A., Mills, E. J., & Forrest, J. I. (2022). Interferon Treatments for SARS-CoV-2: Challenges and Opportunities. Infectious Diseases and Therapy, 11(3), 953–972. https://doi.org/10.1007/s40121-022-00633-9

Jia, R., Xu, F., Qian, J., Yao, Y., Miao, C., Zheng, Y.-M., Liu, S.-L., Guo, F., Geng, Y., Qiao, W., & Liang, C. (2014). Identification of an endocytic signal essential for the antiviral action of IFITM3. Cellular Microbiology, 16(7), 1080–1093. https://doi.org/10.1111/cmi.12262

Jocher, G., Grass, V., Tschirner, S. K., Riepler, L., Breimann, S., Kaya, T., Oelsner, M., Hamad, M. S., Hofmann, L. I., Blobel, C. P., Schmidt-Weber, C. B., Gokce, O., Jakwerth, C. A., Trimpert, J., Kimpel, J., Pichlmair, A., & Lichtenthaler, S. F. (2022). ADAM10 and ADAM17 promote SARS-CoV-2 cell entry and spike protein-mediated lung cell fusion. EMBO Reports, 23(6). https://doi.org/10.15252/embr.202154305

Kafri, T., van Praag, H., Ouyang, L., Gage, F. H., & Verma, I. M. (1999). A Packaging Cell Line for Lentivirus Vectors. Journal of Virology, 73(1), 576-584. https://doi.org/10.1128/jvi.73.1.576-584.1999

Ketterer, S., Gomez-Auli, A., Hillebrand, L. E., Petrera, A., Ketscher, A., & Reinheckel, T. (2017). Inherited diseases caused by mutations in cathepsin protease genes. The FEBS Journal, 284(10), 1437–1454. https://doi.org/10.1111/febs.13980

Kim, D., Lee, J. Y., Yang, J. S., Kim, J. W., Kim, V. N., & Chang, H. (2020). The Architecture of SARS-CoV-2 Transcriptome. Cell, 181(4), 914–921.e10. https://doi.org/10.1016/j.cell.2020.04.011

Koch, J., Uckeley, Z. M., Doldan, P., Stanifer, M., Boulant, S., & Lozach, P. (2021). TMPRSS2 expression dictates the entry route used by SARS-CoV-2 to infect host cells. The EMBO Journal, 40(16). https://doi.org/10.15252/embj.2021107821

Kozak, M. (1986). Point mutations define a sequence flanking the AUG initiator codon that modulates translation by eukaryotic ribosomes. Cell, 44(2), 283-292. https://doi.org/10.1016/0092-8674(86)90762-2

Kozak, M. (2005). Regulation of translation via mRNA structure in prokaryotes and eukaryotes. Gene, 361, 13-37. https://doi.org/10.1016/j.gene.2005.06.037

Kung, Y. A., Lee, K. M., Chiang, H. J., Huang, S. Y., Wu, C. J., & Shih, S. R. (2022). Molecular Virology of SARS-CoV-2 and Related Coronaviruses. Microbiology and molecular biology reviews : MMBR, 86(2), e0002621. https://doi.org/10.1128/mmbr.00026-21

Kutner, R. H., Zhang, X. Y., & Reiser, J. (2009). Production, concentration and titration of pseudotyped HIV-1-based lentiviral vectors. Nature Protocols, 4(4), 495-505. https://doi.org/10.1038/nprot.2009.22

Le Bon, A., & Tough, D. F. (2002). Links between innate and adaptive immunity via type I interferon. Current Opinion in Immunology, 14(4), 432-436. https://doi.org/10.1016/S0952-7915(02)00354-0

Lei, X., Dong, X., Ma, R., Wang, W., Xiao, X., Tian, Z., Wang, C., Wang, Y., Li, L., Ren, L., Guo, F., Zhao, Z., Zhou, Z., Xiang, Z., Wang, J., & Xu, L. (2020). Activation and evasion of type I interferon responses by SARS-CoV-2. Nature Communications, 11, 3810. https://doi.org/10.1038/s41467-020-17665-9

Li, F. (2016). Structure, Function, and Evolution of Coronavirus Spike Proteins. Annual Review of Virology, 3(1), 237–261. https://doi.org/10.1146/annurev-virology-110615-042301

Li, K., Markosyan, R. M., Zheng, Y.-M., Golfetto, O., Bungart, B., Li, M., Ding, S., He, Y., Liang, C., & Lee, J. C. (2013). IFITM proteins restrict viral membrane hemifusion. PLOS Pathogens, 9(1), e1003124. https://doi.org/10.1371/journal.ppat.1003124

Li, T., Cui, Z., Jia, Y., Liang, Z., Nie, J., Zhang, L., Wang, M., Li, Q., Wu, J., Xu, N., Liu, S., Li, X., An, Y., Han, P., Zhang, M., Li, Y., Qu, X., Wang, Q., Huang, W., & Wang, Y. (2022). Aggregation of high-frequency RBD mutations of SARS-CoV-2 with three VOCs did not cause significant antigenic drift. Journal of Medical Virology, 94(5), 2108-2125. https://doi.org/10.1002/jmv.27596

Long, S. (2021). SARS-CoV-2 Subgenomic RNAs: Characterization, Utility, and Perspectives. Viruses, 13(10), 1923. https://doi.org/10.3390/v13101923

Lukassen, S., Chua, R. L., Trefzer, T., Kahn, N. C., Schneider, M. A., Muley, T., Eils, R. (2020). SARS-CoV-2 receptor ACE2 and TMPRSS2 are primarily expressed in bronchial transient secretory cells. The EMBO Journal, 39(10), e105114. https://doi.org/10.15252/embj.20105114

Mahoney, M., Damalanka, V., Tartell, M., Chung, D., Lourenço, A., Pwee, D., & Janetka, J. (2021). A novel class of tmprss2 inhibitors potently block sars-cov-2 and mers-cov viral entry and protect human epithelial lung cells. Proceedings of the National Academy of Sciences, 118(43). https://doi.org/10.1073/pnas.2108728118

Marceau, T., & Braibant, M. (2024). Role of Viral Envelope Proteins in Determining Susceptibility of Viruses to IFITM Proteins. Viruses, 16(2), 254–254. https://doi.org/10.3390/v16020254

Marie-Pierre Confort, Maëva Duboeuf, Thiesson, A., Pons, L., Marziali, F., Desloire, S., Maxime Ratinier, Cimarelli, A., & Arnaud, F. (2023). IFITMs from Naturally Infected Animal Species Exhibit Distinct Restriction Capacities against Toscana and Rift Valley Fever Viruses. Viruses, 15(2), 306-306. https://doi.org/10.3390/v15020306

Maslo, C., Friedland, R., Toubkin, M., Laubscher, A., Akaloo, T., & Kama, B. (2021). Characteristics and Outcomes of Hospitalized Patients in South Africa During the COVID-19 Omicron Wave Compared With Previous Waves. JAMA. https://doi.org/10.1001/jama.2021.24868

McKee, D. L., Sternberg, A., Stange, U., Laufer, S., & Naujokat, C. (2020). Candidate drugs against SARS-CoV-2 and COVID-19. Pharmacological Research, 157, 104859. https://doi.org/10.1016/j.phrs.2020.104859

McMahan, K., Giffin, V., Tostanoski, L. H., Chung, B., Siamatu, M., Suthar, M. S., Halfmann, P., Kawaoka, Y., Piedra-Mora, C., Jain, N., Ducat, S., Kar, S., Andersen, H., Lewis, M. G., Martinot, A. J., & Barouch, D. H. (2022). Reduced pathogenicity of the SARS-CoV-2 omicron variant in hamsters. Med, 3(4), 262-268.e4. https://doi.org/10.1016/j.medj.2022.03.004

McNab, F., Mayer-Barber, K., Sher, A., Wack, A., & O'Garra, A. (2015). Type I interferons in infectious disease. Nature Reviews Immunology, 15(2), 87-103. https://doi.org/10.1038/nri3787

Meischel, T., Fritzlar, S., Villalon-Letelier, F., Tessema, M. B., Brooks, A. G., Reading, P. C., & Londrigan, S. L. (2021). IFITM proteins that restrict the early stages of respiratory virus infection do not influence late-stage replication. Journal of Virology, 95(20), e00837-21. https://doi.org/10.1128/JVI.00837-21

Meng, B., Abdullahi, A., Ferreira, I. A. T. M., Goonawardane, N., Saito, A., Kimura, I., Yamasoba, D., Gerber, P. P., Fatihi, S., Rathore, S., Zepeda, S. K., Papa, G., Kemp, S. A., Ikeda, T., Toyoda, M., Tan, T. S., Kuramochi, J., Mitsunaga, S., Ueno, T., & Shirakawa, K. (2022). Altered TMPRSS2 usage by SARS-CoV-2 Omicron impacts tropism and fusogenicity. Nature. https://doi.org/10.1038/s41586-022-04474-x

Milone, M. C., & O'Doherty, U. (2018). Clinical use of lentiviral vectors. Leukemia, 32(7), 1529-1541. https://doi.org/10.1038/s41375-018-0106-0

Miorin, L., et al. (2020). SARS-CoV-2 Orf6 hijacks Nup98 to block STAT nuclear import and antagonize interferon signaling. Proceedings of the National Academy of Sciences of the United States of America, 117(45), 28344-28354. https://doi.org/10.1073/pnas.2016650117

Mlcochova, P., Kemp, S., Dhar, M. S., Papa, G., Meng, B., Ferreira, I. A. T. M., Datir, R., Collier, D. A., Albecka, A., Singh, S., Pandey, R., Brown, J., Zhou, J., Goonawardane, N., Mishra, S., Whittaker, C., Mellan, T., Marwal, R., Datta, M., & Sengupta, S. (2021). SARS-CoV-2 B.1.617.2 Delta variant replication and immune evasion. Nature, 599, 1–8. https://doi.org/10.1038/s41586-021-03944-y

Mohandas, S., Yadav, P. D., Sapkal, G., Shete, A. M., Deshpande, G., Nyayanit, D. A., Patil, D., Kadam, M., Kumar, A., Mote, C., & Jain, R. (2022). Pathogenicity of SARS-CoV-2 Omicron (R346K) variant in Syrian hamsters and its cross-neutralization with different variants of concern. EBioMedicine, 79, 103997. https://doi.org/10.1016/j.ebiom.2022.103997

Mühlemann, B., Wilks, S. H., Baracco, L., Meriem Bekliz, Carreño, J. M., Corman, V. M., Davis-Gardner, M. E., Wanwisa Dejnirattisai, Diamond, M. S., Douek, D. C., Drosten, C., Eckerle, I., Venkata-Viswanadh Edara, Ellis, M., Fouchier, R. A. M., Frieman, M., Godbole, S., Haagmans, B., Halfmann, P. J., & Henry, A. R. (2023). Comparative Analysis of SARS-CoV-2 Antigenicity across Assays and in Human and Animal Model Sera. BioRxiv (Cold Spring Harbor Laboratory). https://doi.org/10.1101/2023.09.27.559689

Muik, A., Lui, B. G., Wallisch, A. K., Bacher, M., Mühl, J., Reinholz, J., Ozhelvaci, O., Beckmann, N., Güimil Garcia, R. C., Poran, A., Shpyro, S., Finlayson, A., Cai, H., Yang, Q., Swanson, K. A., Türeci, Ö., & Şahin, U. (2022). Neutralization of SARS-CoV-2 Omicron by BNT162b2 mRNA vaccine-elicited human sera. Science (New York, N.Y.), 375(6581), 678-680. https://doi.org/10.1126/science.abn7591

Müller, U., Steinhoff, U., Reis, L. F. L., Hemmi, S., Pavlovic, J., Zinkernagel, R. M., & Aguet, M. (1994). Functional role of type I and type II interferons in antiviral defense. Science, 264(5167), 1918-1921. https://doi.org/10.1126/science.8009221

Muus, C., Luecken, M. D., Eraslan, G., Sikkema, L., Waghray, A., Heimberg, G., The Human Cell Atlas Lung Biological Network. (2021). Single-cell meta-analysis of SARS-CoV-2 entry genes across tissues and demographics. Nature Medicine, 27, 546-559. https://doi.org/10.1038/s41591-020-01227-z

Naldini, L. (2015). Gene therapy returns to centre stage. Nature, 526(7573), 351-360. https://doi.org/10.1038/nature15818

Naldini, L., Blomer, U., Gallay, P., Ory, D., Mulligan, R., Gage, F. H., & Trono, D. (1996). In vivo gene delivery and stable transduction of nondividing cells by a lentiviral vector. Science, 272(5259), 263-267. https://doi.org/10.1126/science.272.5259.263

Narayana, S. K., Helbig, K. J., McCartney, E. M., Eyre, N. S., Bull, R. A., Eltahla, A., Lloyd, A. R., & Beard, M. R. (2015). The Interferon-induced Transmembrane Proteins, IFITM1, IFITM2, and IFITM3 Inhibit Hepatitis C Virus Entry. The Journal of biological chemistry, 290(43), 25946–25959. https://doi.org/10.1074/jbc.M115.657346

Nchioua, R., Schundner, A., Kmiec, D., Prelli Bozzo, C., Zech, F., Koepke, L., Graf, A., Krebs, S., Blum, H., Frick, M., Sparrer, K. M. J., & Kirchhoff, F. (2022). SARS-CoV-2 Variants of Concern

Hijack IFITM2 for Efficient Replication in Human Lung Cells. Journal of virology, 96(11), e0059422. https://doi.org/10.1128/jvi.00594-22

Neerukonda, S. N., Vassell, R., Herrup, R., Liu, S., Wang, T., Takeda, K., Yang, Y., Lin, T. L., Wang, W., & Weiss, C. D. (2021). Establishment of a well-characterized SARS-CoV-2 lentiviral pseudovirus neutralization assay using 293T cells with stable expression of ACE2 and TMPRSS2. PloS one, 16(3), e0248348. https://doi.org/10.1371/journal.pone.0248348

Nie, J., Li, Q., Wu, J., Zhao, C., Hao, H., Liu, H., Zhang, L., Nie, L., Qin, H., Wang, M., Lu, Q., Li, X., Sun, Q., Liu, J., Fan, C., Huang, W., Xu, M., & Wang, Y. (2020). Establishment and validation of a pseudovirus neutralization assay for SARS-CoV-2. Emerging microbes & infections, 9(1), 680-686. https://doi.org/10.1080/22221751.2020.1743767

Ou, X., Liu, Y., Lei, X., Li, P., Mi, D., Ren, L., Guo, L., Guo, R., Chen, T., Hu, J., Xiang, Z., Mu, Z., Chen, X., Chen, J., Hu, K., Jin, Q., Wang, J., & Qian, Z. (2020). Characterization of spike glycoprotein of SARS-CoV-2 on virus entry and its immune cross-reactivity with SARS-CoV. Nature Communications, 11, Article 1620. https://doi.org/10.1038/s41467-020-15562-9

Padmanabhan, P., Desikan, R., & Dixit, N. M. (2020). Targeting TMPRSS2 and Cathepsin B/L together may be synergistic against SARS-CoV-2 infection. PLOS Computational Biology, 16(12), e1008461. https://doi.org/10.1371/journal.pcbi.1008461

Patoine, A., Husseini, A., Bahar Kasaai, Gaumond, M.-H., & Moffatt, P. (2017). The osteogenic cell surface marker BRIL/IFITM5 is dispensable for bone development and homeostasis in mice. PloS One, 12(9), e0184568–e0184568. https://doi.org/10.1371/journal.pone.0184568

Peacock, T. P., Brown, J. C., Zhou, J., Thakur, N., Sukhova, K., Newman, J., Kugathasan, R., Yan, A. W. C., Furnon, W., De Lorenzo, G., Cowton, V. M., Reuss, D., Moshe, M., Martinez, M., Stockwell, R., Major, J., Goldhill, D. H., Barclay, W. S. (2022). The SARS-CoV-2 variant, Omicron, shows

rapid replication in human primary nasal epithelial cultures and efficiently uses an endosomal route of entry. https://doi.org/10.1101/2021.12.31.474653

Peacock, T. P., Goldhill, D. H., Zhou, J., Baillon, L., Frise, R., Swann, O. C., Kugathasan, R., Penn, R., Brown, J. C., Sanchez-David, R. Y., Braga, L., Williamson, M. K., Hassard, J. A., Staller, E., Hanley, B., Osborn, M., Giacca, M., Davidson, A. D., Matthews, D. A., & Barclay, W. S. (2021). The furin cleavage site in the SARS-CoV-2 spike protein is required for transmission in ferrets. Nature microbiology, 6(7), 899-909. https://doi.org/10.1038/s41564-021-00908-w

Perreira, J. M., Chin, C. R., Feeley, E. M., & Brass, A. L. (2013). IFITMs restrict the replication of multiple pathogenic viruses. Journal of Molecular Biology, 425(24), 4937-4955. https://doi.org/10.1016/j.jmb.2013.09.024

Pfaffl, M. W. (2001). A new mathematical model for relative quantification in real-time RT-PCR. Nucleic Acids Research, 29(9), e45. https://doi.org/10.1093/nar/29.9.e45

Platanias, L. C. (2005). Mechanisms of type-I- and type-II-interferon-mediated signalling. Nature Reviews Immunology, 5(5), 375-386. https://doi.org/10.1038/nri1604

Prelli Bozzo, C., Nchioua, R., Volcic, M., Koepke, L., Krüger, J., Schütz, D., Heller, S., Stürzel, C. M., Kmiec, D., Conzelmann, C., Müller, J., Zech, F., Braun, E., Groß, R., Wettstein, L., Weil, T., Weiß, J., Diofano, F., Rodríguez Alfonso, A. A., & Wiese, S. (2021). IFITM proteins promote SARS-CoV-2 infection and are targets for virus inhibition in vitro. Nature Communications, 12(1). https://doi.org/10.1038/s41467-021-24817-y

Qian, J., Yann Le Duff, Wang, Y., Pan, Q., Ding, S., Zheng, Y.-M., Liu, S.-L., & Liang, C. (2015). Primate lentiviruses are differentially inhibited by interferon-induced transmembrane proteins. Virology, 474, 10-18. https://doi.org/10.1016/j.virol.2014.10.015

Qian, Z., Dominguez, S. R., & Holmes, K. V. (2013). Role of the spike glycoprotein of human Middle East respiratory syndrome coronavirus (MERS-CoV) in virus entry and syncytia formation. PloS one, 8(10), e76469. https://doi.org/10.1371/journal.pone.0076469

Qu B, Miskey, C., Goemer, A., Potmus, D., Maximillian Nocke, Kleinert, R., Itotia, T. K., Valder, L., Brueckmann, J., Hoeck, S., Hastert, F. D., Christine von Rhein, Schuermann, C., Ebenig, A., Marek Widera, Ciesek, S., Pfaender, S., Zoltán Ivics, Schnierle, B. S., & Tarr, A. W. (2022). SARS-CoV-2 entry route impacts a range of downstream viral and cellular processes. BioRxiv (Cold Spring Harbor Laboratory). https://doi.org/10.1101/2022.08.05.502936

Sa Ribero, M., Jouvenet, N., Dreux, M., & Nisole, S. (2020). Interplay between SARS-CoV-2 and the type I interferon response. PLoS Pathogens, 16(7), e1008737. https://doi.org/10.1371/journal.ppat.1008737

Scarpa, F., Sanna, D., Azzena, I., Casu, M., Cossu, P., Fiori, P. L., Benvenuto, D., Imperia, E., Giovanetti, M., Ceccarelli, G., Cauda, R., Cassone, A., Pascarella, S., & Ciccozzi, M. (2023). Genome-based comparison between the recombinant SARS-CoV-2 XBB and its parental lineages. Journal of Medical Virology, 95(3), e28625. https://doi.org/10.1002/jmv.28625

Schneider, W. M., Chevillotte, M. D., & Rice, C. M. (2014). Interferon-stimulated genes: A complex web of host defenses. Annual Review of Immunology, 32, 513-545. https://doi.org/10.1146/annurev-immunol-032713-120231

Schoggins, J. W., & Rice, C. M. (2011). Interferon-stimulated genes and their antiviral effector functions. Current opinion in virology, 1(6), 519–525. https://doi.org/10.1016/j.coviro.2011.10.008

Schuler, B. A., Habermann, A. C., Plosa, E. J., Taylor, C. J., Jetter, C., Negretti, N. M., Sucre, J. M. (2021). Age-determined expression of priming protease TMPRSS2 and localization of SARS-CoV-2 in lung epithelium. Journal of Clinical Investigation, 131(1), e140766. https://doi.org/10.1172/JCI140766

Shang, J., Wan, Y., Luo, C., Ye, G., Geng, Q., Auerbach, A., & Li, F. (2020). Cell entry mechanisms of SARS-CoV-2. Proceedings of the National Academy of Sciences, 117(21). https://doi.org/10.1073/pnas.2003138117

Shang, J., Ye, G., Shi, K., Wan, Y., Luo, C., Aihara, H., Geng, Q., Auerbach, A., & Li, F. (2020). Structural basis of receptor recognition by SARS-CoV-2. Nature, 581(7807). https://doi.org/10.1038/s41586-020-2179-y

Shi, G., Kenney, A. D., Kudryashova, E., Zani, A., Zhang, L., Lai, K. K., Hall-Stoodley, L., Robinson, R. T., Kudryashov, D. S., Compton, A. A., & Yount, J. S. (2020). Opposing activities of IFITM proteins in SARS-CoV-2 infection. The EMBO Journal. https://doi.org/10.15252/embj.2020106501

Shi, G., Li, T., Lai, K. K., Johnson, R. F., Yewdell, J. W., & Compton, A. A. (2024). Omicron Spike confers enhanced infectivity and interferon resistance to SARS-CoV-2 in human nasal tissue. Nature Communications, 15(1), 889. https://doi.org/10.1038/s41467-024-45075-8

Shi, G., Schwartz, O., & Compton, A. A. (2017). More than meets the I: The diverse antiviral and cellular functions of interferon-induced transmembrane proteins. Retrovirology, 14(1), 53. https://doi.org/10.1186/s12977-017-0377-y

Sia, S. F., Yan, L.-M., Chin, A. W. H., Fung, K., Choy, K.-T., Wong, A. Y. L., Kaewpreedee, P., Perera, R. A. P. M., Poon, L. L. M., Nicholls, J. M., Peiris, M., & Yen, H.-L. (2020). Pathogenesis and transmission of SARS-CoV-2 in golden hamsters. Nature. https://doi.org/10.1038/s41586-020-2342-5

Simões, R. S. Q., & Rodríguez-Lázaro, D. (2022). Classical and Next-Generation Vaccine Platforms to SARS-CoV-2: Biotechnological Strategies and Genomic Variants. International journal of environmental research and public health, 19(4), 2392. https://doi.org/10.3390/ijerph19042392

Siwak, K. C., LeBlanc, E. V., Scott, H. M., Kim, Y., Pellizzari-Delano, I., Ball, A. M., Temperton, N. J., Capicciotti, C. J., & Colpitts, C. C. (2024). Cellular sialoglycans are differentially required for endosomal and cell-surface entry of SARS-CoV-2 in lung cell lines. PLoS pathogens, 20(12), e1012365. https://doi.org/10.1371/journal.ppat.1012365

Smith, S., Weston, S., Kellam, P., & Marsh, M. (2014). IFITM proteins—cellular inhibitors of viral entry. Current Opinion in Virology, 4, 71–77. https://doi.org/10.1016/j.coviro.2013.11.004

Starr, T. N., Greaney, A. J., Hilton, S. K., Ellis, D., Crawford, K. H. D., Dingens, A. S., Navarro, M. J., Bowen, J. E., Tortorici, M. A., Walls, A. C., King, N. P., Veesler, D., & Bloom, J. D. (2020). Deep Mutational Scanning of SARS-CoV-2 Receptor Binding Domain Reveals Constraints on Folding and ACE2 Binding. Cell, 182(5), 1295-1310.e20. https://doi.org/10.1016/j.cell.2020.08.012

Su, S., Wong, G., Shi, W., Liu, J., Lai, A. C. K., Zhou, J., Liu, W., Bi, Y., & Gao, G. F. (2016). Epidemiology, Genetic Recombination, and Pathogenesis of Coronaviruses. Trends in microbiology, 24(6), 490–502. https://doi.org/10.1016/j.tim.2016.03.003

Sun, L., Li, P., Ju, X., Ren, R., Huang, W., Ren, L., Wu, Y., Xiong, T., Xu, K., Zhou, X., Gong, M., Miska, E. A., Ding, Q., Wang, J., & Qiangfeng Cliff Zhang. (2021). In vivo structural characterization of the SARS-CoV-2 RNA genome identifies host proteins vulnerable to repurposed drugs. 184(7), 1865-1883.e20. https://doi.org/10.1016/j.cell.2021.02.008

Sun, X., Zeng, H., Kumar, A., Belser, J. A., Maines, T. R., & Tumpey, T. M. (2016). Constitutively Expressed IFITM3 Protein in Human Endothelial Cells Poses an Early Infection Block to Human Influenza Viruses. Journal of virology, 90(24), 11157–11167. https://doi.org/10.1128/JVI.01254-16

Sundaram, V. K., Sampathkumar, N. K., Massaad, C., & Grenier, J. (2019). Optimal use of statistical methods to validate reference gene stability in longitudinal studies. PloS one, 14(7), e0219440. https://doi.org/10.1371/journal.pone.0219440

Sungnak, W., Huang, N., Bécavin, C., Berg, M., Queen, R., Litvinukova, M., HCA Lung Biological Network. (2020). SARS-CoV-2 entry factors are highly expressed in nasal epithelial cells together with innate immune genes. Nature Medicine, 26, 681-687. https://doi.org/10.1038/s41591-020-0868-6

Taboada, B. I., Zárate, S., García-López, R., Muñoz-Medina, J. E., Gómez-Gil, B., Herrera-Estrella, A., Sanchez-Flores, A., Salas-Lais, A. G., Roche, B., Martínez-Morales, G., Domínguez Zárate, H., Duque Molina, C., Avilés Hernández, R., López, S., & Arias, C. F. (2023). SARS-CoV-2 Omicron variants BA.4 and BA.5 dominated the fifth COVID-19 epidemiological wave in Mexico. Microbial genomics, 9(12), 001120. https://doi.org/10.1099/mgen.0.001120

Tamura, T., Ito, J., Uriu, K., Zahradnik, J., Kida, I., Anraku, Y., Nasser, H., Shofa, M., Oda, Y., Lytras, S., Nao, N., Itakura, Y., Deguchi, S., Suzuki, R., Wang, L., Begum, M. M., Kita, S., Yajima, H., Sasaki, J., Sato, K. (2023). Virological characteristics of the SARS-CoV-2 XBB variant derived from recombination of two Omicron subvariants. Nature Communications, 14(1), 2800. https://doi.org/10.1038/s41467-023-38435-3

Tanneti, N. S., Patel, A. K., Tan, L. H., Marques, A. D., Perera, R. A. P. M., Sherrill-Mix, S., Kelly, B. J., Renner, D. M., Collman, R. G., Rodino, K., Lee, C., Bushman, F. D., Cohen, N. A., & Weiss, S. R. (2024). Comparison of SARS-CoV-2 variants of concern in primary human nasal cultures demonstrates Delta as most cytopathic and Omicron as fastest replicating. mBio, 15(4), e0312923. https://doi.org/10.1128/mbio.03129-23

Tegally, H., Wilkinson, E., Giovanetti, M., Iranzadeh, A., Fonseca, V., Giandhari, J., Doolabh, D., Pillay, S., San, E. J., Msomi, N., Mlisana, K., von Gottberg, A., Walaza, S., Allam, M., Ismail, A., Mohale, T., Glass, A. J., Engelbrecht, S., Van Zyl, G., Preiser, W., de Oliveira, T. (2021). Detection of a SARS-CoV-2 variant of concern in South Africa. Nature, 592(7854), 438-443. https://doi.org/10.1038/s41586-021-03402-9

Thimmiraju, S. R., Kimata, J. T., & Pollet, J. (2024). Pseudoviruses, a safer toolbox for vaccine development against enveloped viruses. Expert review of vaccines, 23(1), 174–185. https://doi.org/10.1080/14760584.2023.2299380

Torjesen I. (2022). Covid-19: Omicron variant is linked to steep rise in hospital admissions of very young children. BMJ (Clinical research ed.), 376, o110. https://doi.org/10.1136/bmj.o110

Torjesen, I. (2022). Covid-19: Omicron variant is linked to steep rise in hospital admissions of very young children. BMJ, 376, o110. https://doi.org/10.1136/bmj.o110

Tsai, W.-Y., Ching, L. L., Hsieh, S.-C., Melish, M. E., Nerurkar, V. R., & Wang, W.-K. (2021). A real-time and high-throughput neutralization test based on SARS-CoV-2 pseudovirus containing monomeric infrared fluorescent protein as reporter. Emerging Microbes & Infections, 10(1), 894-904. https://doi.org/10.1080/22221751.2021.1925163

V'kovski, P., Kratzel, A., Steiner, S., Stalder, H., & Thiel, V. (2020). Coronavirus biology and replication: Implications for SARS-CoV-2. Nature Reviews Microbiology, 19(1), 1–16. https://doi.org/10.1038/s41579-020-00468-6

Vandesompele, J., De Preter, K., Pattyn, F., Poppe, B., Van Roy, N., De Paepe, A., & Speleman, F. (2002). Accurate normalization of real-time quantitative RT-PCR data by geometric averaging of multiple internal control genes. Genome biology, 3(7), RESEARCH0034. https://doi.org/10.1186/gb-2002-3-7-research0034

Viana, R., Moyo, S., Amoako, D. G., Tegally, H., Scheepers, C., Althaus, C. L., Anyaneji, U. J., Bester, P. A., Boni, M. F., Chand, M., Choga, W. T., Colquhoun, R., Davids, M., Deforche, K., Doolabh, D., du Plessis, L., Engelbrecht, S., Everatt, J., Giandhari, J., Giovanetti, M., de Oliveira, T. (2022). Rapid epidemic expansion of the SARS-CoV-2 Omicron variant in southern Africa. Nature, 603(7902), 679-686. https://doi.org/10.1038/s41586-022-04411-y

Walls, A. C., Park, Y. J., Tortorici, M. A., Wall, A., McGuire, A. T., & Veesler, D. (2020). Structure, Function, and Antigenicity of the SARS-CoV-2 Spike Glycoprotein. Cell, 181(2), 281–292.e6. https://doi.org/10.1016/j.cell.2020.02.058

Wang, J., Luo, Y., Katiyar, H., Liang, C., & Liu, Q. (2024). The Antiviral Activity of Interferon-Induced Transmembrane Proteins and Virus Evasion Strategies. Viruses, 16(5), 734. https://doi.org/10.3390/v16050734

Wang, Q., Iketani, S., Li, Z., Liu, L., Guo, Y., Huang, Y., Bowen, A. D., Liu, M., Wang, M., Yu, J., Valdez, R., Lauring, A. S., Sheng, Z., Wang, H. H., Gordon, A., Liu, L., & Ho, D. D. (2023). Alarming antibody evasion properties of rising SARS-CoV-2 BQ and XBB subvariants. Cell, 186(2), 279-286.e8. https://doi.org/10.1016/j.cell.2022.12.018

Welch, S. R., Guerrero, L. W., Chakrabarti, A. K., McMullan, L. K., Flint, M., Bluemling, G. R., Painter, G. R., Nichol, S. T., Spiropoulou, C. F., & Albariño, C. G. (2016). Lassa and Ebola virus inhibitors identified using minigenome and recombinant virus reporter systems. Antiviral research, 136, 9-18. https://doi.org/10.1016/j.antiviral.2016.10.007

Weston, S., Czieso, S., White, I. J., Smith, S. E., Kellam, P., & Marsh, M. (2014). A Membrane Topology Model for Human Interferon Inducible Transmembrane Protein 1. PLoS ONE, 9(8), e104341. https://doi.org/10.1371/journal.pone.0104341

Wilks, S. H., Mühlemann, B., Shen, X., Türeli, S., LeGresley, E. B., Netzl, A., Caniza, M. A., Chacaltana-Huarcaya, J. N., Corman, V. M., Daniell, X., Datto, M. B., Dawood, F. S., Denny, T. N., Drosten, C., Fouchier, R. A. M., Garcia, P. J., Halfmann, P. J., Jassem, A., Jeworowski, L. M., Jones, T. C., Smith, D. J. (2023). Mapping SARS-CoV-2 antigenic relationships and serological responses. Science (New York, N.Y.), 382(6666), eadj0070. https://doi.org/10.1126/science.adj0070

Willett, B. J., Grove, J., MacLean, O. A., Wilkie, C., De Lorenzo, G., Furnon, W., Thomson, E. C. (2022). SARS-CoV-2 Omicron is an immune escape variant with an altered cell entry pathway. Nature Microbiology, 7, 1161-1179. https://doi.org/10.1038/s41564-022-01143-7

Wolter, N., Jassat, W., Walaza, S., Welch, R., Moultrie, H., Groome, M., Amoako, D. G., Everatt, J., Bhiman, J. N., Scheepers, C., Tebeila, N., Chiwandire, N., du Plessis, M., Govender, N., Ismail, A., Glass, A., Mlisana, K., Stevens, W., Treurnicht, F. K., Makatini, Z., Cohen, C. (2022). Early assessment of the clinical severity of the SARS-CoV-2 omicron variant in South Africa: a data linkage study. Lancet (London, England), 399(10323), 437-446. https://doi.org/10.1016/S0140-6736(22)00017-4

Wong, M.-T., & Chen, S. S-L. (2014). Emerging roles of interferon-stimulated genes in the innate immune response to hepatitis C virus infection. Cellular & Molecular Immunology, 13(1), 11–35. https://doi.org/10.1038/cmi.2014.127

World Health Organization. (2022, March 29). COVID-19 weekly epidemiological update: Edition 85. https://www.who.int/docs/default-source/coronaviruse/situation-reports/20220329_weekly_epi_update_85.pdf

Wrensch, F., Winkler, M., & Pöhlmann, S. (2014). IFITM proteins inhibit entry driven by the MERS-coronavirus spike protein: evidence for cholesterol-independent mechanisms. Viruses, 6(9), 3683–3698. https://doi.org/10.3390/v6093683

Wu, Y. C., Chen, C. S., & Chan, Y. J. (2020). The outbreak of COVID-19: An overview. Journal of the Chinese Medical Association : JCMA, 83(3), 217–220. https://doi.org/10.1097/JCMA.0000000000000270

Xiang, Q., Li, L., Wu, J., Tian, M., & Fu, Y. (2022). Application of pseudovirus system in the development of vaccine, antiviral-drugs, and neutralizing antibodies. Microbiological research, 258, 126993. https://doi.org/10.1016/j.micres.2022.126993

Xie, J., Bi, Y., Xu, S., Han, Y., Idris, A., Zhang, H., Li, X., Bai, J., Zhang, Y., & Feng, R. (2020). Host antiviral protein IFITM2 restricts pseudorabies virus replication. Virus Research, 287, 198105-198105. https://doi.org/10.1016/j.virusres.2020.198105

Xie, Q., Caterina Prelli Bozzo, Eiben, L., Nöttger, S., Dorota Kmieć, Rayhane Nchioua, Niemeyer, D., Volcic, M., Lee, J.-H., Zech, F., Konstantin, Drosten, C., & Kirchhoff, F. (2023). Endogenous IFITMs boost SARS-coronavirus 1 and 2 replication whereas overexpression inhibits infection by relocalizing ACE2. IScience, 26(4), 106395-106395. https://doi.org/10.1016/j.isci.2023.106395

Xu, J., Zhao, S., Teng, T., Abdalla, A., Zhu, W., Xie, L., & Guo, X. (2020). Systematic comparison of two animal-to-human transmitted human coronaviruses: sars-cov-2 and sars-cov. Viruses, 12(2), 244. https://doi.org/10.3390/v12020244

Xu, Z., Choi, J. H., Dai, D. L., Luo, J., Ladak, R. J., Li, Q., Wang, Y., Zhang, C., Wiebe, S., Liu, A. C. H., Ran, X., Yang, J., Naeli, P., Garzia, A., Zhou, L., Mahmood, N., Deng, Q., Elaish, M., Lin, R., Mahal, L. K., Sonenberg, N. (2022). SARS-CoV-2 impairs interferon production via NSP2-induced repression of mRNA translation. Proceedings of the National Academy of Sciences of the United States of America, 119(32), e2204539119. https://doi.org/10.1073/pnas.2204539119

Yadati, T., Houben, T., Bitorina, A., & Shiri-Sverdlov, R. (2020). The ins and outs of cathepsins: Physiological function and role in disease management. Cells, 9(7), 1679. https://doi.org/10.3390/cells9071679

Yamasoba, D., Kimura, I., Nasser, H., Morioka, Y., Nao, N., Ito, J., Uriu, K., Tsuda, M., Zahradnik, J., Shirakawa, K., Suzuki, R., Kishimoto, M., Kosugi, Y., Kobiyama, K., Hara, T., Toyoda, M., Tanaka, Y. L., Butlertanaka, E. P., Shimizu, R., Ito, H., Sato, K. (2022). Virological characteristics of the SARS-CoV-2 Omicron BA.2 spike. Cell, 185(12), 2103-2115.e19. https://doi.org/10.1016/j.cell.2022.04.035

Yánez, D. C., Ross, S., & Crompton, T. (2020). The IFITM protein family in adaptive immunity. Immunology, 159(4), 365–372. https://doi.org/10.1111/imm.13163

Yang, H., & Rao, Z. (2021). Structural biology of SARS-CoV-2 and implications for therapeutic development. Nature Reviews Microbiology, 19(11), 685–700. https://doi.org/10.1038/s41579-021-00630-8

Yang, R., Huang, B., Ruhan, A., Li, W., Wang, W., Deng, Y., & Tan, W. (2020). Development and effectiveness of pseudotyped SARS-CoV-2 system as determined by neutralizing efficiency and entry inhibition test in vitro. Biosafety and Health, 2(4), 226–231. https://doi.org/10.1016/j.bsheal.2020.08.004

Yang, W., & Shaman, J. (2021). COVID-19 pandemic dynamics in India, the SARS-CoV-2 Delta variant, and implications for vaccination. medRxiv. https://doi.org/10.1101/2021.06.21.21259268

Yang, Y., Ye, F., Zhu, N., Wang, W., Deng, Y., Zhao, Z., Tan, W., & Liu, W. (2015). Middle East respiratory syndrome coronavirus ORF4b protein inhibits type I interferon production through both cytoplasmic and nuclear targets. Scientific Reports, 5, 17554. https://doi.org/10.1038/srep17554 PMC

Yu, J., Li, M., Wilkins, J., Ding, S., Swartz, T. H., Esposito, A. M., Zheng, Y. M., Freed, E. O., Liang, C., Chen, B. K., & Liu, S. L. (2015). IFITM Proteins Restrict HIV-1 Infection by Antagonizing the Envelope Glycoprotein. Cell reports, 13(1), 145-156. https://doi.org/10.1016/j.celrep.2015.08.055

Zhao, H., Lu, L., Peng, Z., Chen, L. L., Meng, X., Zhang, C., Ip, J. D., Chan, W. M., Chu, A. W., Chan, K. H., Jin, D. Y., Chen, H., Yuen, K. Y., & To, K. K. (2022). SARS-CoV-2 Omicron variant shows less efficient replication and fusion activity when compared with Delta variant in TMPRSS2-expressed cells. Emerging microbes & infections, 11(1), 277-283. https://doi.org/10.1080/22221751.2021.2023329

Zhao, M. M., Yang, W. L., Yang, F. Y., Zhang, L., Huang, W. J., Hou, W., Fan, C. F., Jin, R. H., Feng, Y. M., Wang, Y. C., & Yang, J. K. (2021). Cathepsin L plays a key role in SARS-CoV-2 infection in humans and humanized mice and is a promising target for new drug development. Signal transduction and targeted therapy, 6(1), 134. https://doi.org/10.1038/s41392-021-00558-8

Zhao, X., Guo, F., Liu, F., Cuconati, A., Chang, J., Block, T. M., & Guo, J.-T. (2014). Interferon induction of IFITM proteins promotes infection by human coronavirus OC43. Proceedings of the National Academy of Sciences of the United States of America, 111(18), 6756–6761. https://doi.org/10.1073/pnas.1320856111

Zhao, X., Li, J., Winkler, C. A., An, P., & Guo, J. T. (2019). IFITM Genes, Variants, and Their Roles in the Control and Pathogenesis of Viral Infections. Frontiers in microbiology, 9, 3228. https://doi.org/10.3389/fmicb.2018.03228

Zhao, X., Sehgal, M., Hou, Z., Cheng, J., Shu, S., Wu, S., Guo, F., Le Marchand, S. J., Lin, H., Chang, J., & Guo, J. T. (2018). Identification of Residues Controlling Restriction versus Enhancing Activities of IFITM Proteins on Entry of Human Coronaviruses. Journal of virology, 92(6), e01535-17. https://doi.org/10.1128/JVI.01535-17

Zhou, H., Møhlenberg, M., Thakor, J. C., Tuli, H. S., Wang, P., Assaraf, Y. G., Dhama, K., & Jiang, S. (2022). Sensitivity to Vaccines, Therapeutic Antibodies, and Viral Entry Inhibitors and Advances To Counter the SARS-CoV-2 Omicron Variant. Clinical microbiology reviews, 35(3), e0001422. https://doi.org/10.1128/cmr.00014-22

Zhou, Q., Chen, V., Shannon, C. P., Wei, X. S., Xiang, X., Wang, X., Wang, Z. H., Liu, M. Q., Hu, Y., Luo, H., Liu, W., Yang, L., Xie, Y., Wu, W., Shetty, A., Jin, R., Wu, X., Wu, X., & Zhang, Z. (2020). Interferon-α2b treatment for COVID-19. Frontiers in Immunology, 11, 1061. https://doi.org/10.3389/fimmu.2020.01061

Zhou, Y., Vedantham, P., Lu, K., Agudelo, J., Carrion, R., Nunneley, J. W., Barnard, D., Pöhlmann, S., McKerrow, J. H., Renslo, A. R., & Simmons, G. (2015). Protease inhibitors targeting coronavirus and filovirus entry. Antiviral Research, 116, 76-84. https://doi.org/10.1016/j.antiviral.2015.01.011

Zufferey, R., Dull, T., Mandel, R. J., Bukovsky, A., Quiroz, D., Naldini, L., & Trono, D. (1998). Self-inactivating lentivirus vector for safe and efficient in vivo gene delivery. Journal of virology, 72(12), 9873-9880. https://doi.org/10.1128/JVI.72.12.9873-9880.1998

APPENDIX

Amino acid sequences for the S protein of the SARS-CoV-2 variants were retrieved from the NCBI Gene Bank (https://www.ncbi.nlm.nih.gov/gene) and aligned and compared using NIH BLASTp ®, COBALT and EMBL-EBI Clustal Omega tool.

Supplementary Table 1: Spike protein of various variants compared to Wuhan-Hu-1: QHD43416.1.

VARIANTS	ACCESSION	E VALUE	PERCENT %	LENGTH
Beta	WDB12209.1	0	99.14%	1270
BQ.1	WEF88212.1	0	98.90%	1270
Delta	WDV60773.1	0	98.59%	1271
BA.4	UTE11510.1	0	97.25%	1268
BA.5	WED51419.1	0	97.17%	1268
BA.2	WEF79925.1	0	97.17%	1268
BA.2	WDY61995.1	0	96.94%	1270
Alpha	UYX70557.1	0	95.05%	1270
XBB	WED48949.1	0	94.66%	1269

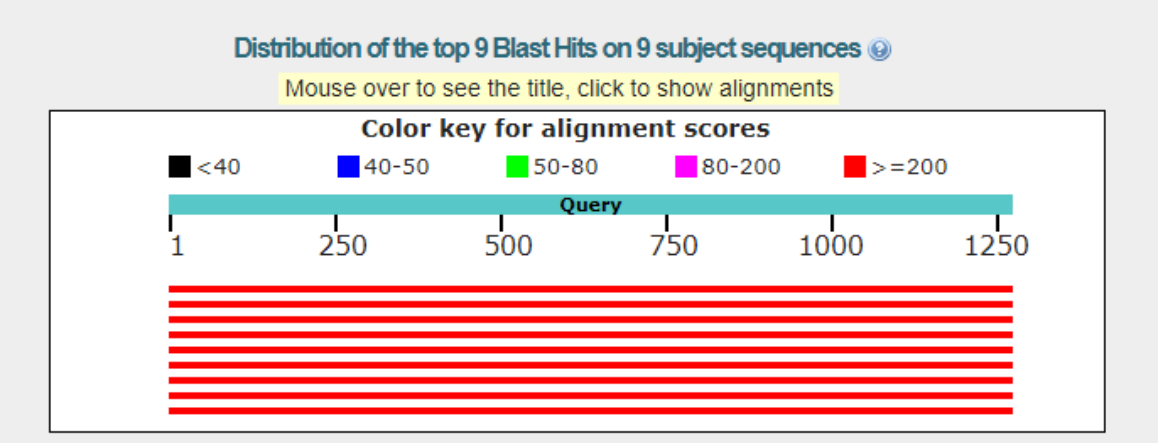

Supplementary Figure 1: Alignment score of Alpha, Beta, Delta, BA.1, BA.2, BA.4, BA.5, BQ.1 and XBB

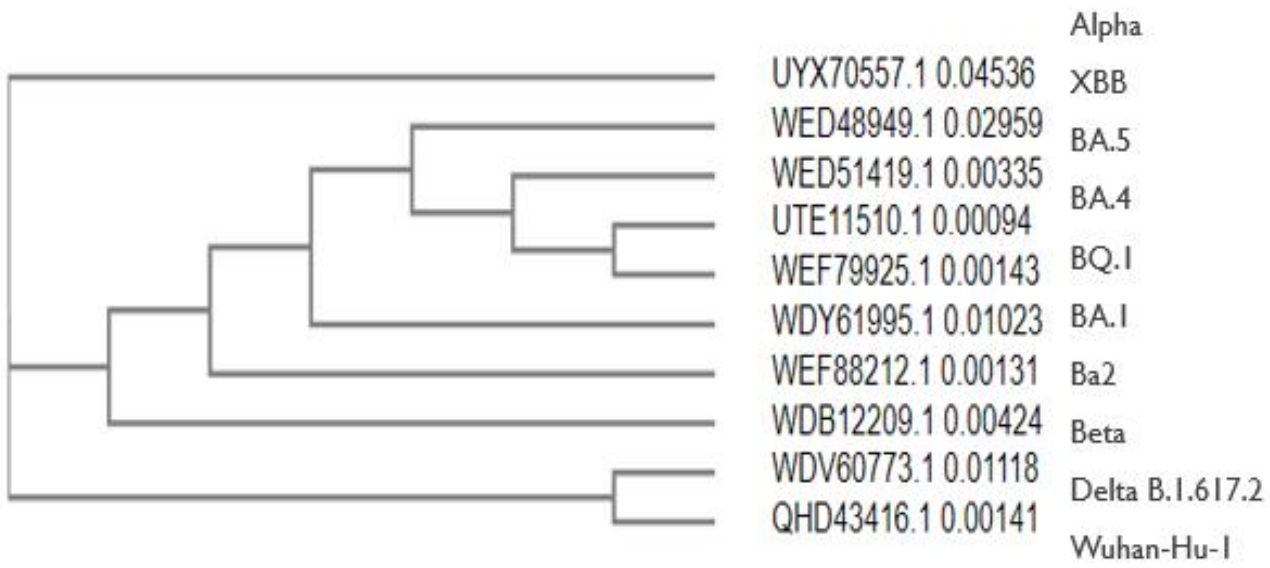

Supplementary Figure 2: Phylogenetic Tree of SARS-CoV-2 variants made with NIH COBLAT.

Supplementary Figure 3.1: Alignment of Alpha, Beta, Delta, BA.1, BA.2, BA.4, BA.5, BQ.1 and XBB variants using the EMBL-EBI Clustal Omega tool

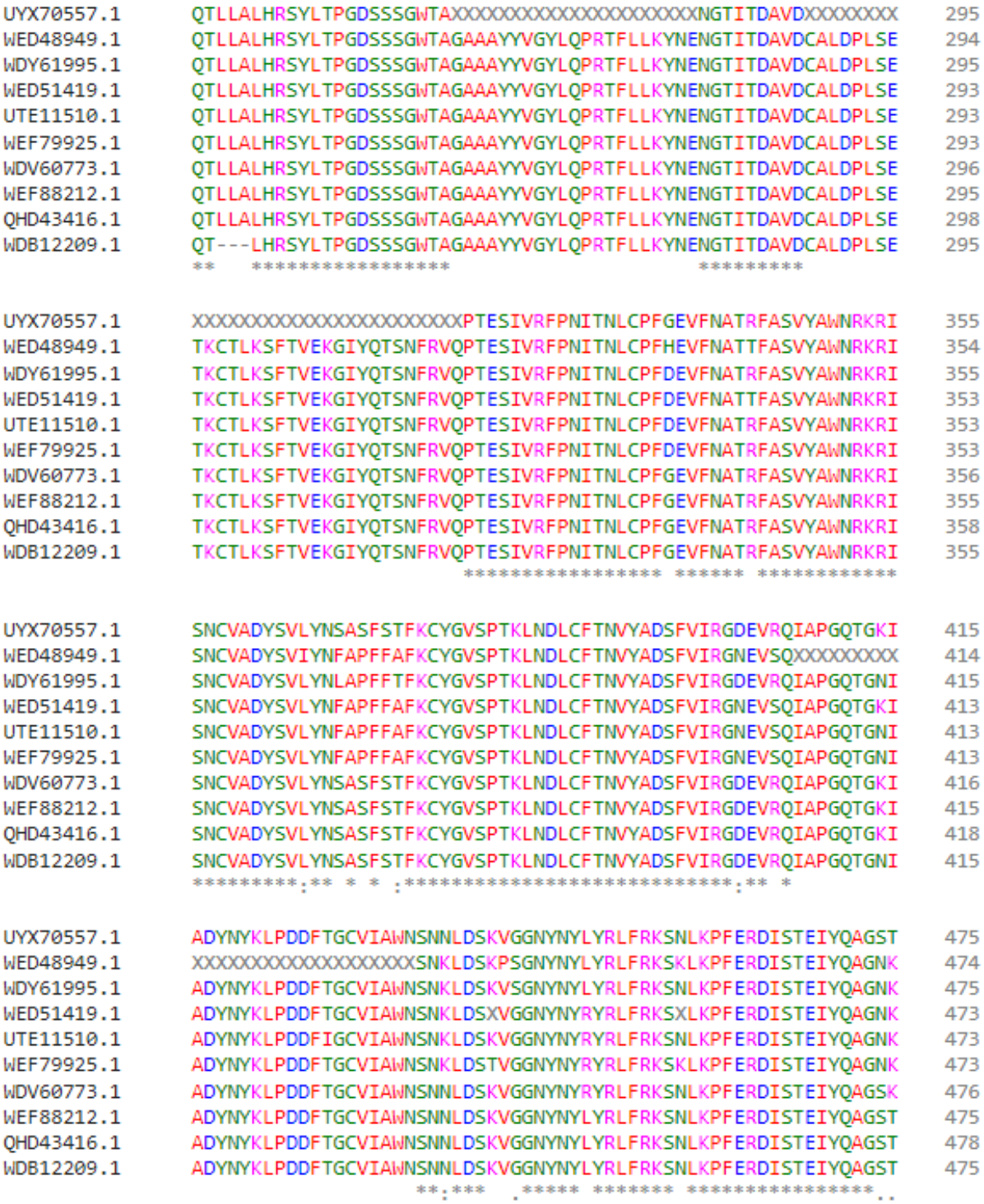

Supplementary Figure 3.2: Alignment of Alpha, Beta, Delta, BA.1, BA.2, BA.4, BA.5, BQ.1 and XBB variants using the EMBL-EBI Clustal Omega tool

Supplementary Figure 3.3: Alignment of Alpha, Beta, Delta, BA.1, BA.2, BA.4, BA.5, BQ.1 and XBB variants using the EMBL-EBI Clustal Omega tool